POGGIO LAB

University of Basel

Scanning SQUID-on-tip microscopy of 2D and chiral magnetism

Quantum sensing and fundamental physics with levitated mechanical systems
ECT, Trento, Italy*
02.08.2023

Prof. Martino Poggio
Department of Physics & Swiss Nanoscience Institute
University of Basel, Switzerland

Swiss Nanoscience Institute
NCCR SPIN
Swiss National Science Foundation
Funded by the European Union
FIBsuperProbes

Faraday’s iron filings

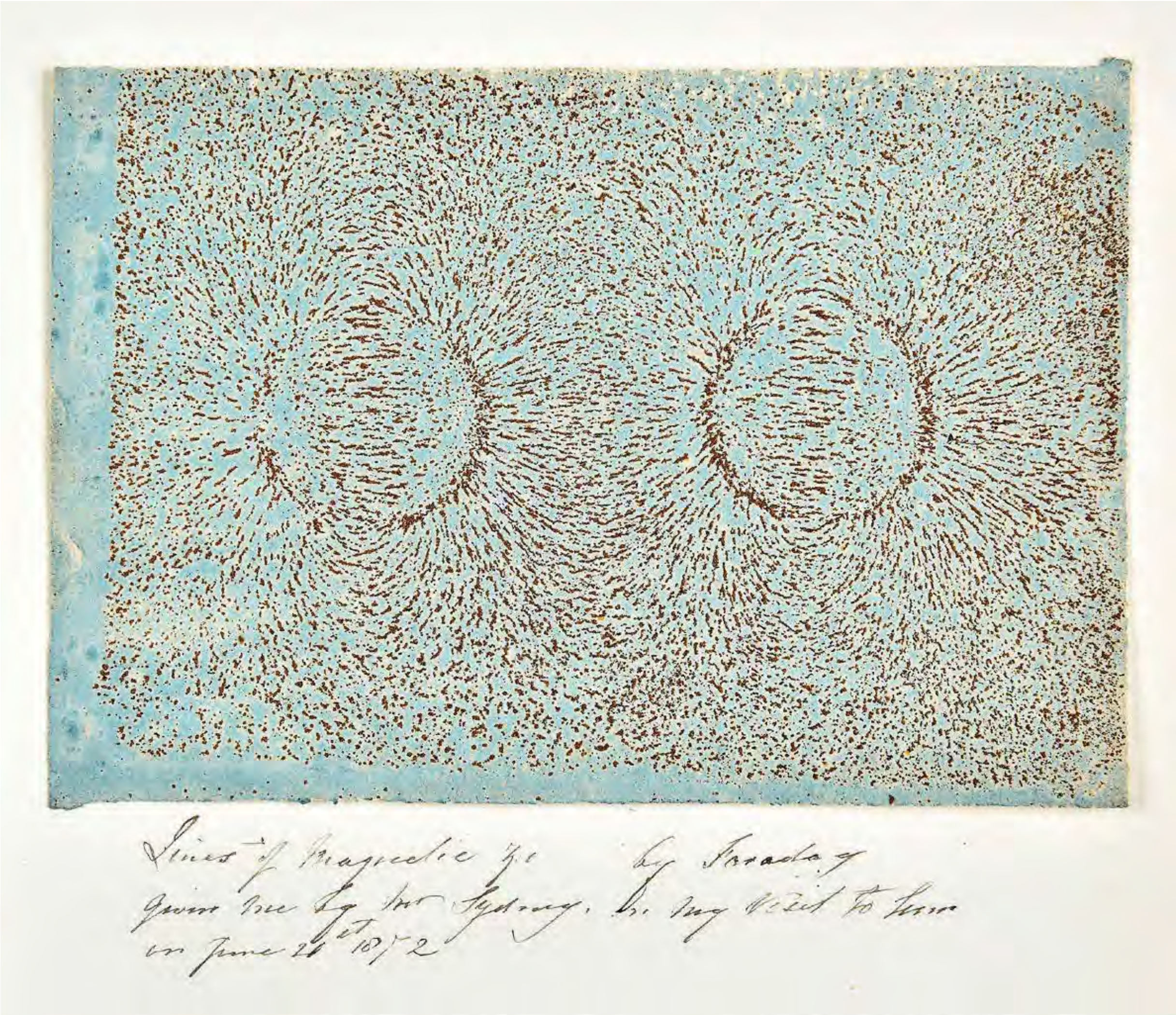

M. Faraday, ca. 1830s

Scanning tunnelling spectroscopy on atomic-scale

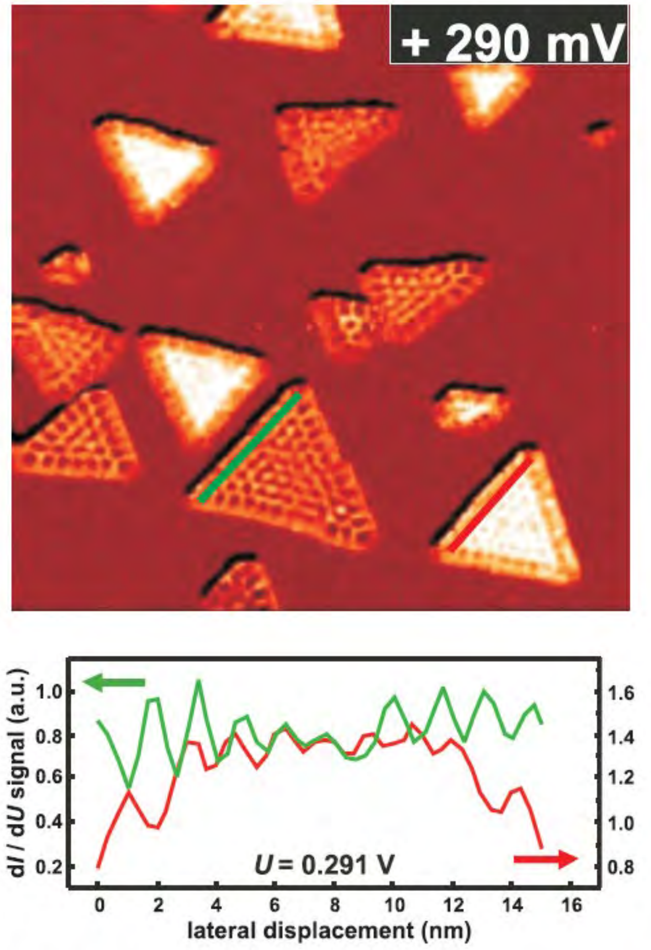

FIG. 44. (Color) SP-STS data (60×60 nm^2) revealing the spin dependence of the 2D electronic confinement states in nanoscale Co islands which manifests itself by a spin-dependent oscillation amplitude of the confinement states for differently magnetized Co nanoislands. From Pietzsch *et al.*, 2006.

Magneto-optical imaging of local spin-polarization

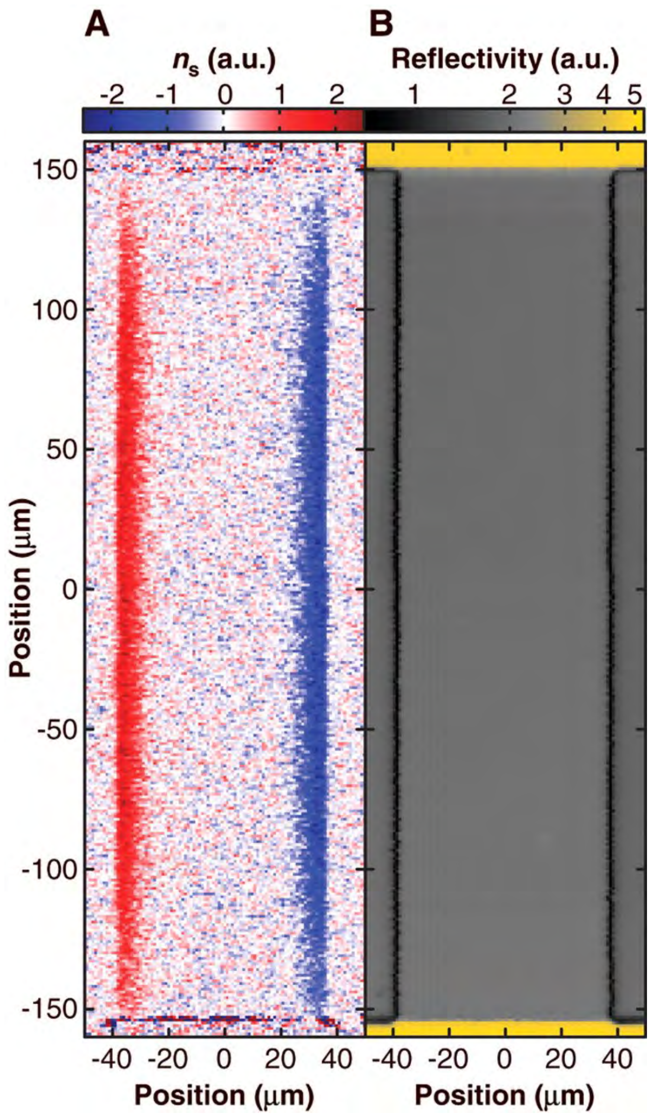

Kato et al., *Science* **306**, 5703 (2004).

Lorentz microscopy of skyrmion crystals

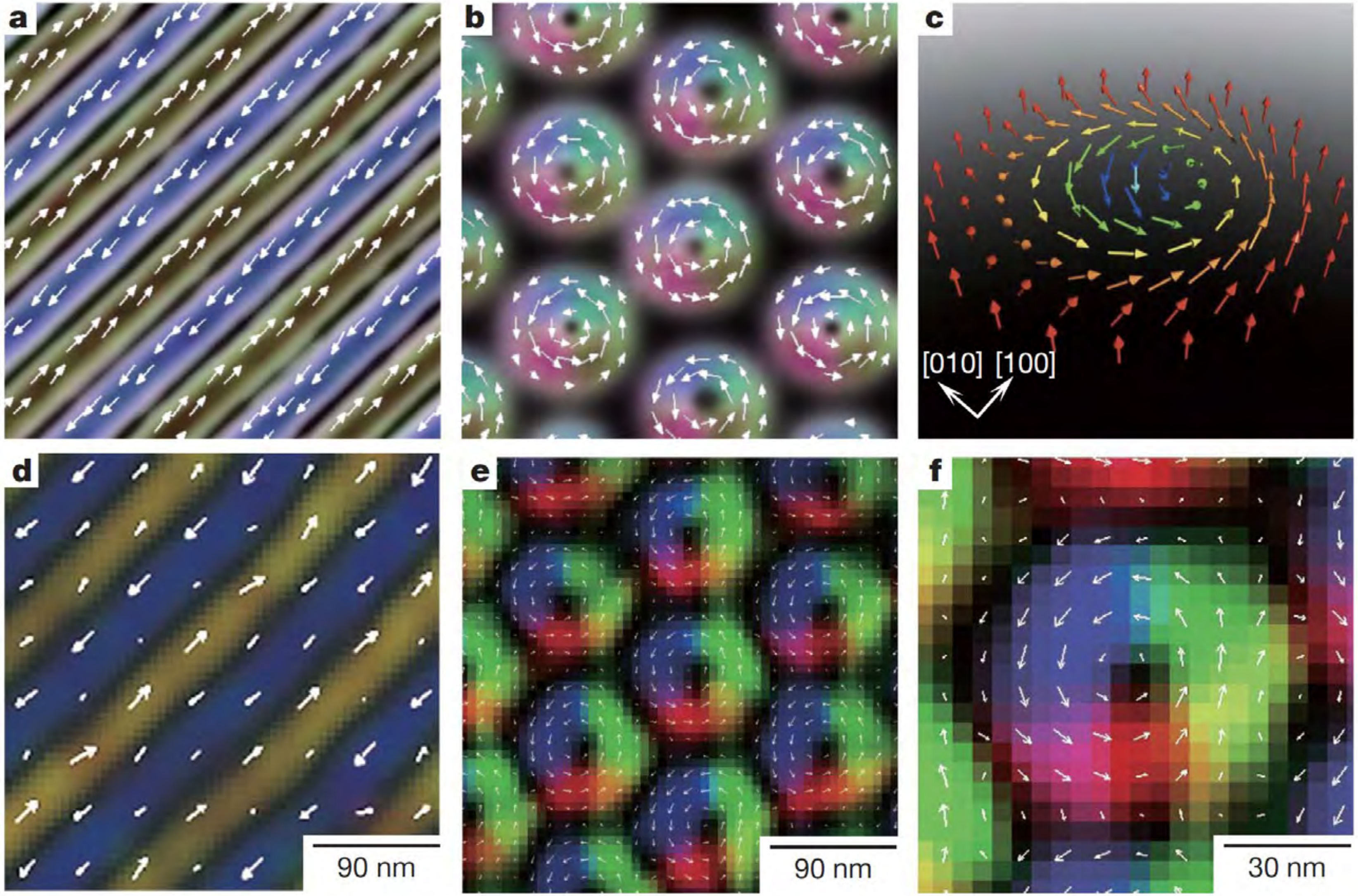

Yu et al., *Nature* **465**, 901 (2010).

SQUID microscopy of edge currents

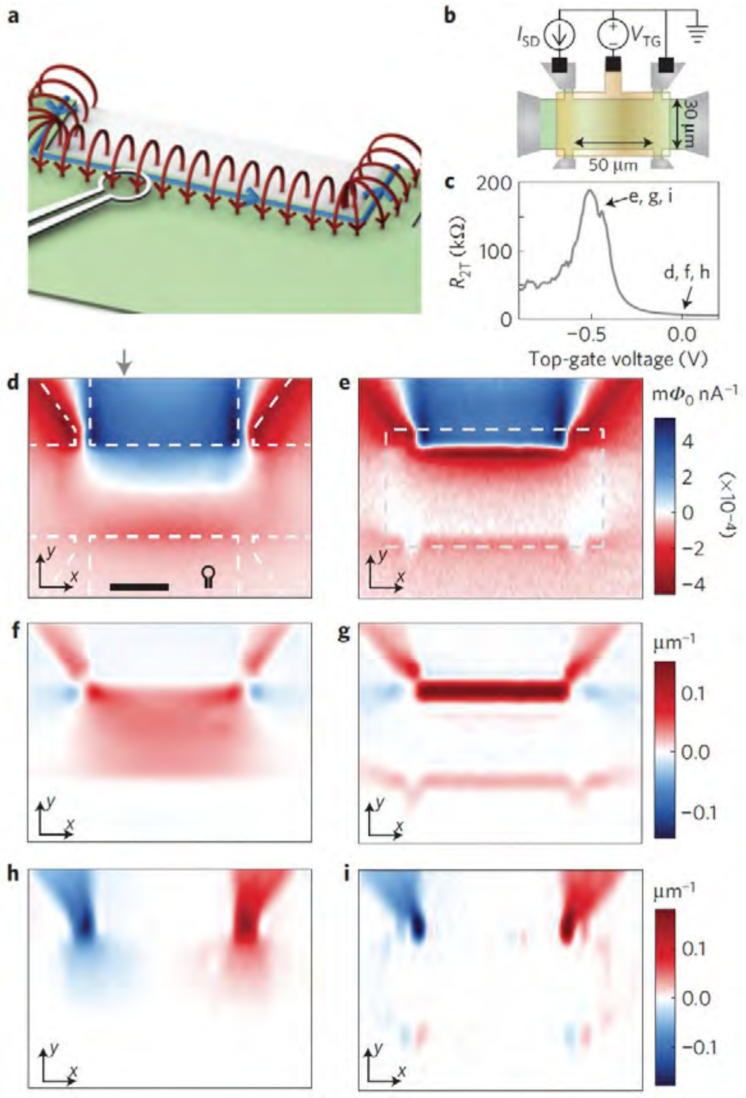

Nowack et al., *Nat. Phys.* **12**, 787 (2013).

SQUID microscopy of twist-angle disorder

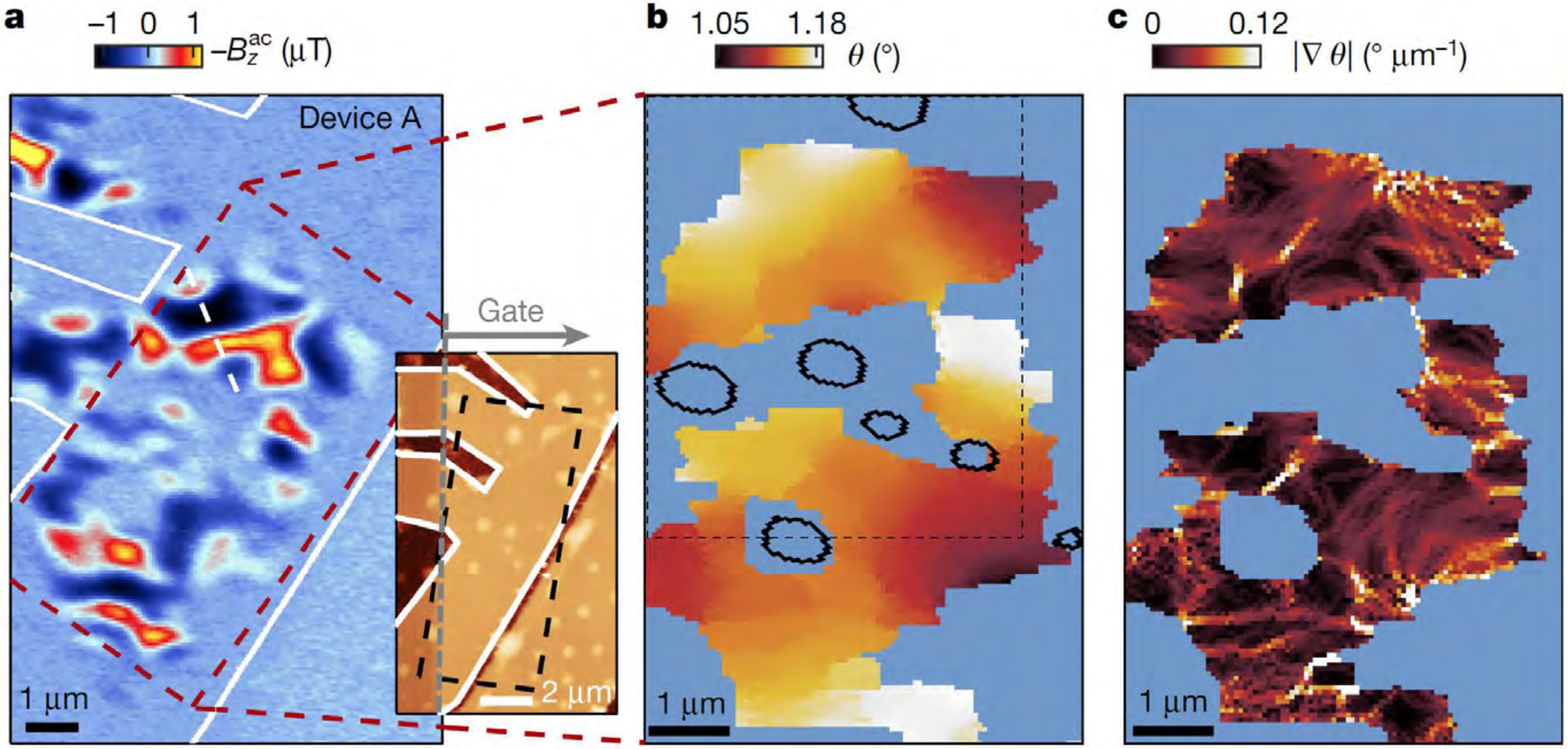

Uri et al., *Nature* **581**, 47 (2020).

Energence of 2D materials and vdW heterostructures

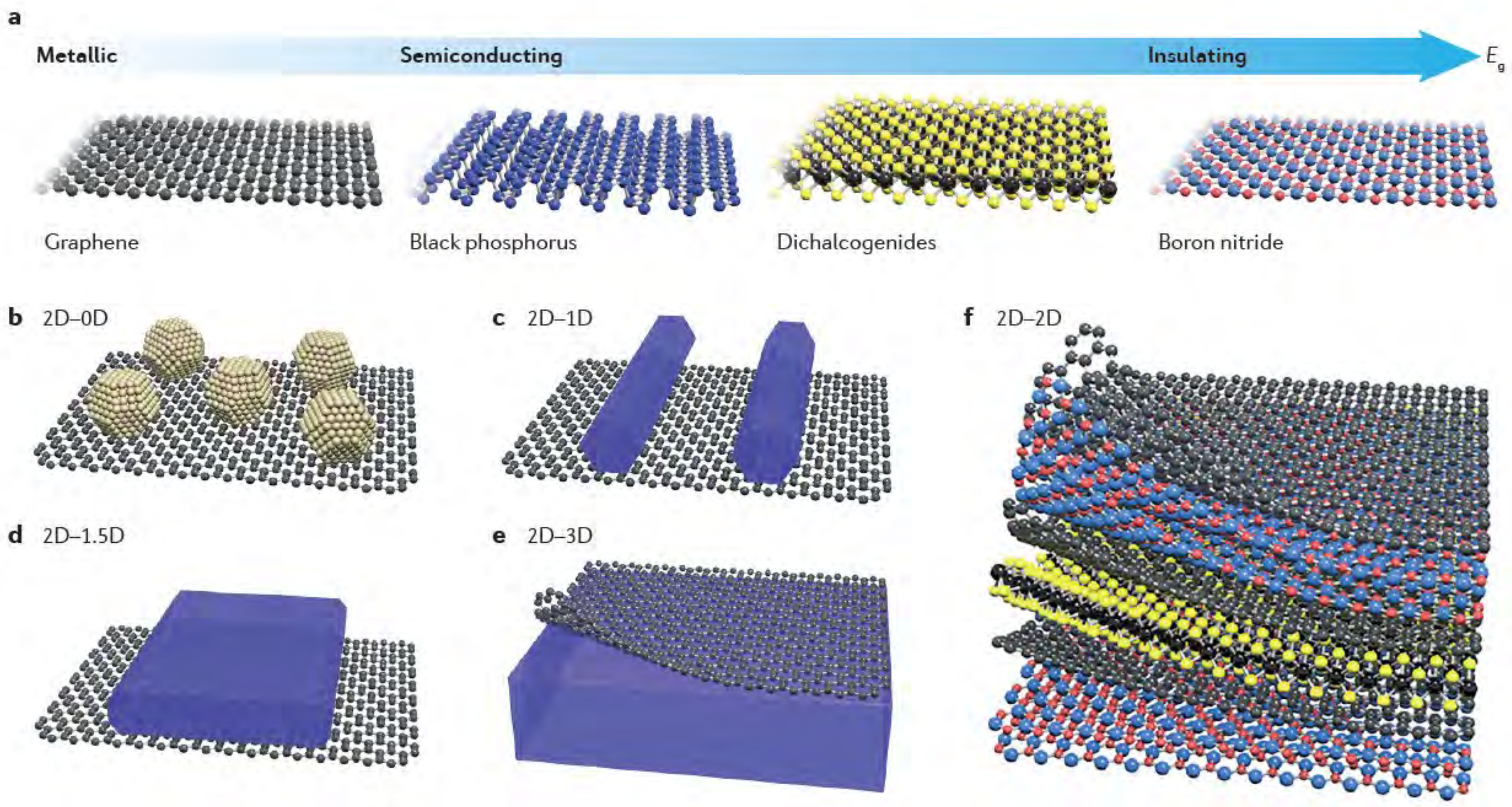

Figure 1 | **Two-dimensional layered materials and van der Waals heterostructures. a** | A broad library of two-dimensional layered materials (2DLMs) with varying chemical composition, atomic structures and electronic properties, with an increasing bandgap from left to right. **b–f** | Van der Waals heterostructures formed by integrating the dangling-bond-free 2DLMs with 0D nanoparticles or quantum dots (panel **b**), 1D nanowires (panel **c**), 1.5D nanoribbons (panel **d**), 3D bulk materials (panel **e**) and 2D nanosheets (panel **f**).

Liu et al., *Nat. Rev. Mater.* **1**, 1 (2016)

Correlated states in atomically layered materials

ARTICLE

doi:10.1038/nature26160

Unconventional superconductivity in magic-angle graphene superlattices

Yuan Cao[1], Valla Fatemi[1], Shiang Fang[2], Kenji Watanabe[3], Takashi Taniguchi[3], Efthimios Kaxiras[2,4] & Pablo Jarillo-Herrero[1]

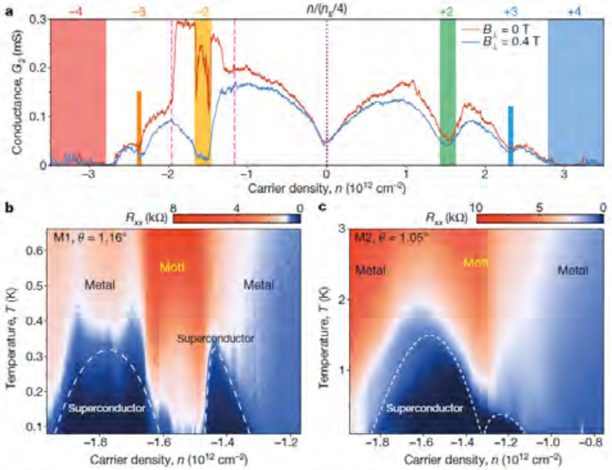

Figure 2 | Gate-tunable superconductivity in magic-angle TBG. **a**, Two-probe conductance $G_2 = I/V_{bias}$ of device M1 ($\theta = 1.16°$) measured in zero magnetic field (red) and at a perpendicular field of $B_\perp = 0.4$ T (blue). The curves exhibit the typical V-shaped conductance near charge neutrality ($n = 0$, vertical purple dotted line) and insulating states at the superlattice bandgaps $n = \pm n_s$, which correspond to filling ±4 electrons in each moiré unit cell (blue and red bars). They also exhibit reduced conductance at intermediate integer fillings of the superlattice owing to Coulomb interactions (other coloured bars). Near a filling of −2 electrons per unit cell, there is considerable conductance enhancement at zero field that is suppressed in $B_\perp = 0.4$ T. This enhancement signals the onset of superconductivity. Measurements were conducted at 70 mK; $V_{bias} = 10$ μV. **b**, Four-probe resistance R_{xx}, measured at densities corresponding to the region bounded by pink dashed lines in **a**, versus temperature. Two superconducting domes are observed next to the half-filling state, which is labelled 'Mott' and centred around $-n_s/2 = -1.58 \times 10^{12}$ cm^{-2}. The remaining regions in the diagram are labelled as 'metal' owing to the metallic temperature dependence. The highest critical temperature observed in device M1 is $T_c = 0.5$ K (at 50% of the normal-state resistance). **c**, As in **b**, but for device M2, showing two asymmetric and overlapping domes. The highest critical temperature in this device is $T_c = 1.7$ K.

LETTER

doi:10.1038/nature22391

Layer-dependent ferromagnetism in a van der Waals crystal down to the monolayer limit

Bevin Huang[1*], Genevieve Clark[2*], Efrén Navarro-Moratalla[3*], Dahlia R. Klein[3], Ran Cheng[4], Kyle L. Seyler[1], Ding Zhong[1], Emma Schmidgall[1], Michael A. McGuire[5], David H. Cobden[1], Wang Yao[6], Di Xiao[4], Pablo Jarillo-Herrero[3] & Xiaodong Xu[1,2]

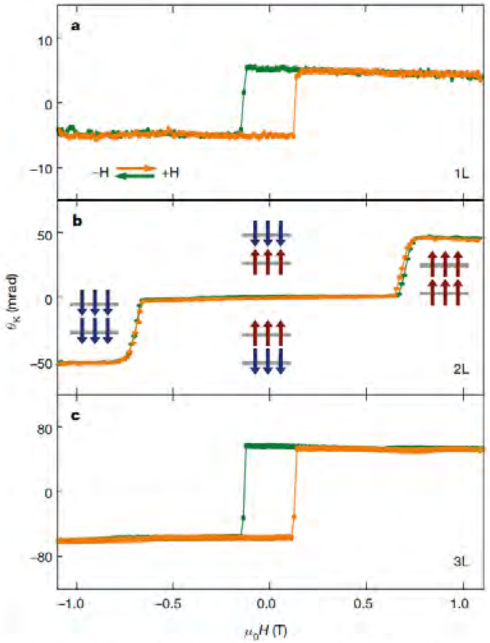

Figure 3 | Layer-dependent magnetic ordering in atomically-thin CrI_3. **a**, MOKE signal on a monolayer (1L) CrI_3 flake, showing hysteresis in the Kerr rotation as a function of applied magnetic field, indicative of ferromagnetic behaviour. **b**, MOKE signal from a bilayer CrI_3 showing vanishing Kerr rotation for applied fields ±0.65 T, suggesting antiferromagnetic behaviour. Insets depict bilayer (2L) magnetic ground states for different applied fields. **c**, MOKE signal on a trilayer (3L) flake, showing a return to ferromagnetic behaviour.

Contrast

Current density $\vec{J}$

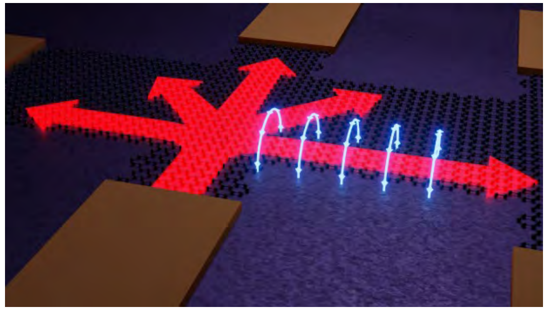

Magnetization $\vec{M}$

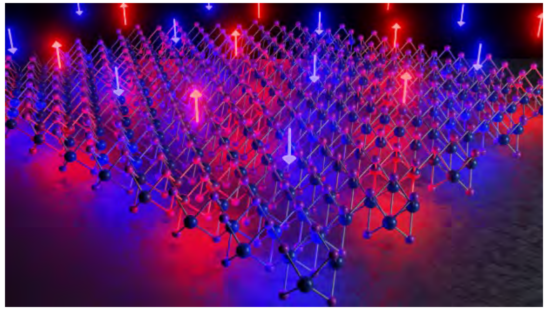

Techniques

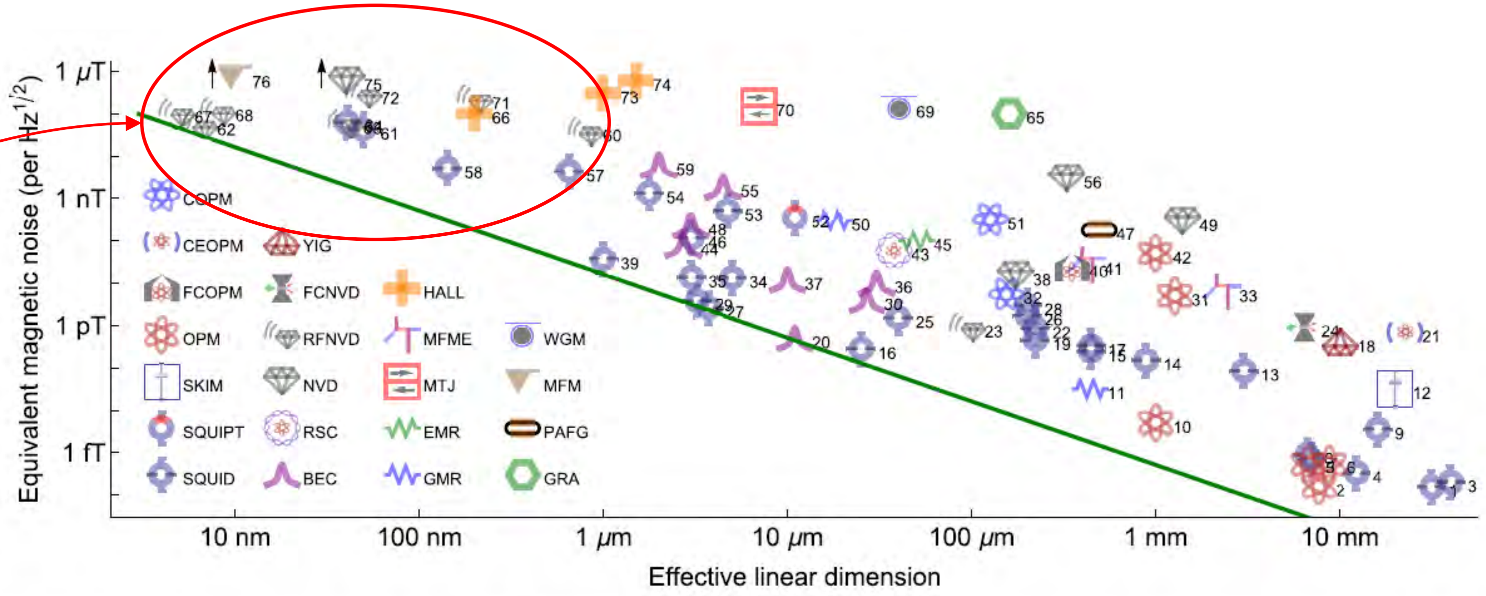

FIG. 2. Reported magnetic sensitivity $\delta B\sqrt{T}$ for different sensor technologies versus size of the sensitive region. Effective linear dimension $l_{\rm eff}$ indicates $\sqrt{\rm area}$ for planar sensors and $\sqrt[3]{\rm volume}$ for volumetric ones. For pointlike systems such as single spins, $l_{\rm eff}$ indicates $\sqrt[3]{\rm volume}$ for a sphere with radius equal to the minimum source-detector distance. For work reporting sensitivity in units of magnetic dipole moment, we convert to field units using the reported sample distance. Excepting RFNVD, noise levels are the lowest reported value at frequency ≤ 1 kHz. An arrow indicates that the value is off the scale. SQUID, superconducting quantum interference device; SQUIPT, superconducting quantum interference proximity transistor; SKIM, superconducting kinetic impedance magnetometer; OPM, optically pumped magnetometer; FCOPM, OPM with flux concentrators; CEOPM, cavity-enhanced OPM; COPM, OPM with cold thermal atoms; BEC, Bose-Einstein condensate; RSC, Rydberg Schrödinger cat; NVD, nitrogen-vacancy center in diamond; RFNVD, radio-frequency NVD; FCNVD, NVD with flux concentrators; YIG, yttrium-aluminum-garnet; GMR, giant magnetoresistance; EMR, extraordinary magnetoresistance; MTJ, magnetic tunnel junction; MEMF, magnetoelectric multiferroic; HALL, Hall-effect sensor; GRA, graphene; PAFG, parallel gating fluxgate; MFM, magnetic force microscope, WGM, whispering-gallery mode magnetostrictive. Line shows $E_R \equiv \langle \delta B^2 \rangle T l_{\rm eff}^3/(2\mu_0) = \hbar$. Numeric labels refer to Table I.

Map weak magnetic field patterns with high spatial resolution

Mitchell & Palacios Alvarez, *Rev. Mod. Phys.* **92**, 021001 (2020)

Contrast & Techniques

Current density $\vec{J}$

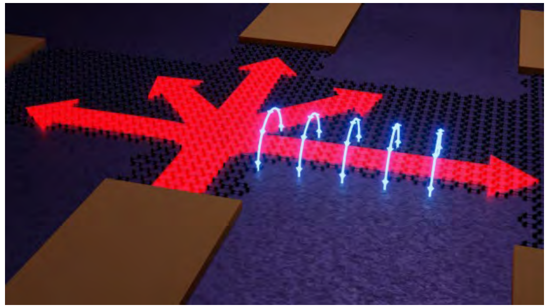

Magnetization $\vec{M}$

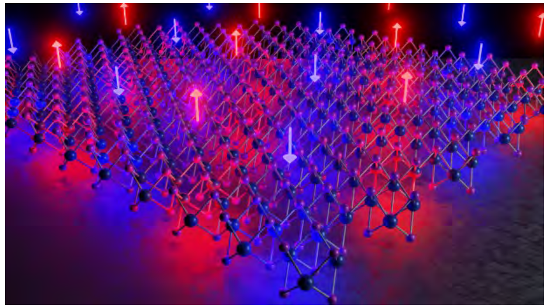

Magnetic field $\vec{B}$

SSM

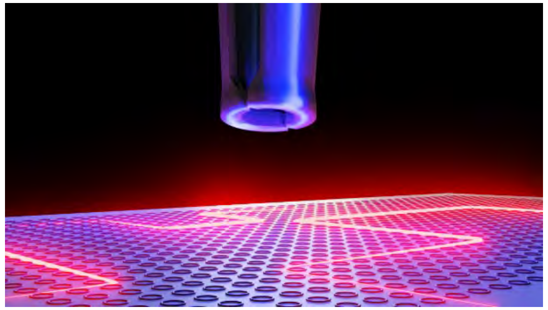

Magnetic flux Φ_z

MFM

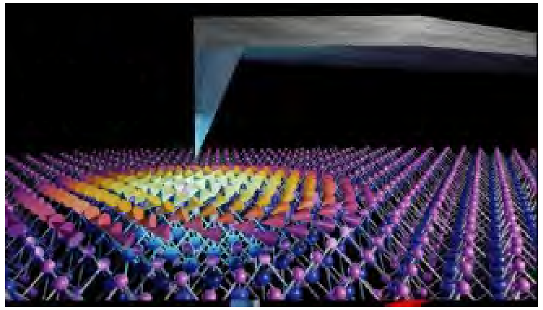

Magnetic field derivative $\frac{\partial B_z}{\partial z}$

SNVM

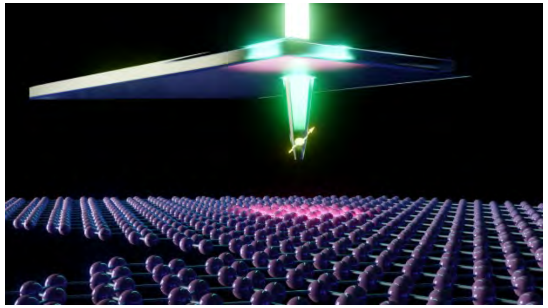

Magnetic field component B_z

TECHNICAL REVIEWS

Check for updates

Nanoscale magnetic field imaging for 2D materials

Estefani Marchiori[1], Lorenzo Ceccarelli[1], Nicola Rossi[1], Luca Lorenzelli[2], Christian L. Degen[2] and Martino Poggio[1,3]✉

Abstract | Nanoscale magnetic imaging can provide microscopic information about length scales, inhomogeneity and interactions of materials systems. As such, it is a powerful tool to probe phenomena such as superconductivity, Mott insulating states and magnetically ordered states in 2D materials, which are sensitive to the local environment. This Technical Review provides an analysis of weak magnetic field imaging techniques that are most promising for the study of 2D materials: magnetic force microscopy, scanning superconducting quantum interference device microscopy and scanning nitrogen-vacancy centre microscopy.

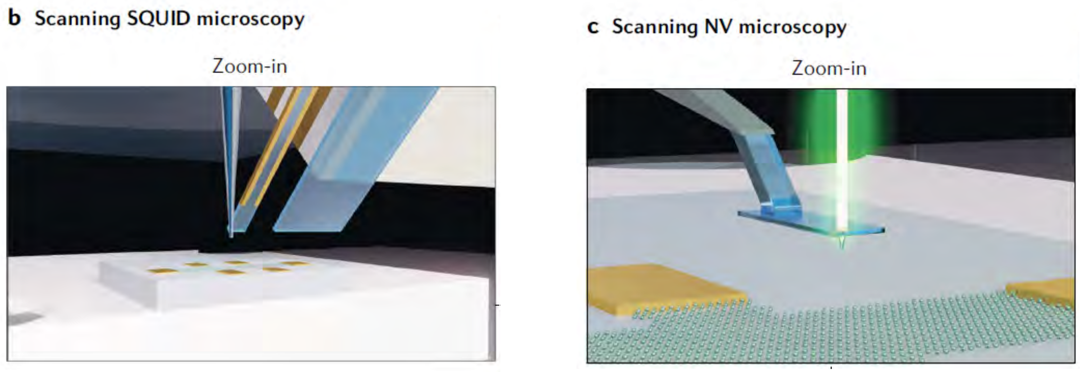

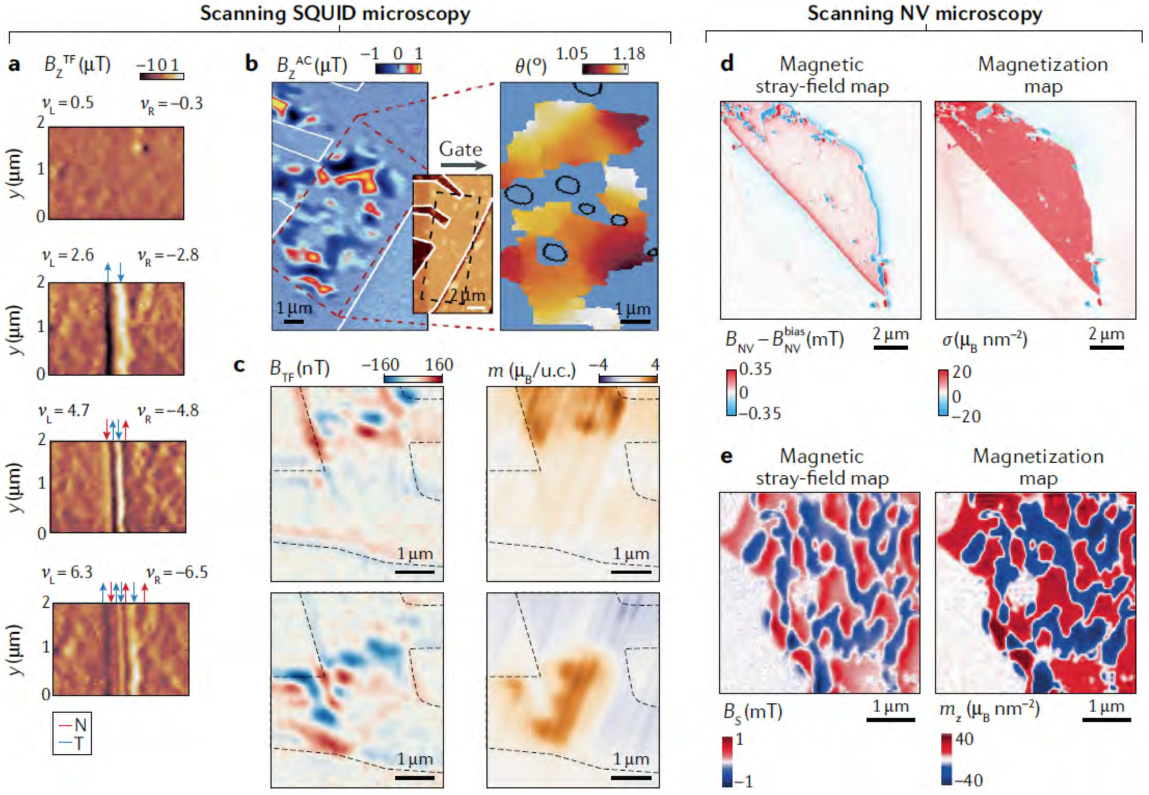

Outline

- Introduction
- Scanning SQUID microscopy (SSM)
  - Imaging the surface of Cu_2OSeO_3 with a SQUID-on-tip probe
  - Imaging 2D $Cr_2Ge_2Te_6$ with a SQUID-on-lever probe
- Nanowire-based magnetic force microscopy (MFM)
  - Imaging magnetic phase transition in 2D $EuGe_2$

Superconducting quantum interference device (SQUID)

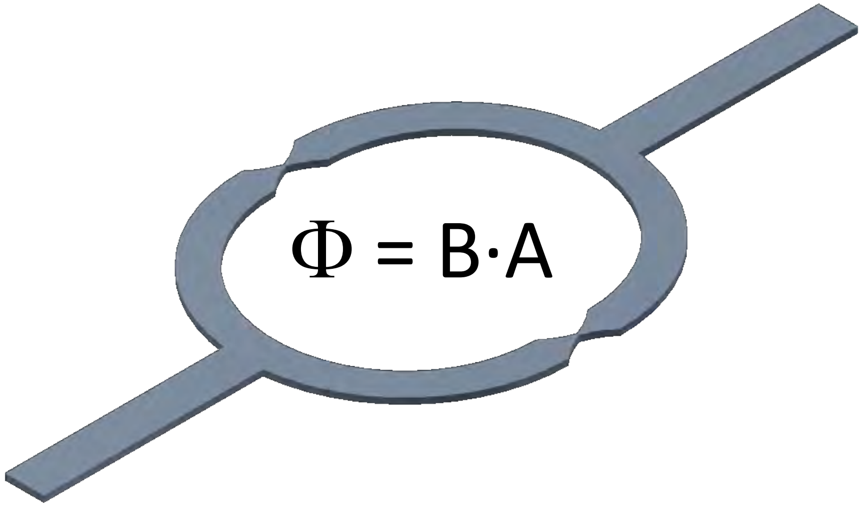

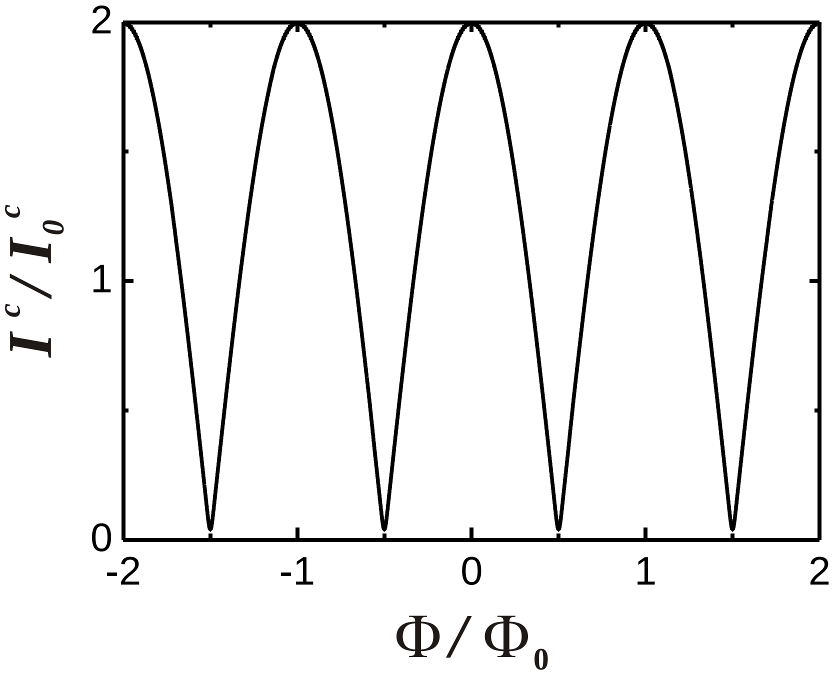

SQUID critical current: $I^{c}(\Phi) = 2I_0^{C}\cos|\square\ /\Phi_0|$

SCANNING SQUID MICROSCOPY

John R. Kirtley
IBM T. J. Watson Research Center, Yorktown Heights, New York 10598;
e-mail: kirtley@watson.ibm.com

John P. Wikswo, Jr.
Department of Physics and Astronomy, Vanderbilt University, Nashville,
Tennessee 37235; e-mail: wikswojp@ctrvax.vanderbilt.edu

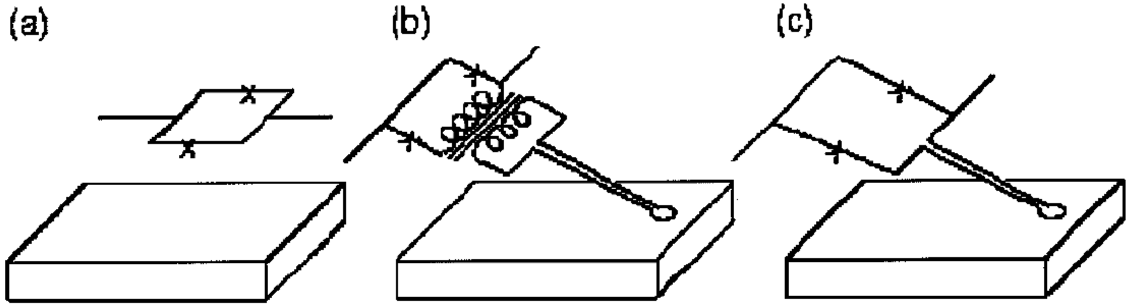

Annu. Rev. Mater. Sci. 1999. 29:117–48

Self-Aligned Nanoscale SQUID on a Tip

Amit Finkler,[*,†] Yehonathan Segev,[†] Yuri Myasoedov,[†] Michael L. Rappaport,[†] Lior Ne'eman,[†] Denis Vasyukov,[†] Eli Zeldov,[†] Martin E. Huber,[‡] Jens Martin,[§] and Amir Yacoby[§]

[†]Department of Condensed Matter Physics, Weizmann Institute of Science, Rehovot 76100, Israel, [‡]Departments of Physics and Electrical Engineering, University of Colorado, Denver, Colorado 80217, and [§]Department of Physics, Harvard University, Cambridge, Massachusetts 02138

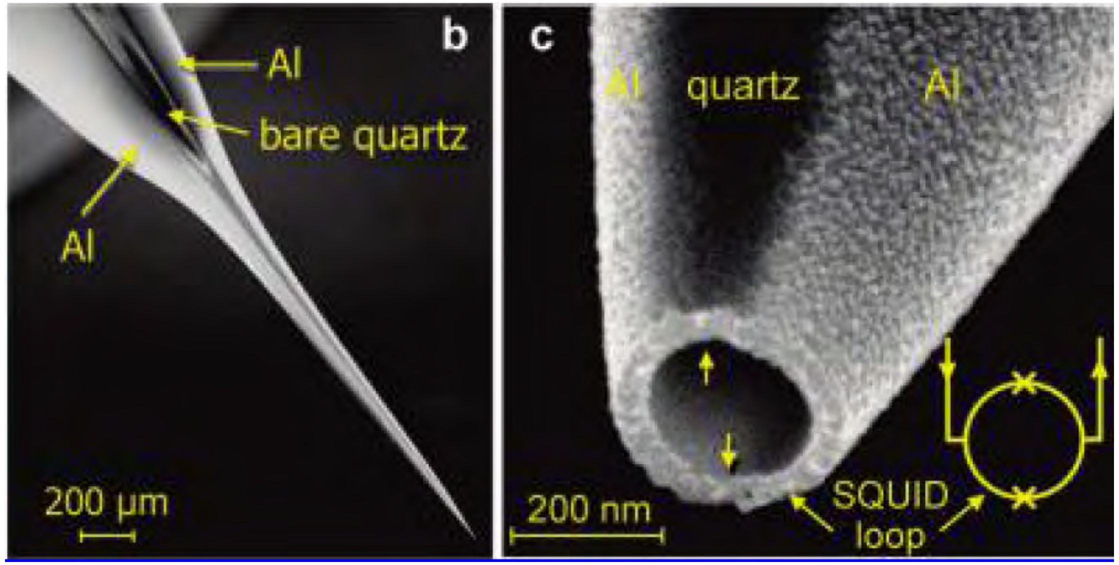

Nano Lett. **2010,** *10,* 1046–1049

SQUID-on-tip sensor

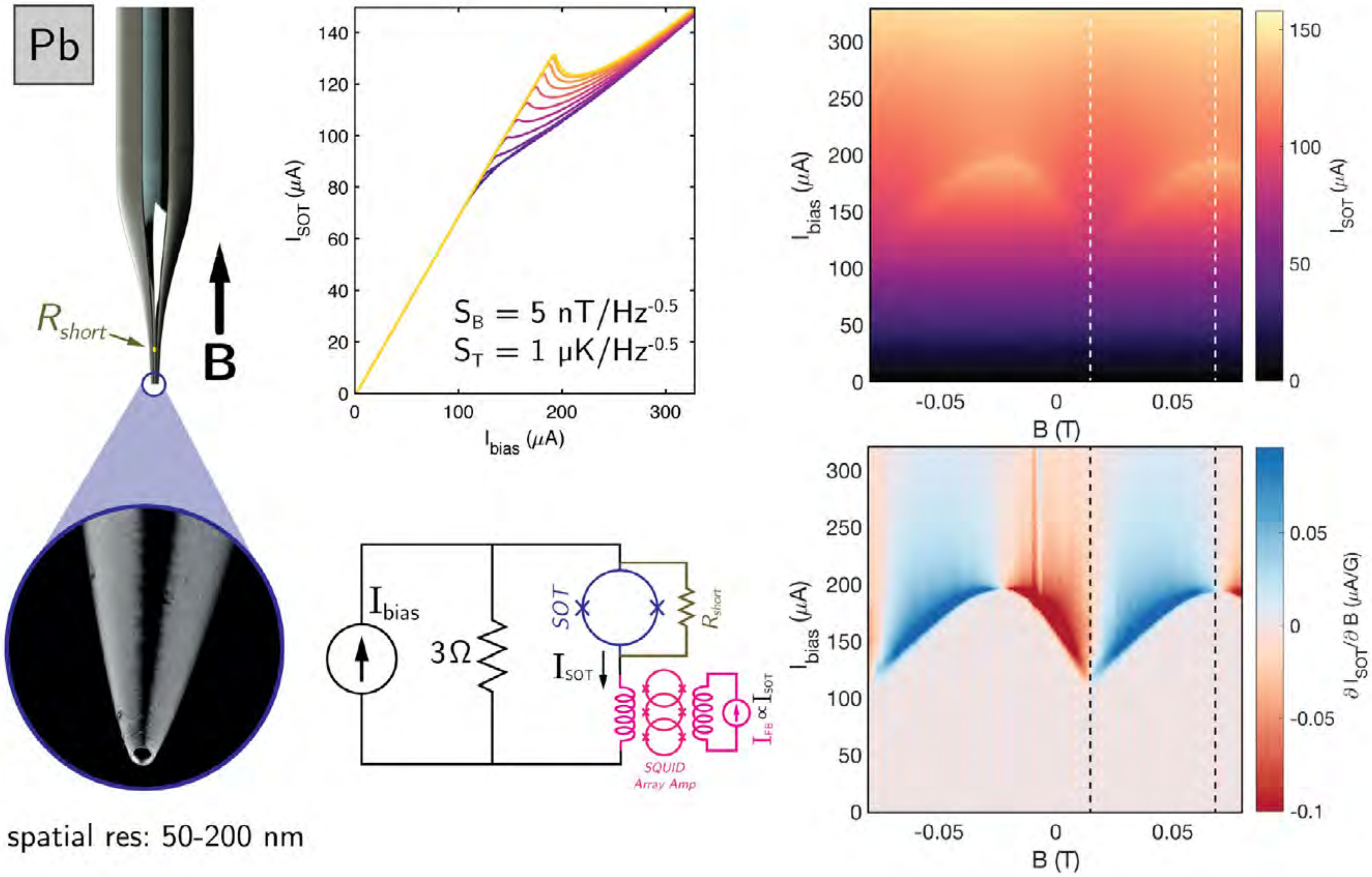

Vasyukov et al., *Nat. Nanotechnol.* **8**, 639 (2013)

Nanometer-scale scanning SQUID microscopy

Imaging current density in superconducting qubit devices from Wallraff group (ETHZ).

Scanning SQUID microscope

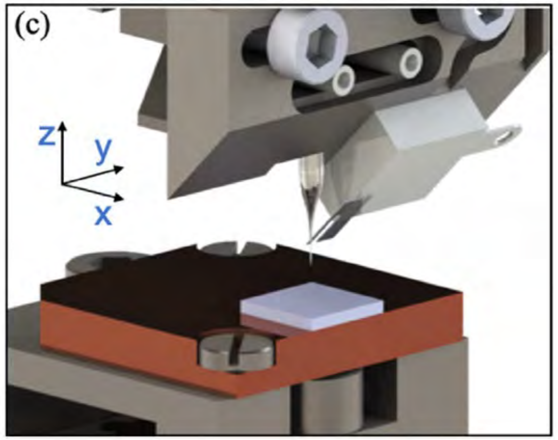

SSM using a SQUID-on-tip probe operating in at 4.2 K.

Superconducting device

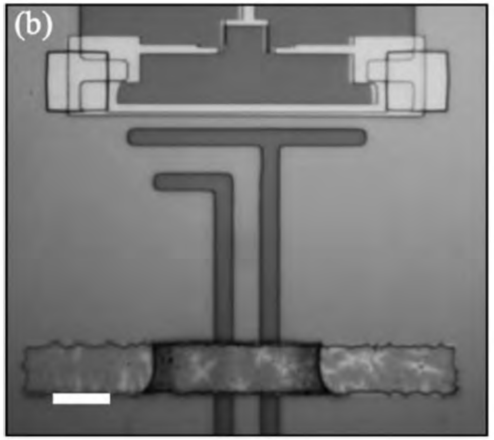

Transmon qubit with flux-control line coming from the bottom (scale bar 10 μm).

Marchiori et al., *Appl. Phys. Lett.* **121**, 052601 (2022)

Imaging magnetic configurations at the surface of bulk Cu_2OSeO_3

Dr. Estefani Marchiori

Post-doctoral Researcher

Giulio Romagnoli

Post-doctoral Researcher

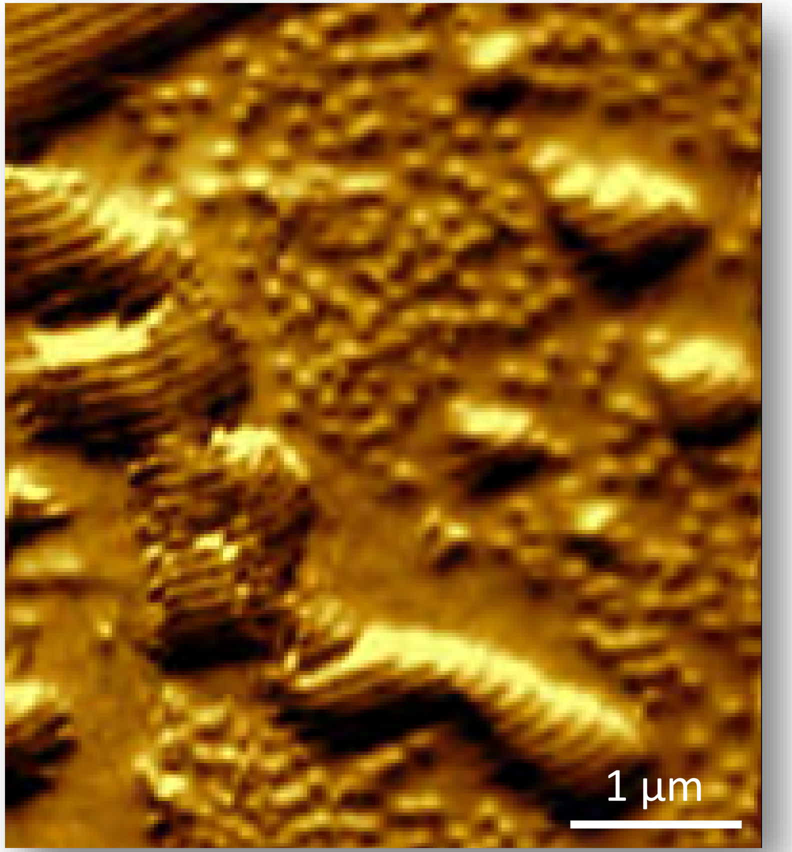

<u>Samples:</u>

Prijaranjan Baral

Arnaud Magrez

EPFL

Cu_2OSeO_3 – Chiral Magnet

- Characteristics:
  - **Insulating** skyrmion-hosting material
  - **Chiral** magnet of the **B20-type** (MnSi, $Mn_{1-x}Co_xSi$, MnGe, FeGe, …)
  - **Cubic** crystal symmetry

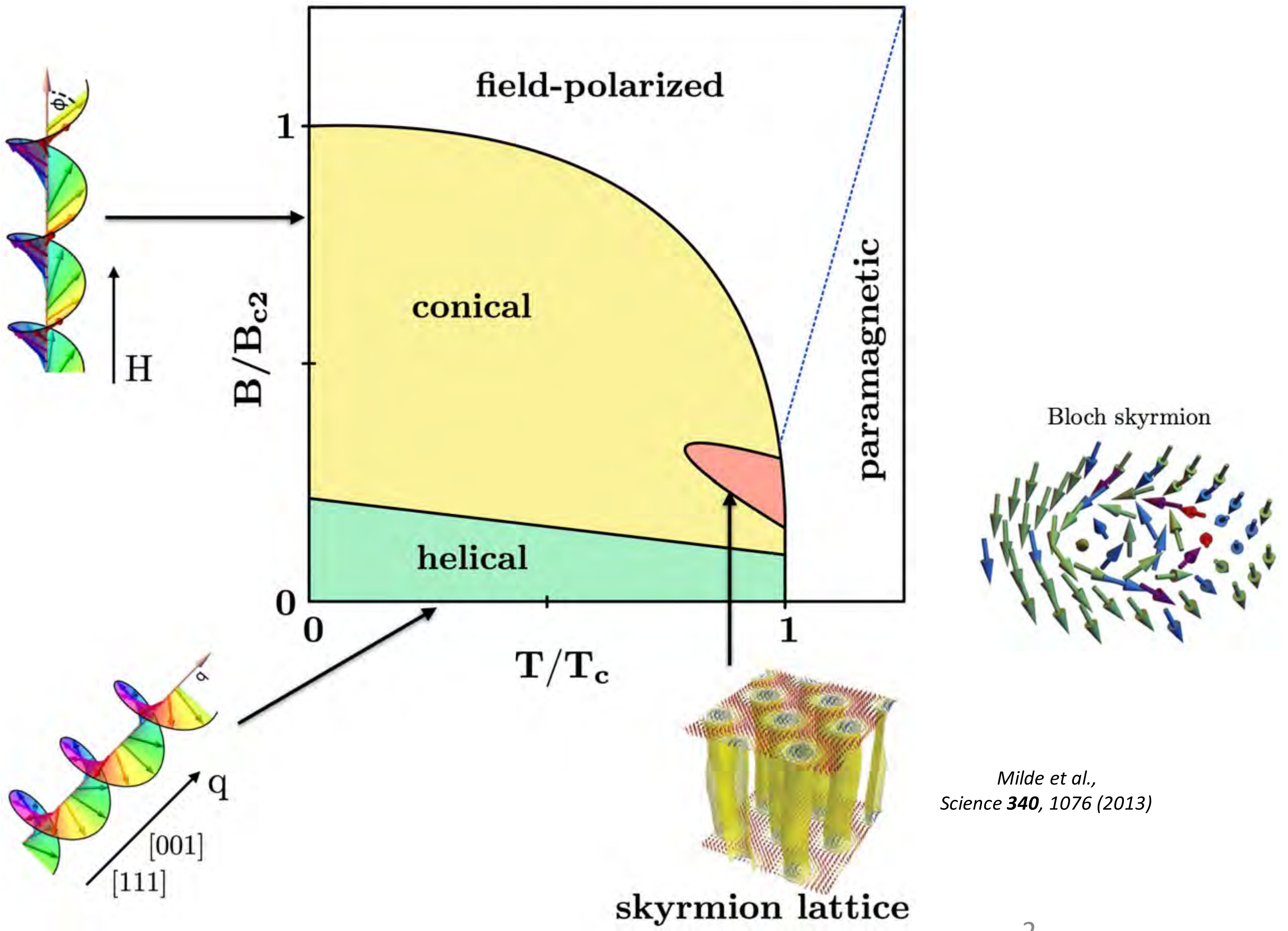

*Masell et al., Phys. Rev. B **102**, 180402 (2020)*

*Milde et al., Science **340**, 1076 (2013)*

Sample & scanning SQUID

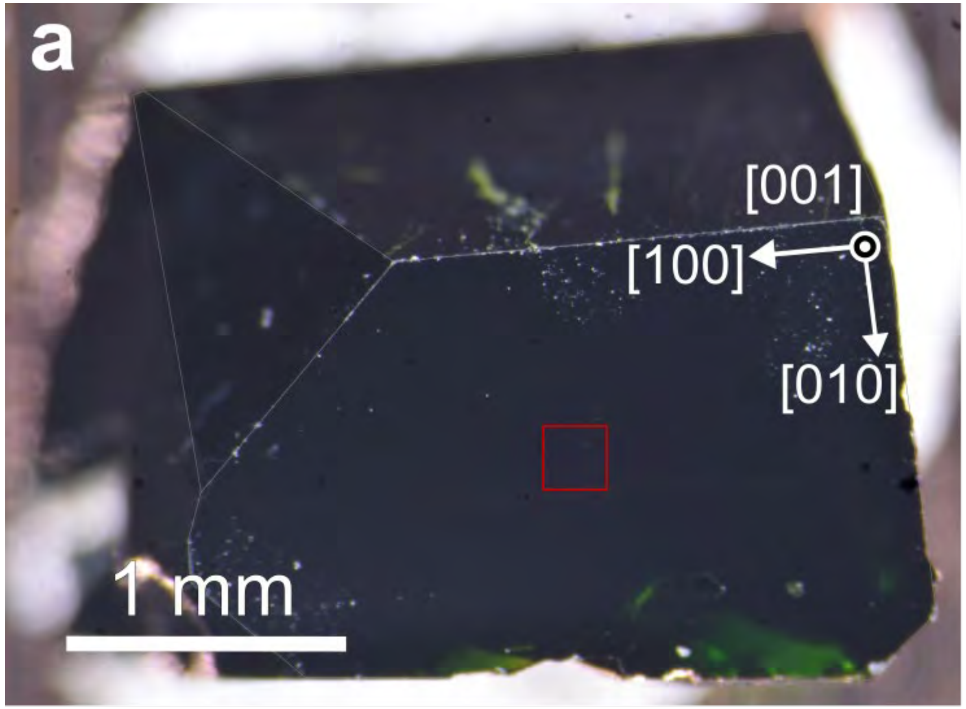

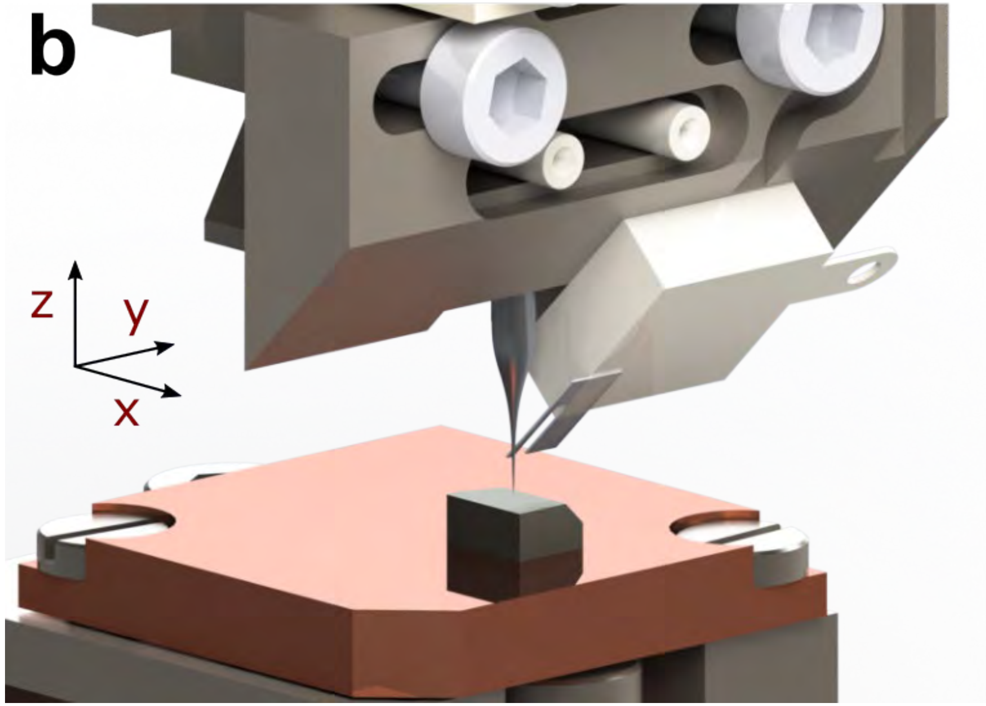

Cu_2OSeO_3 – Field decrease study

University of Basel

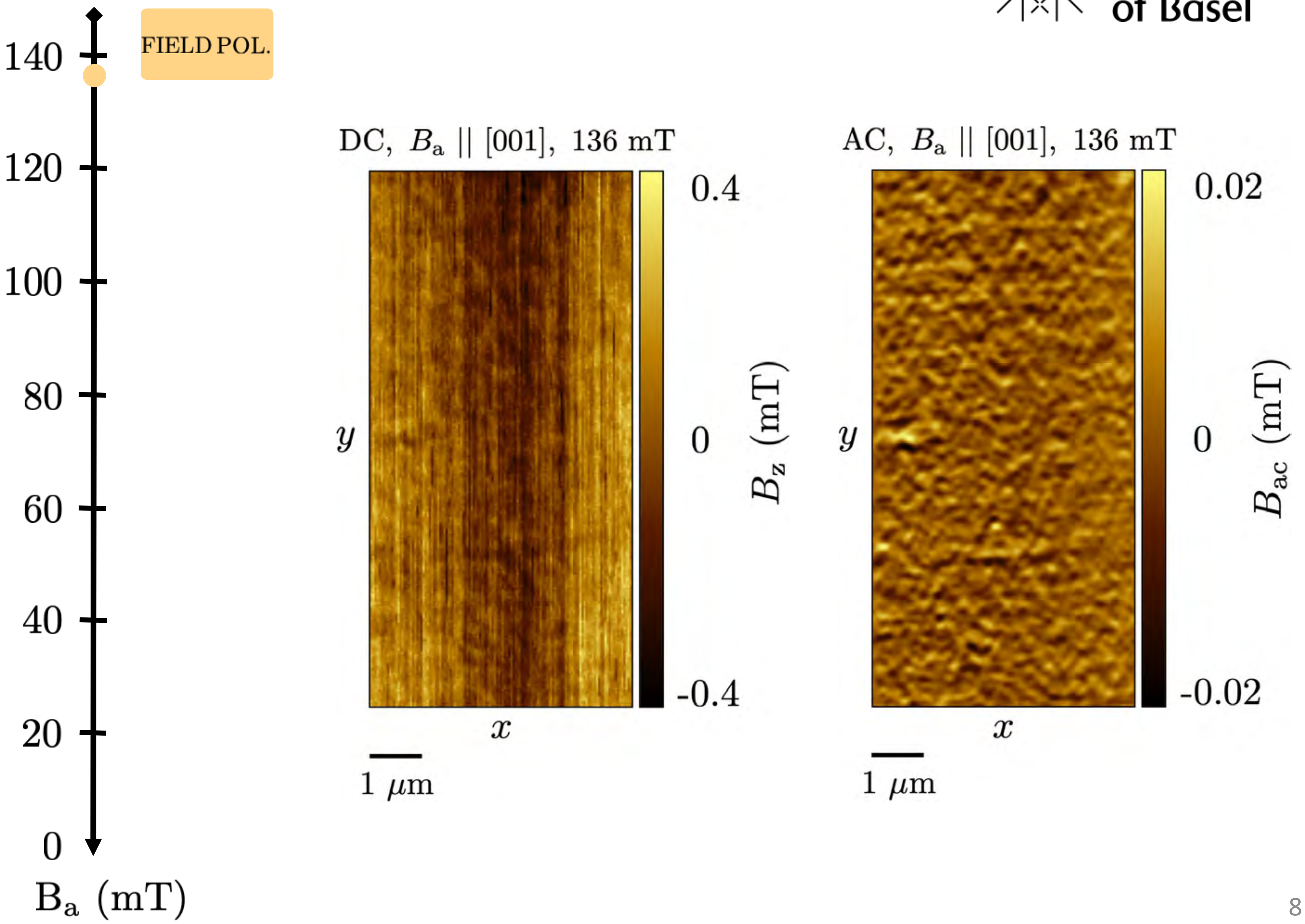

Cu_2OSeO_3 – Field decrease study

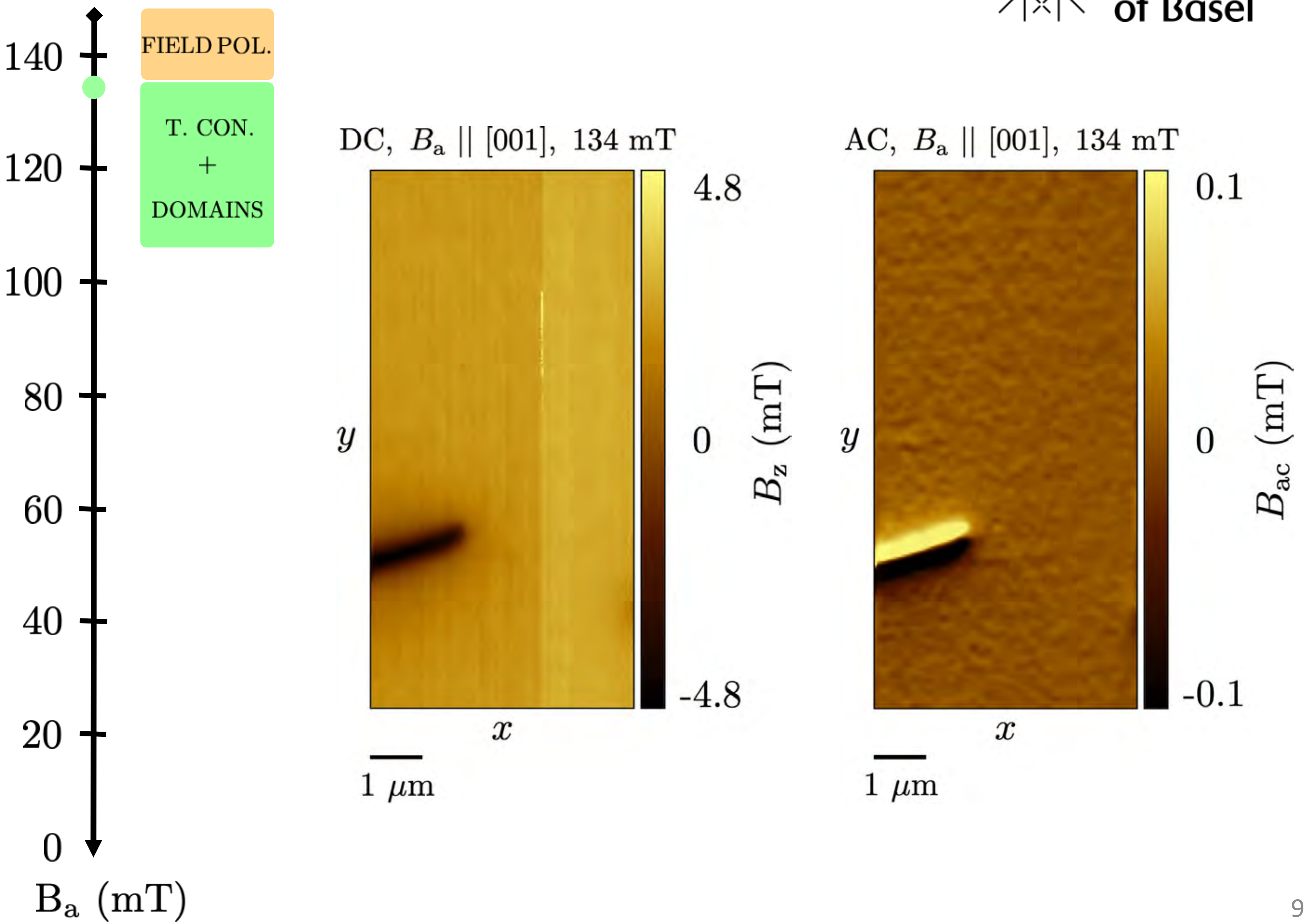

Cu_2OSeO_3 – Field decrease study

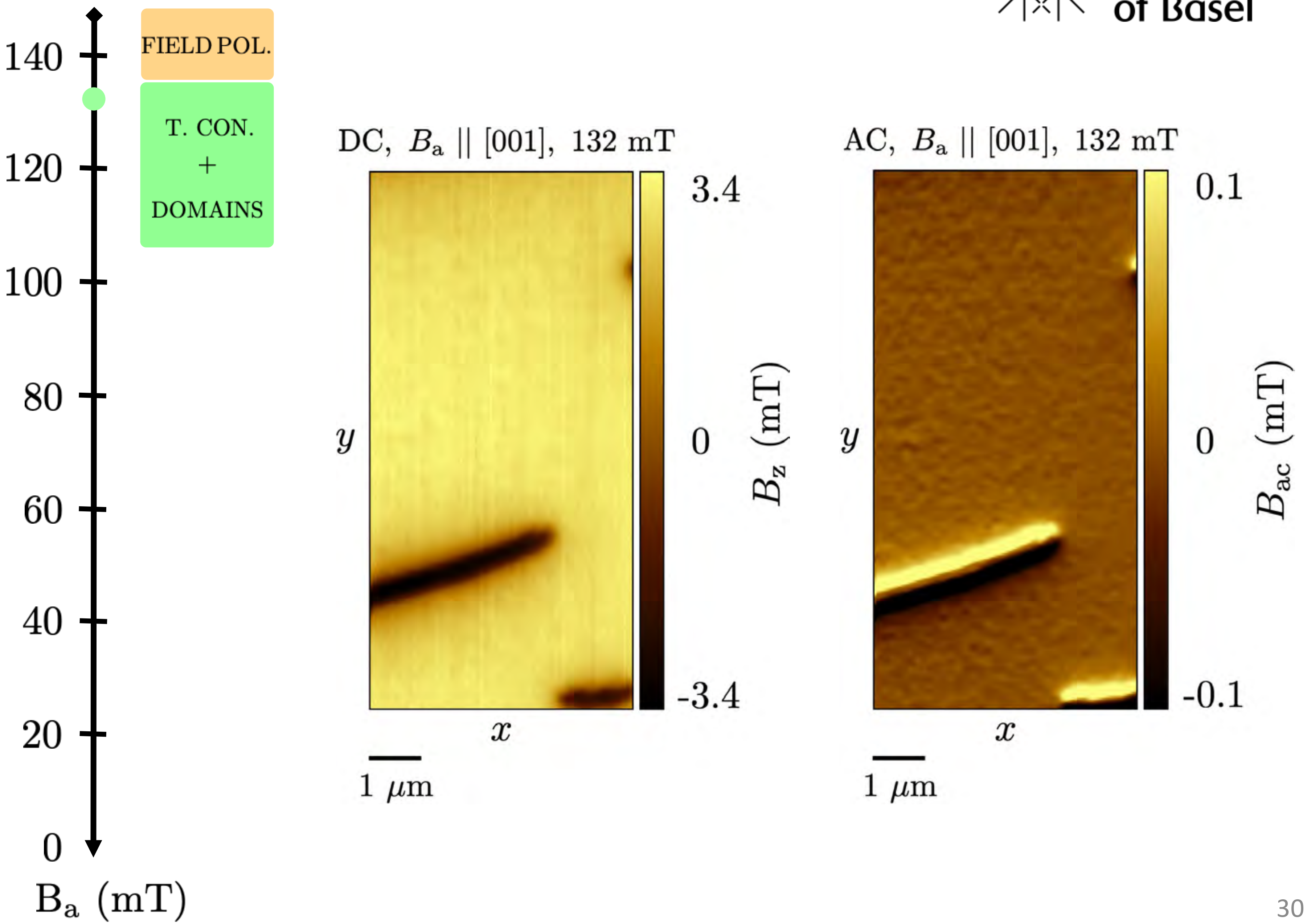

Cu_2OSeO_3 – Field decrease study

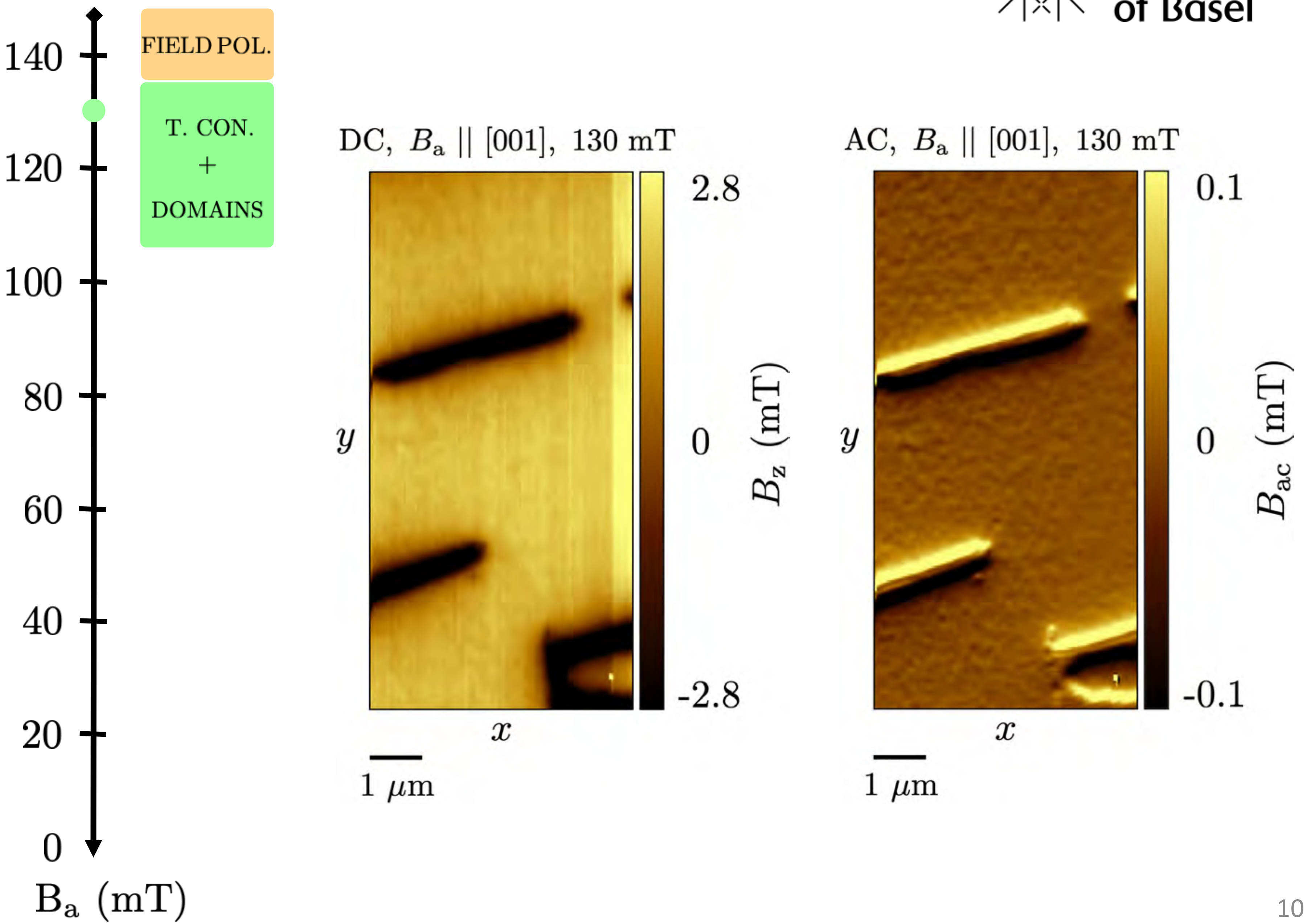

Cu_2OSeO_3 – Field decrease study

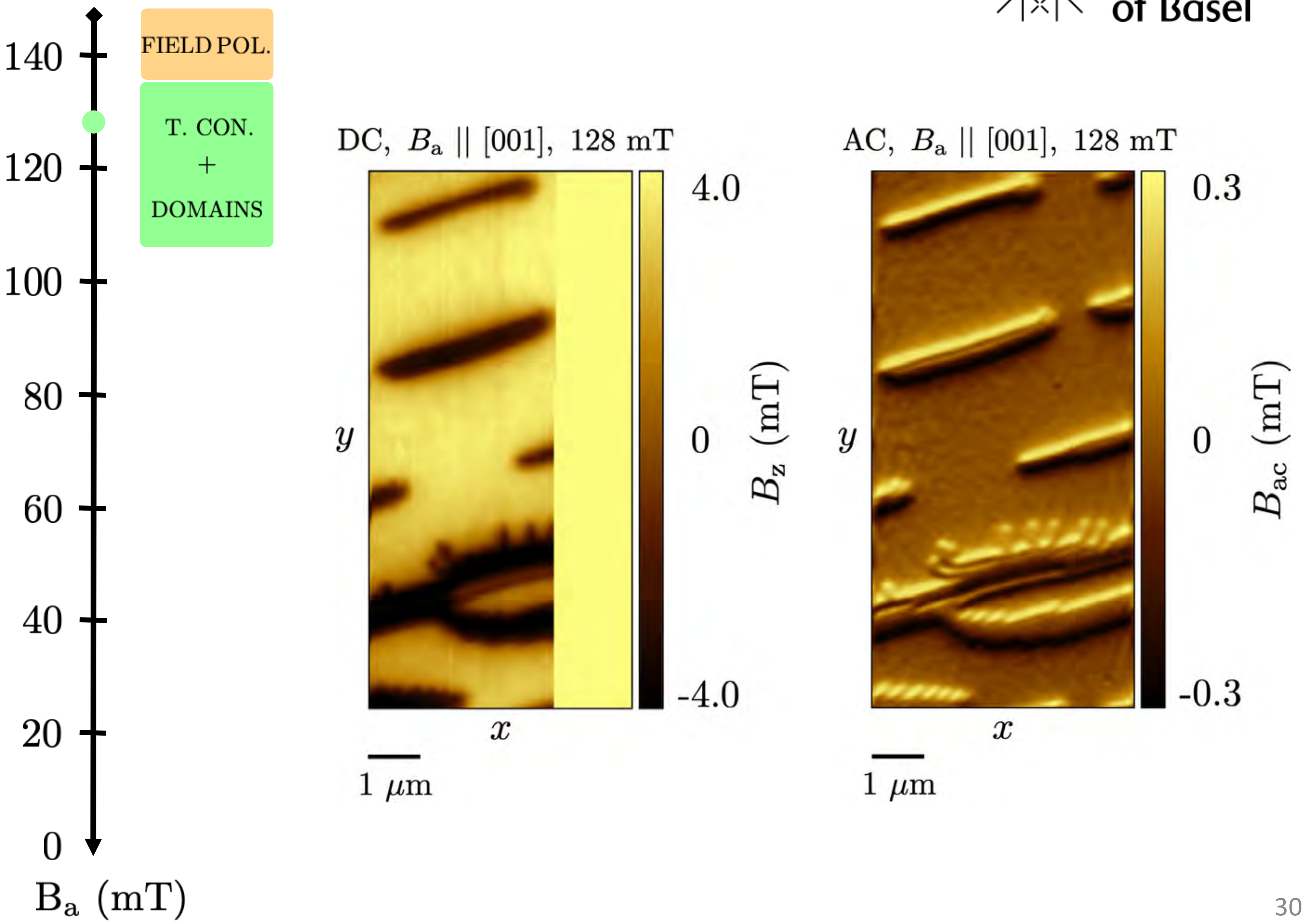

Cu_2OSeO_3 – Field decrease study

University of Basel

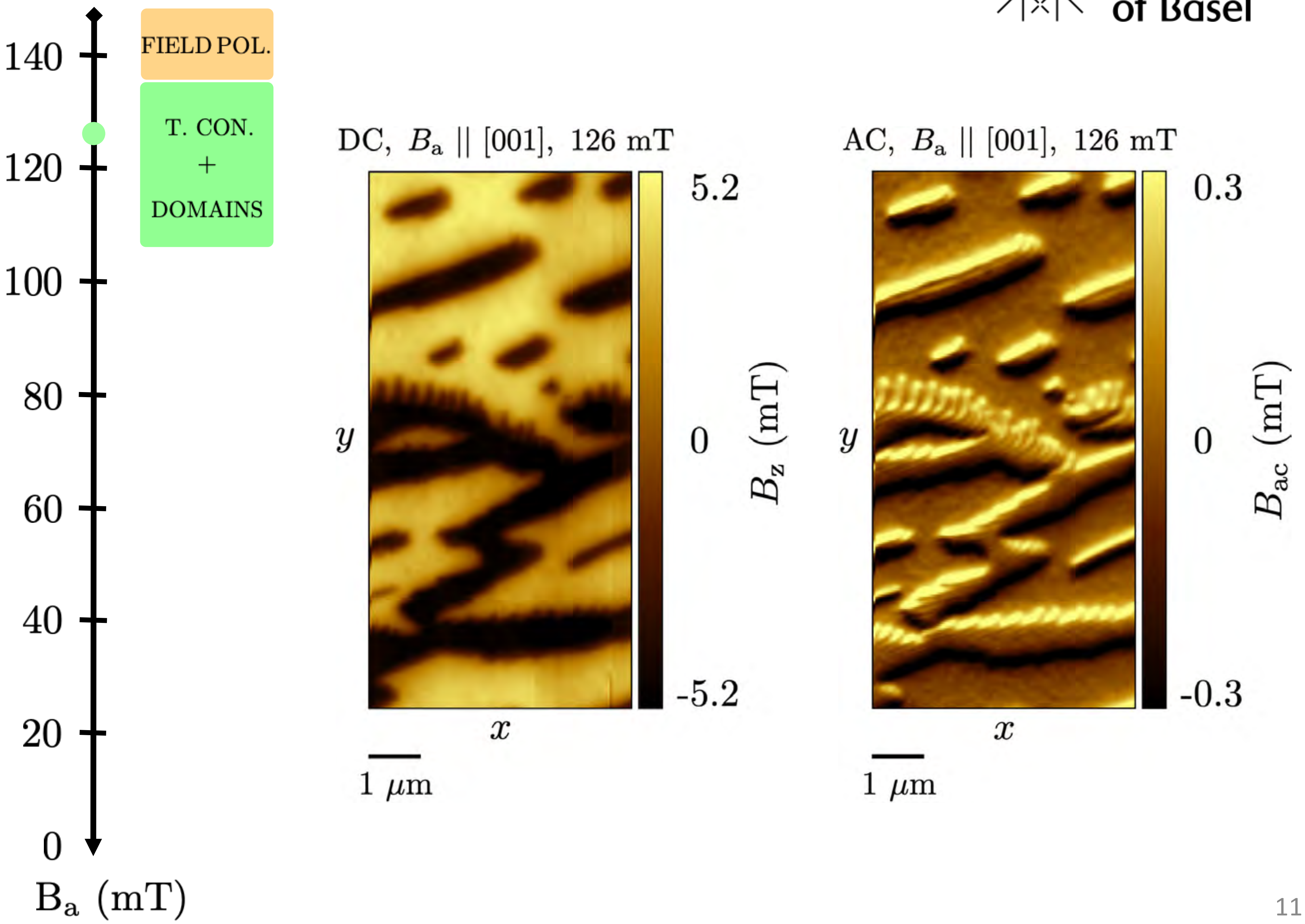

Cu_2OSeO_3 – Field decrease study

University of Basel

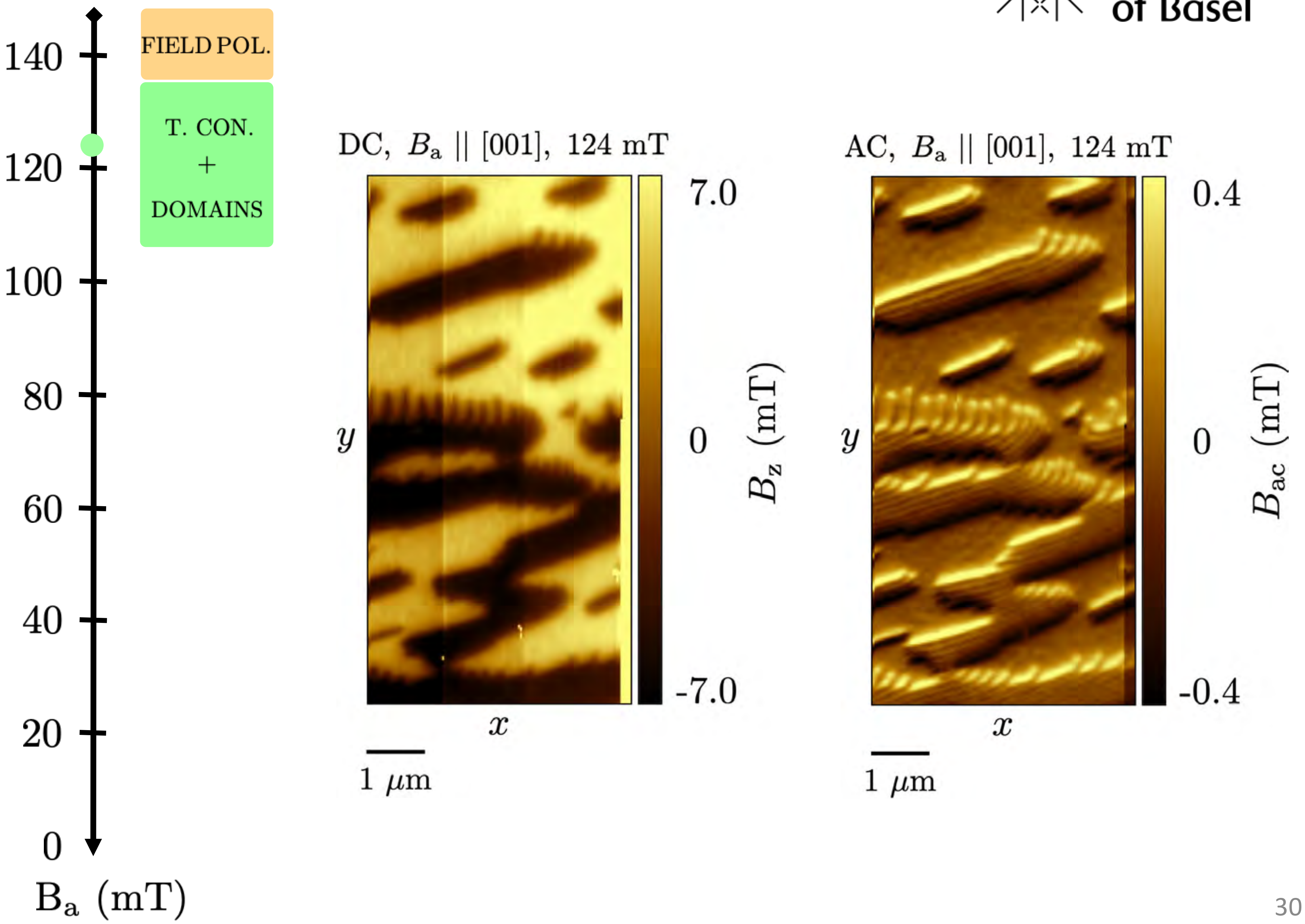

Cu_2OSeO_3 – Field decrease study

University of Basel

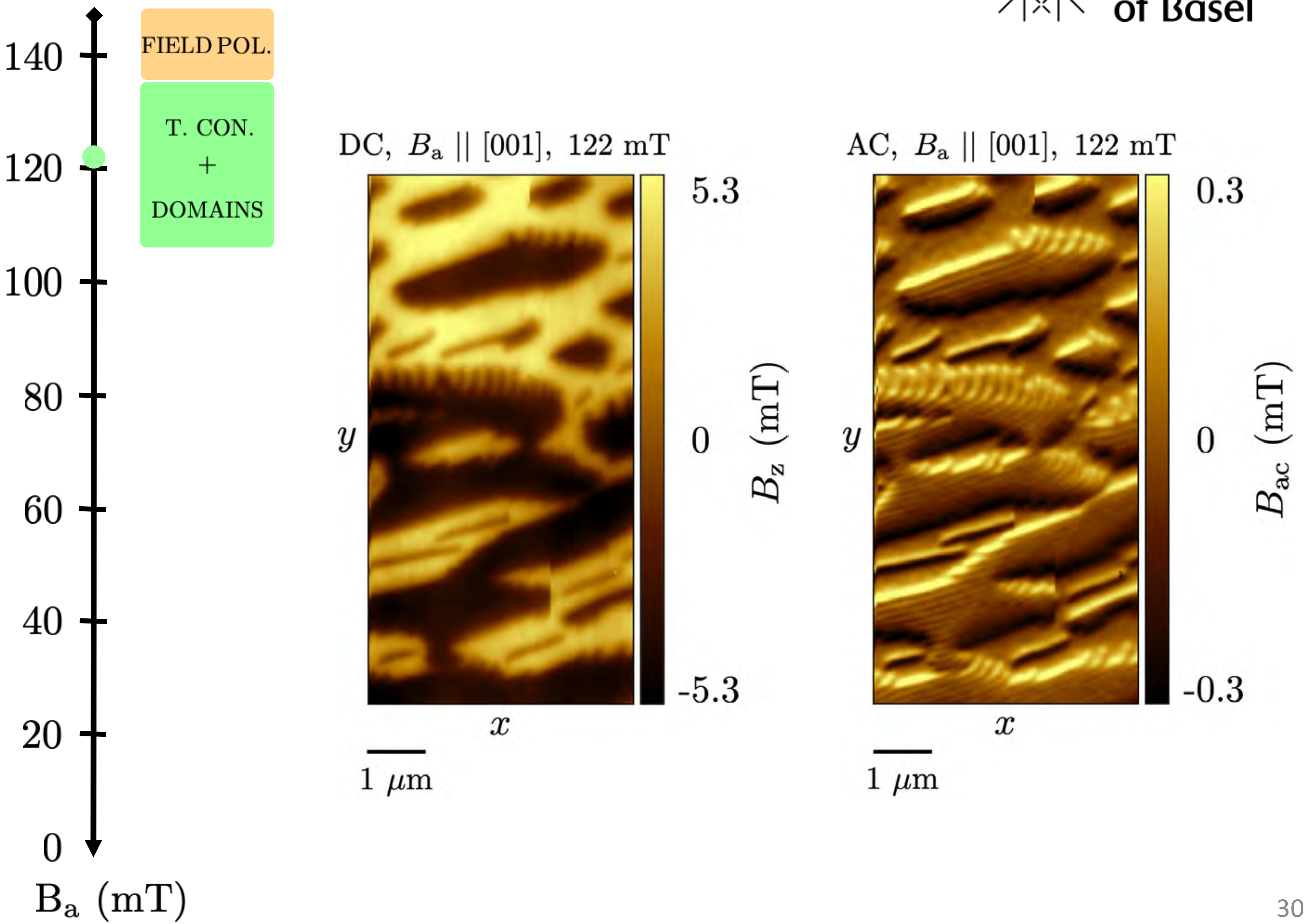

Cu_2OSeO_3 – Field decrease study

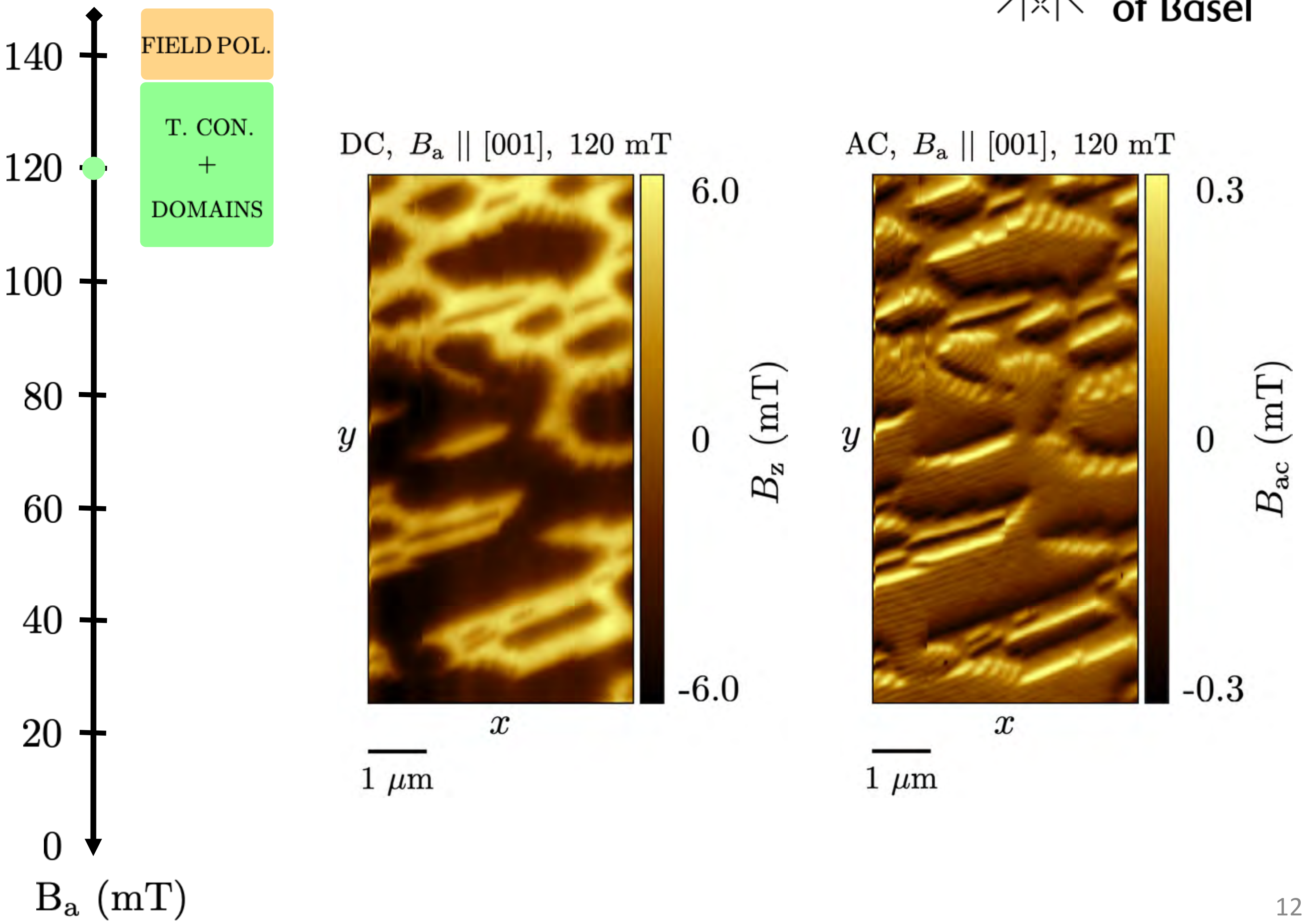

Cu_2OSeO_3 – Field decrease study

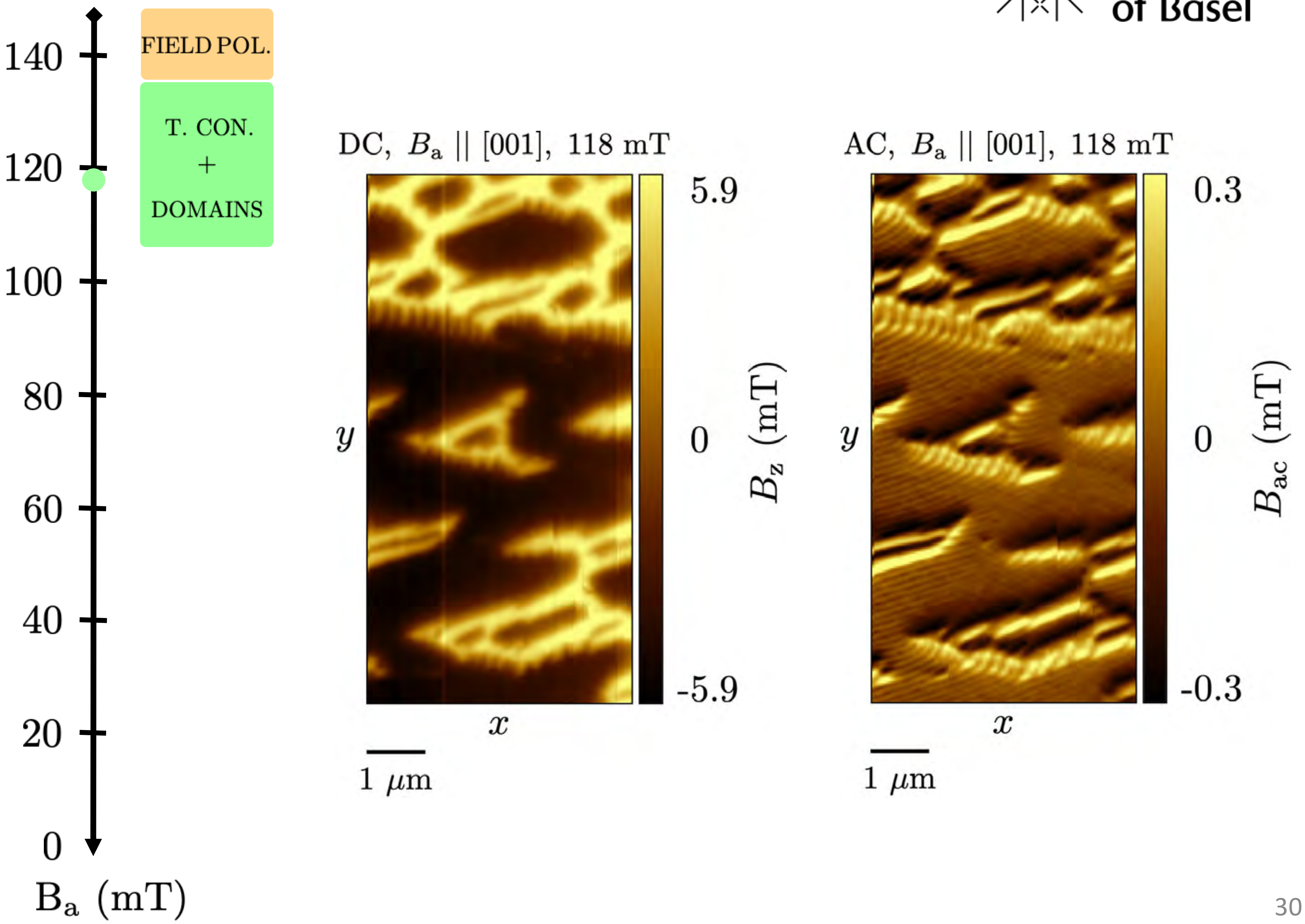

Cu_2OSeO_3 – Field decrease study

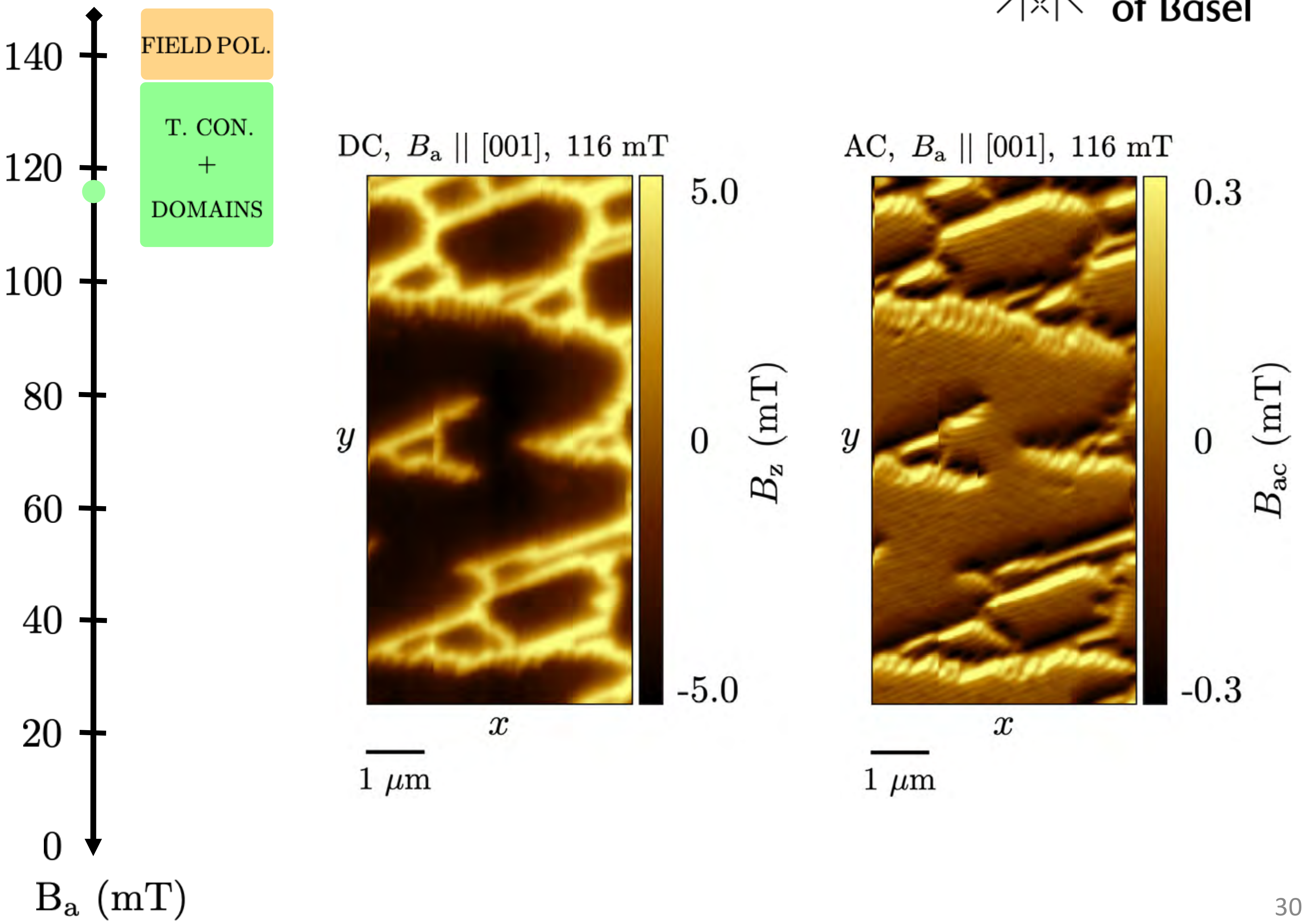

Cu_2OSeO_3 – Field decrease study

University of Basel

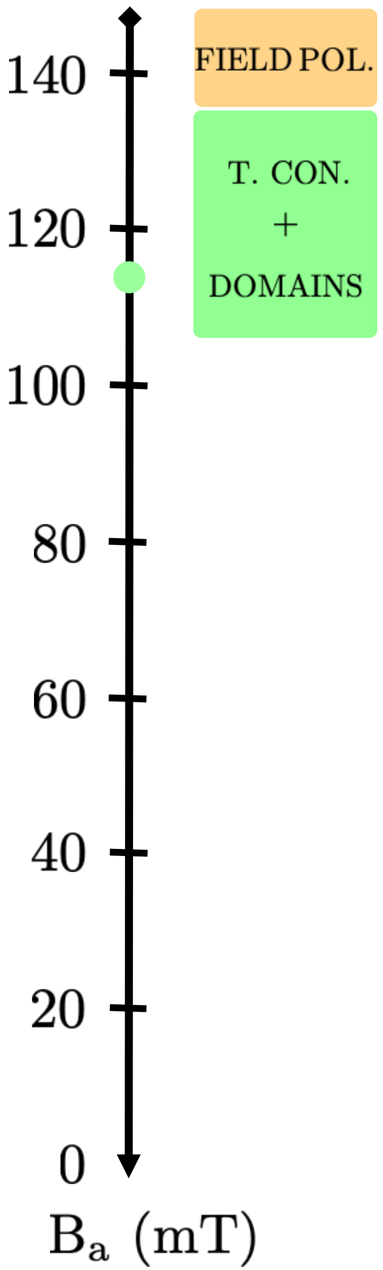

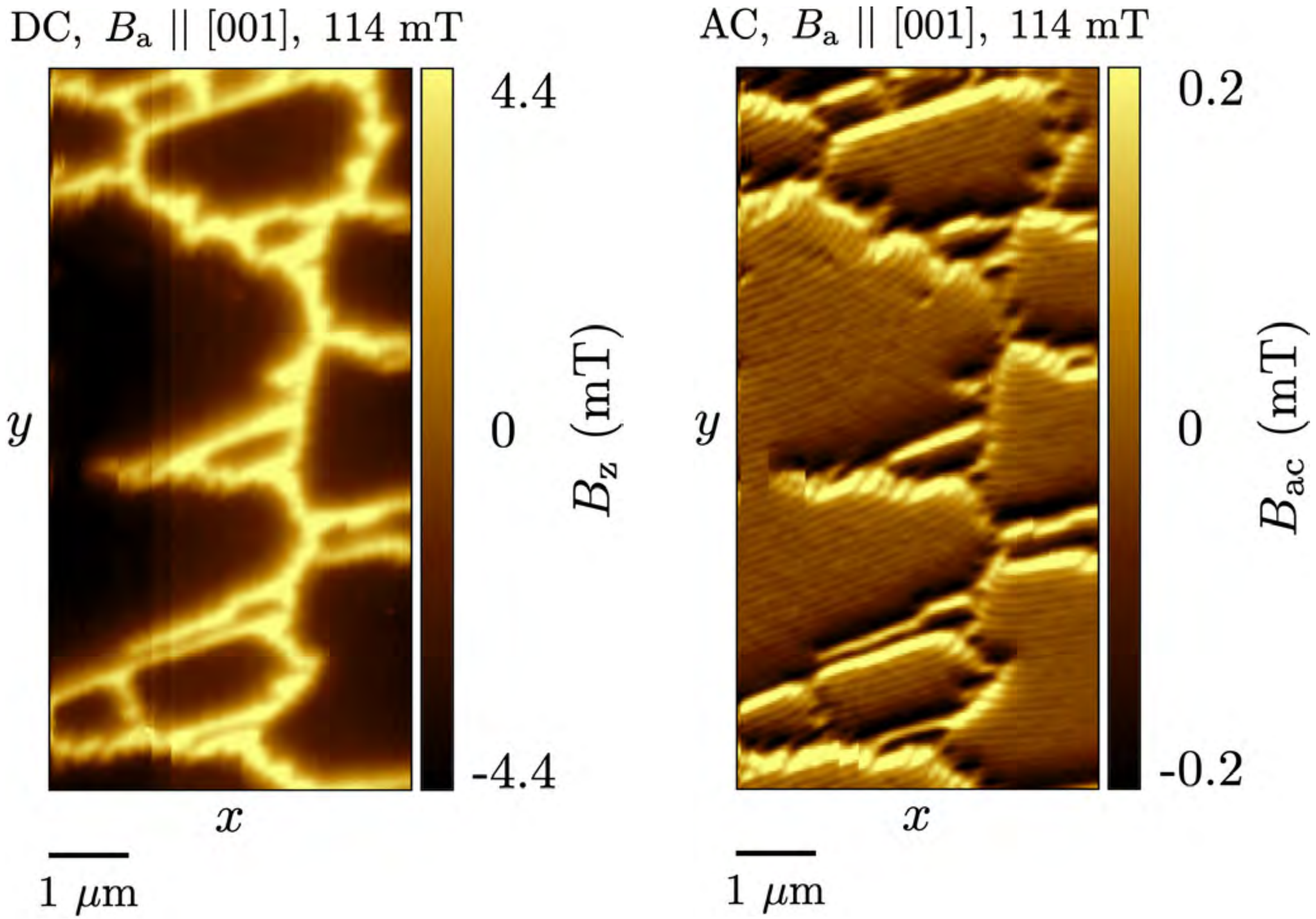

Cu_2OSeO_3 – Field decrease study

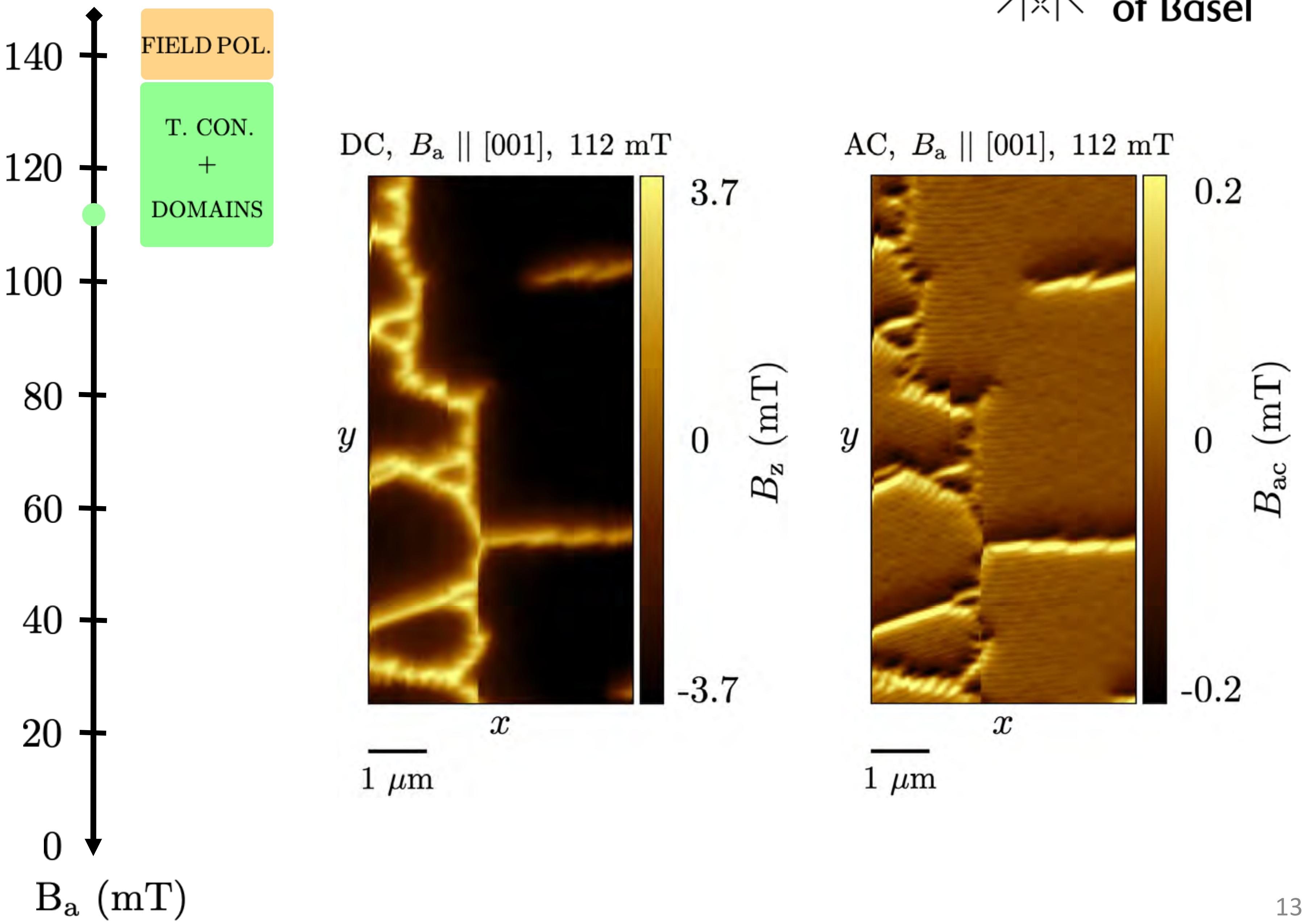

Cu_2OSeO_3 – Field decrease study

University of Basel

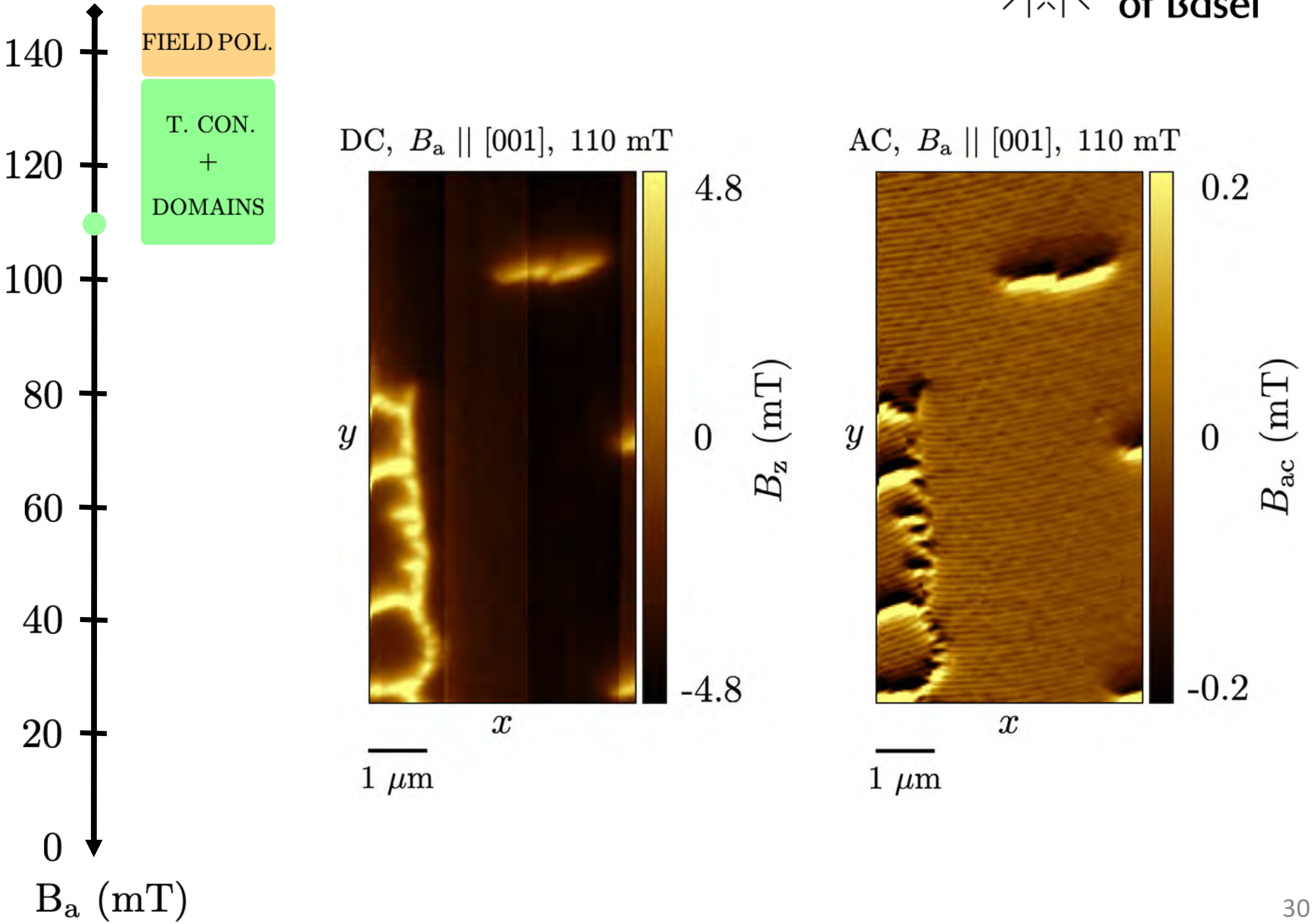

Cu_2OSeO_3 – Field decrease study

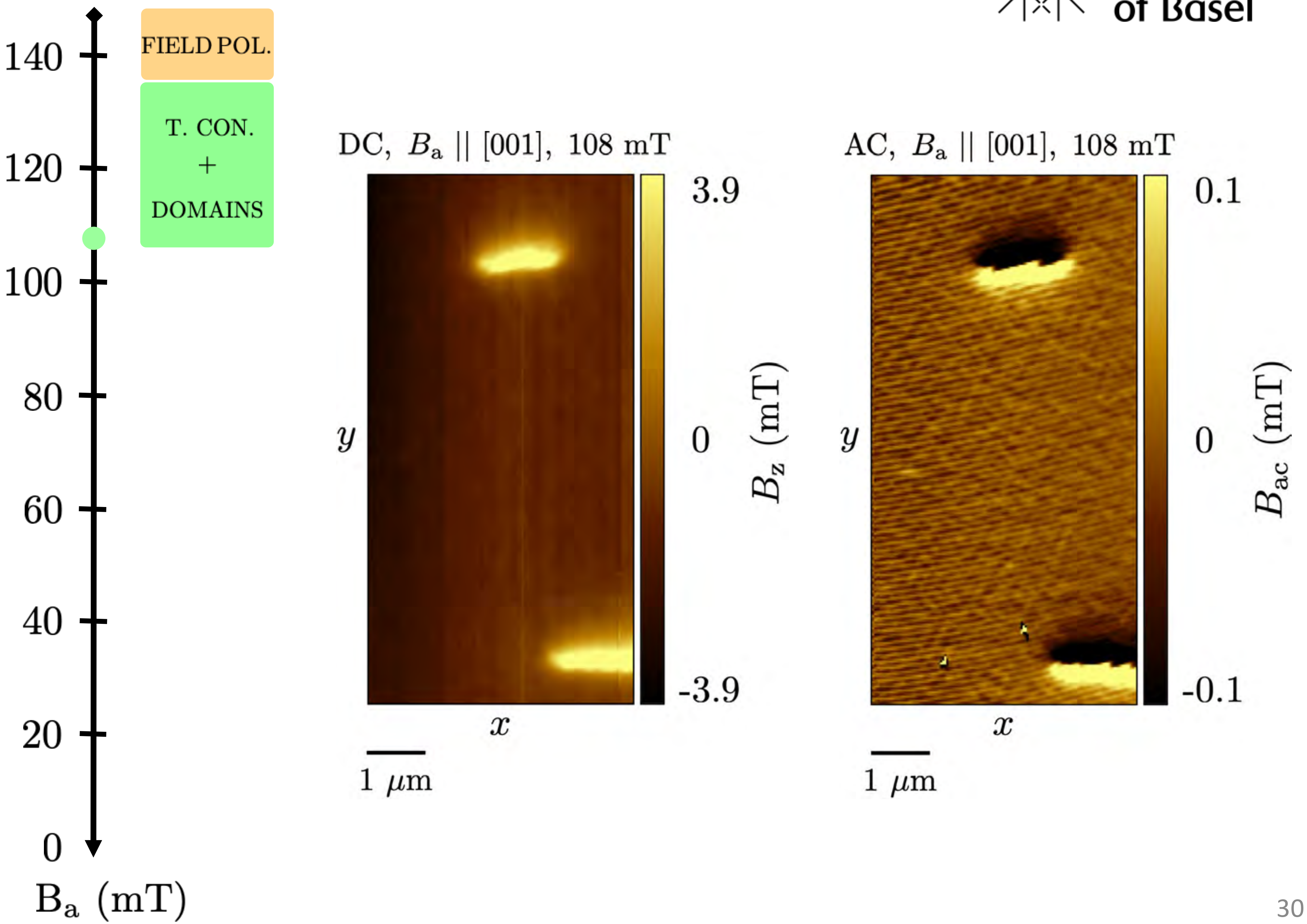

Cu_2OSeO_3 – Field decrease study

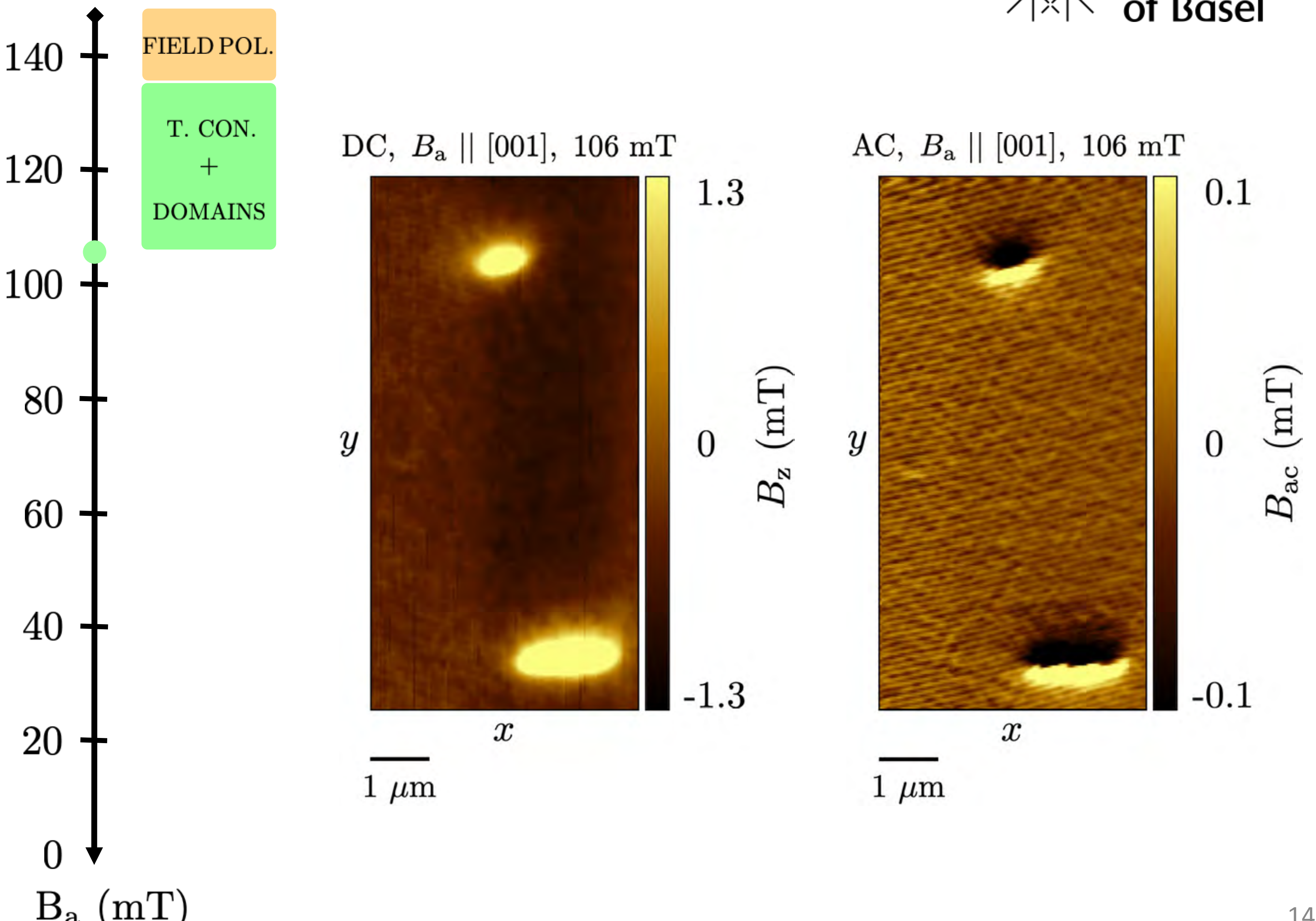

Cu_2OSeO_3 – Field decrease study

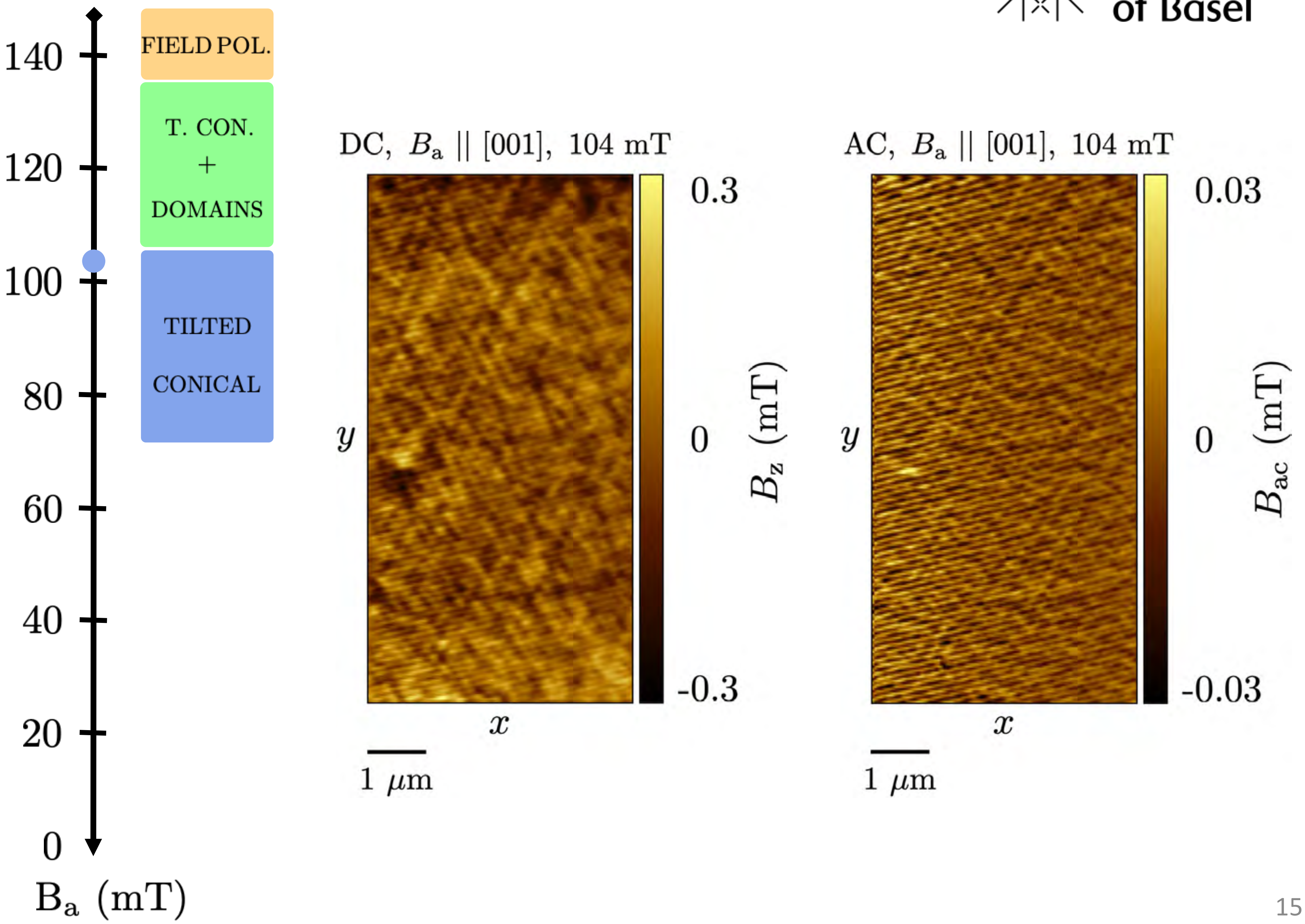

Cu_2OSeO_3 – Field decrease study

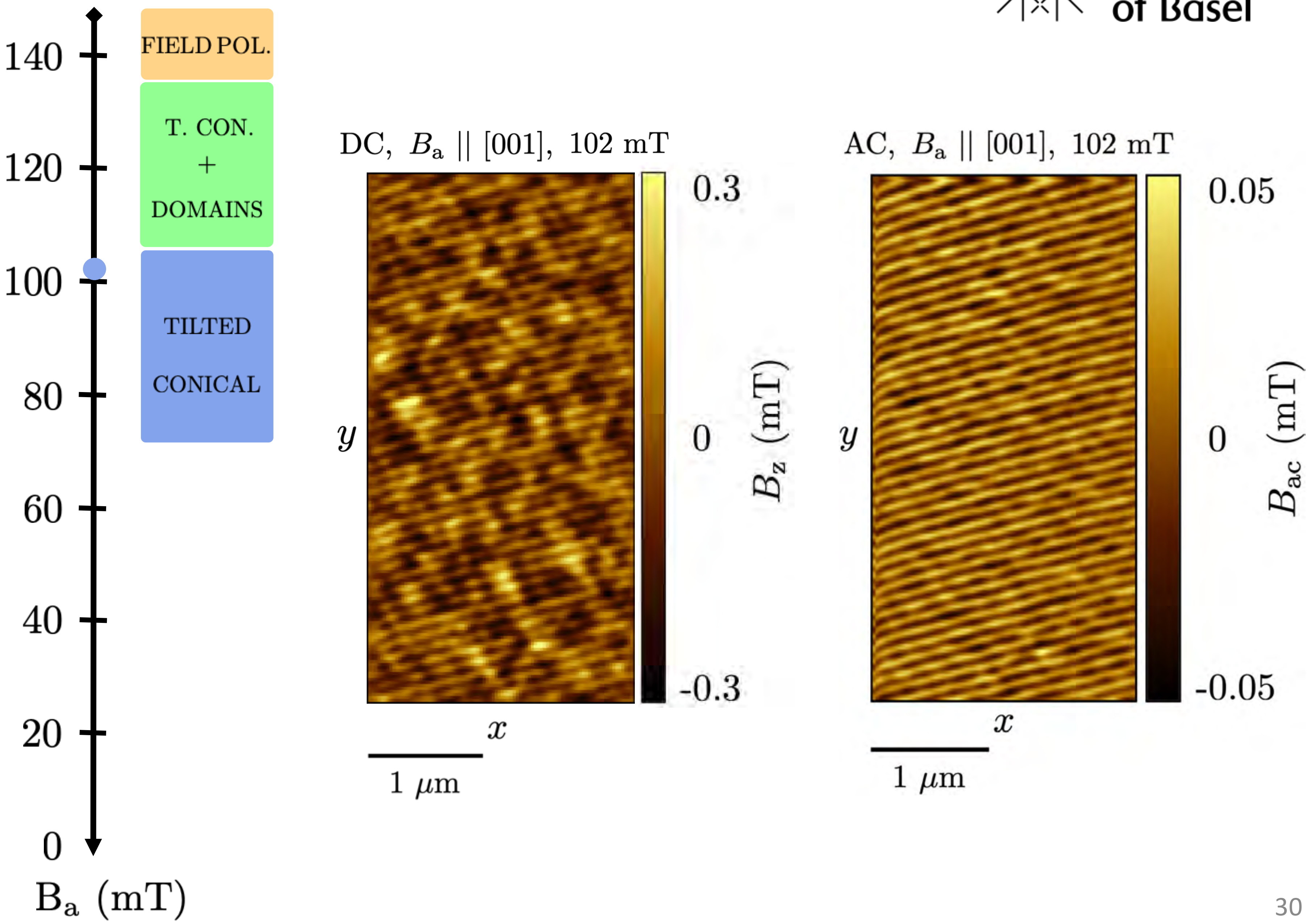

Cu_2OSeO_3 – Field decrease study

University of Basel

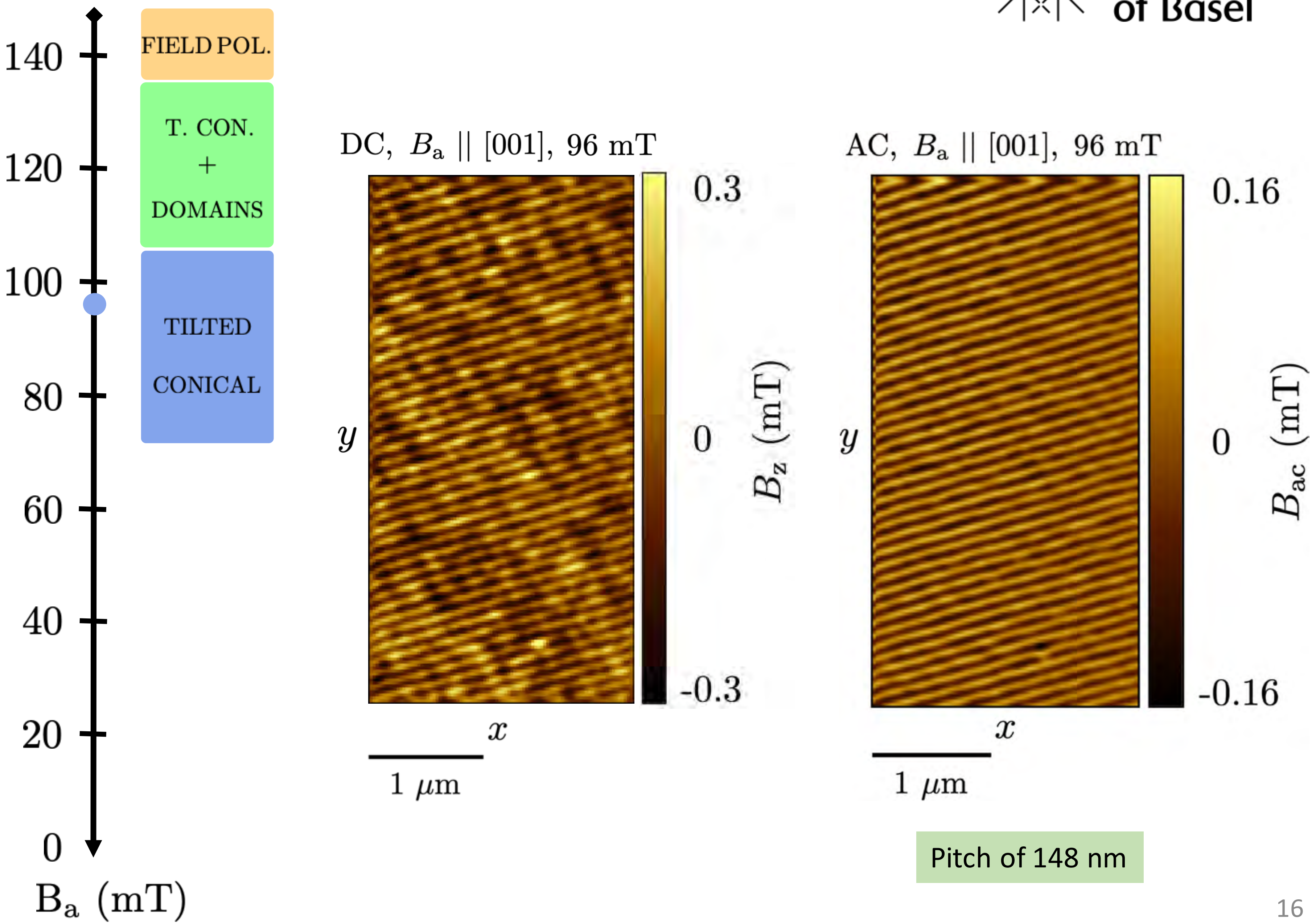

Pitch of 148 nm

Cu_2OSeO_3 – Field decrease study

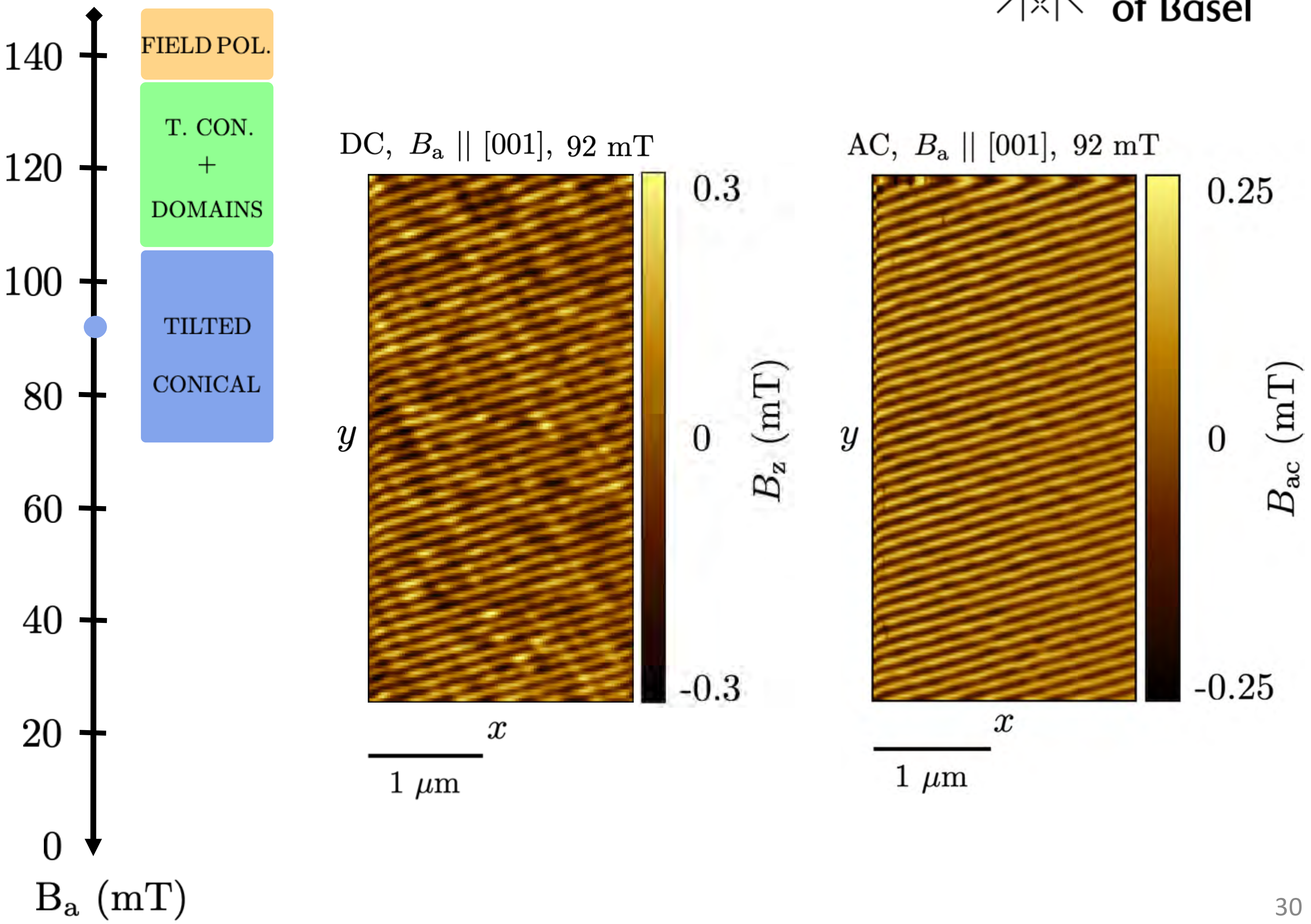

Cu_2OSeO_3 – Field decrease study

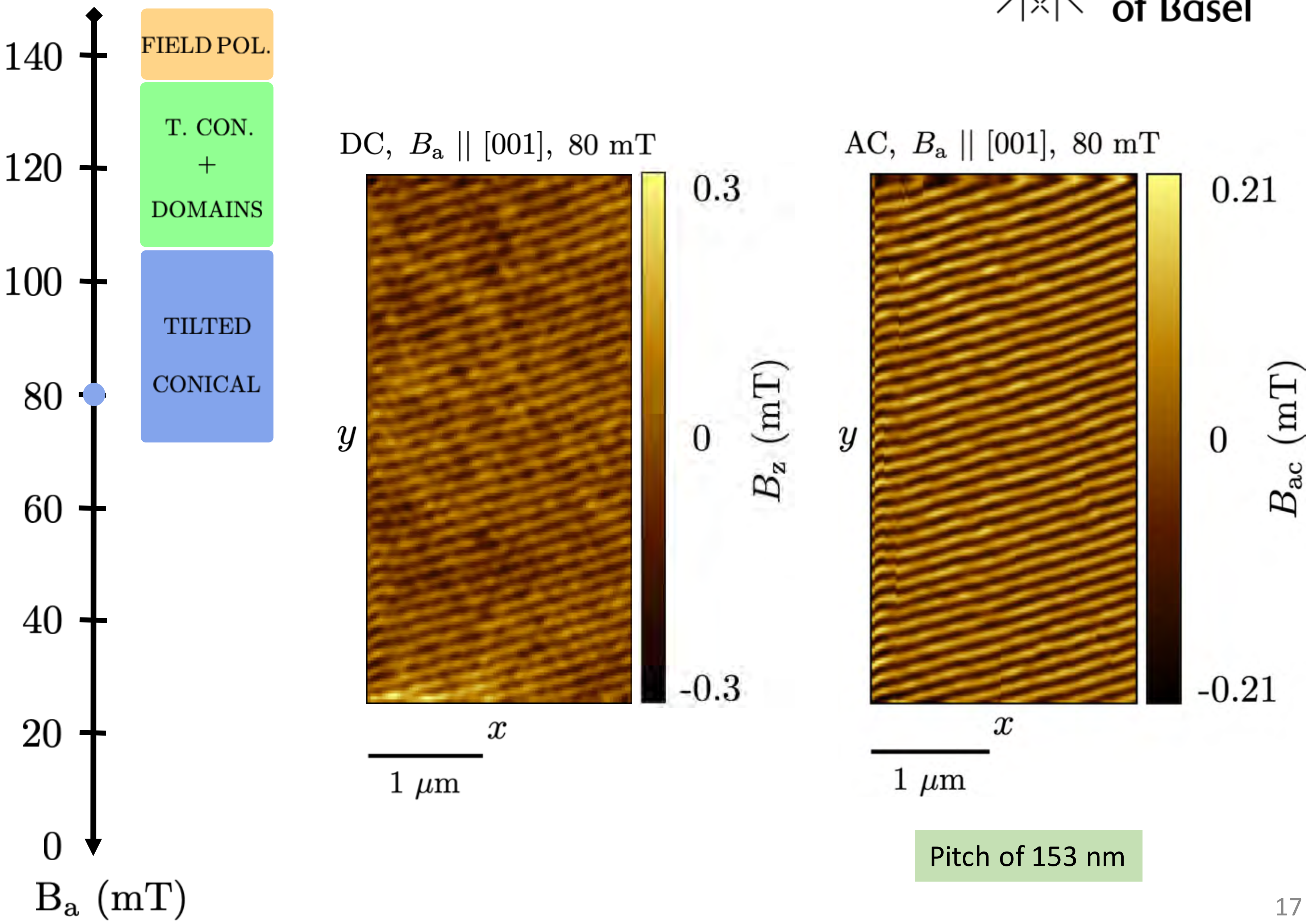

Pitch of 153 nm

Cu_2OSeO_3 – Field decrease study

University of Basel

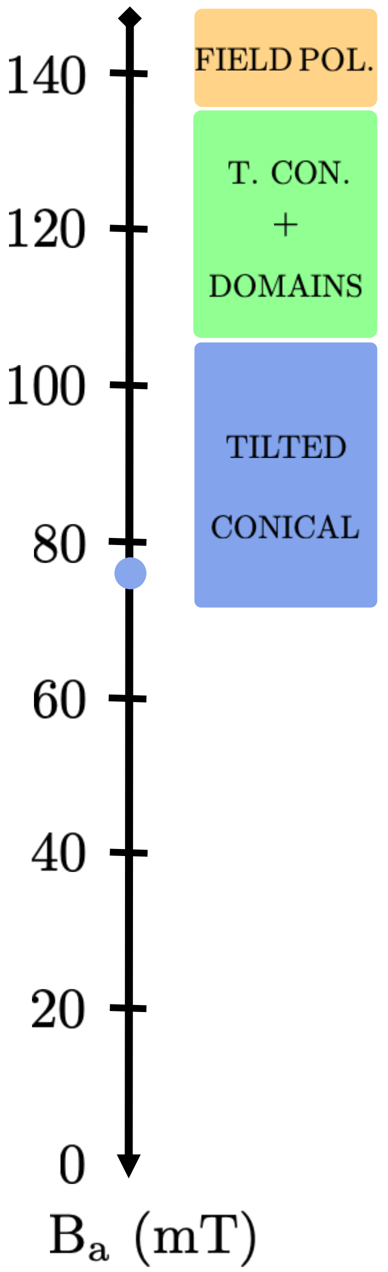

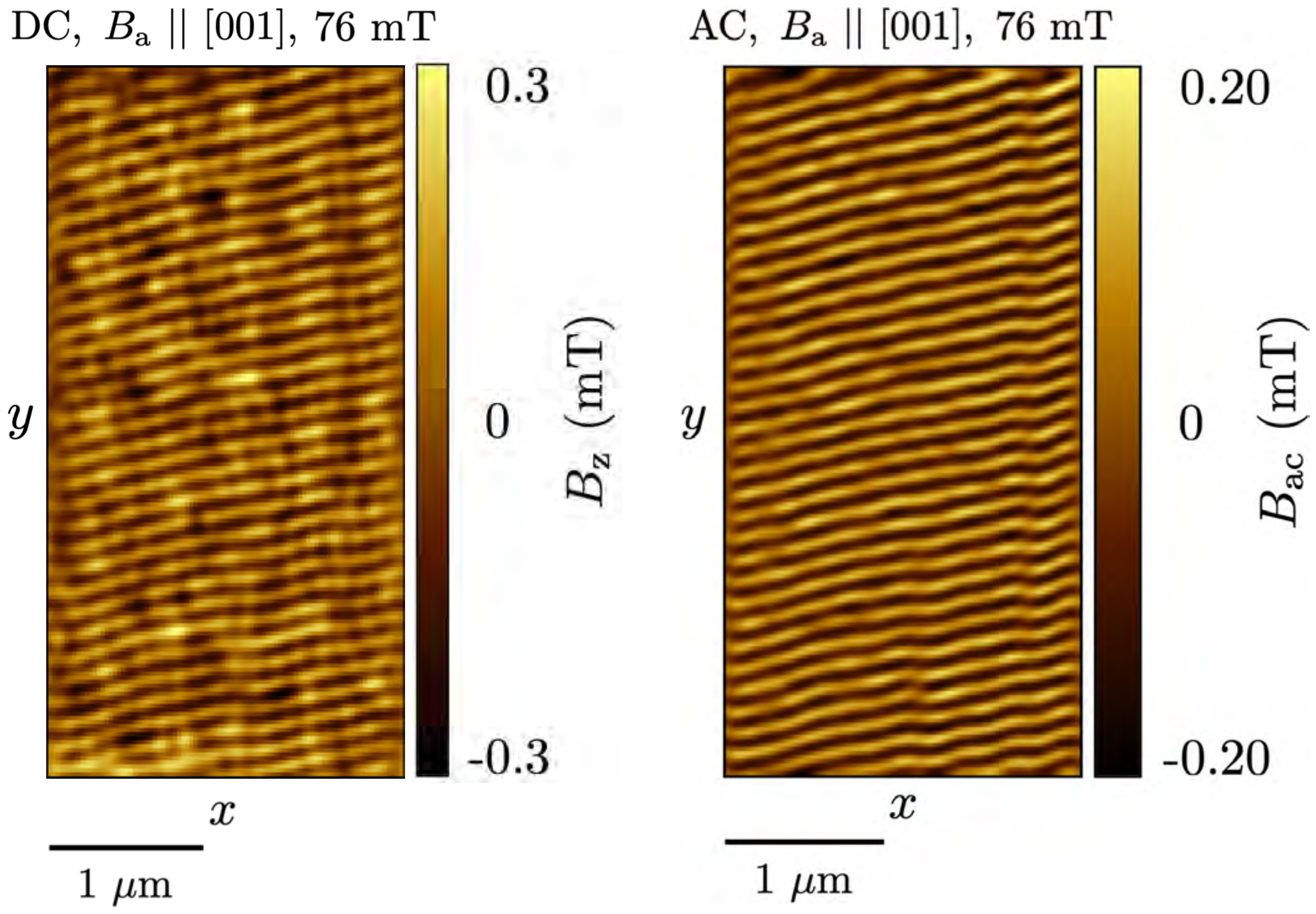

Pitch of 158 nm

Tilted Conical Phase: Θ (B)

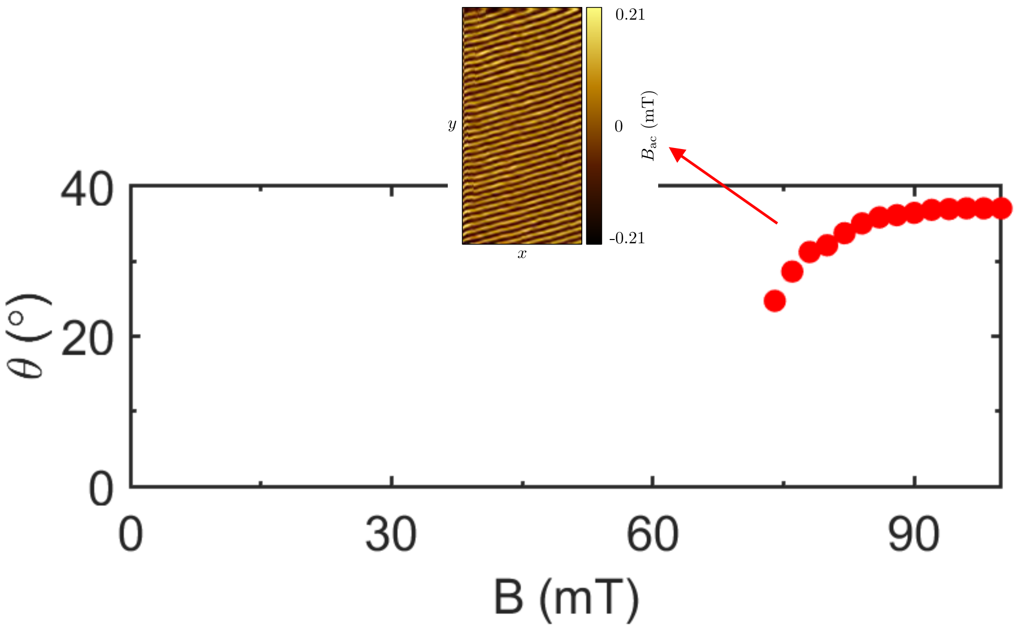

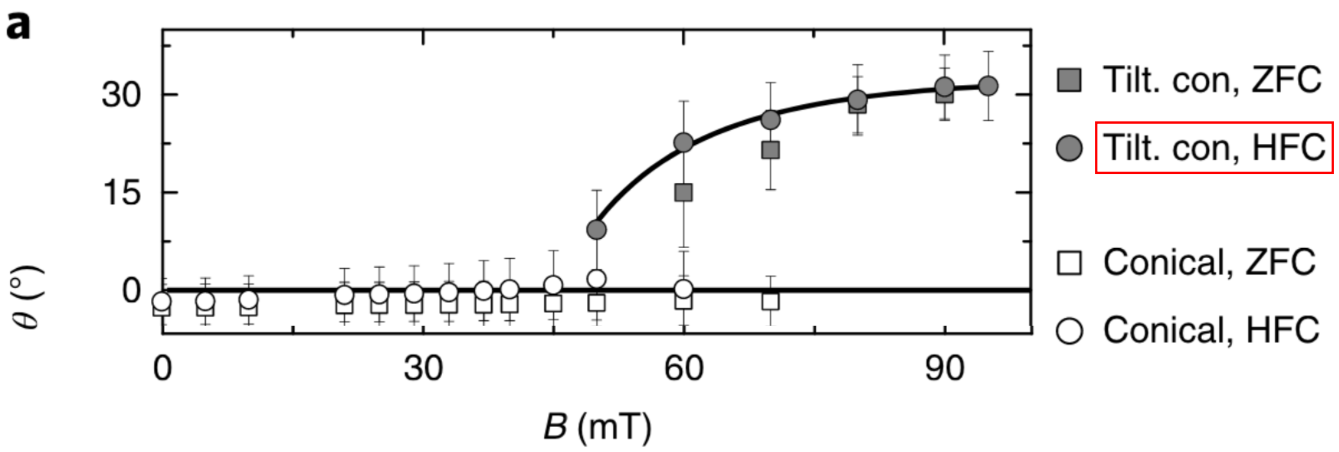

Chacon et al., Nat. Phys. ***14****, 936 (2018)*

Cu_2OSeO_3 – Field decrease study

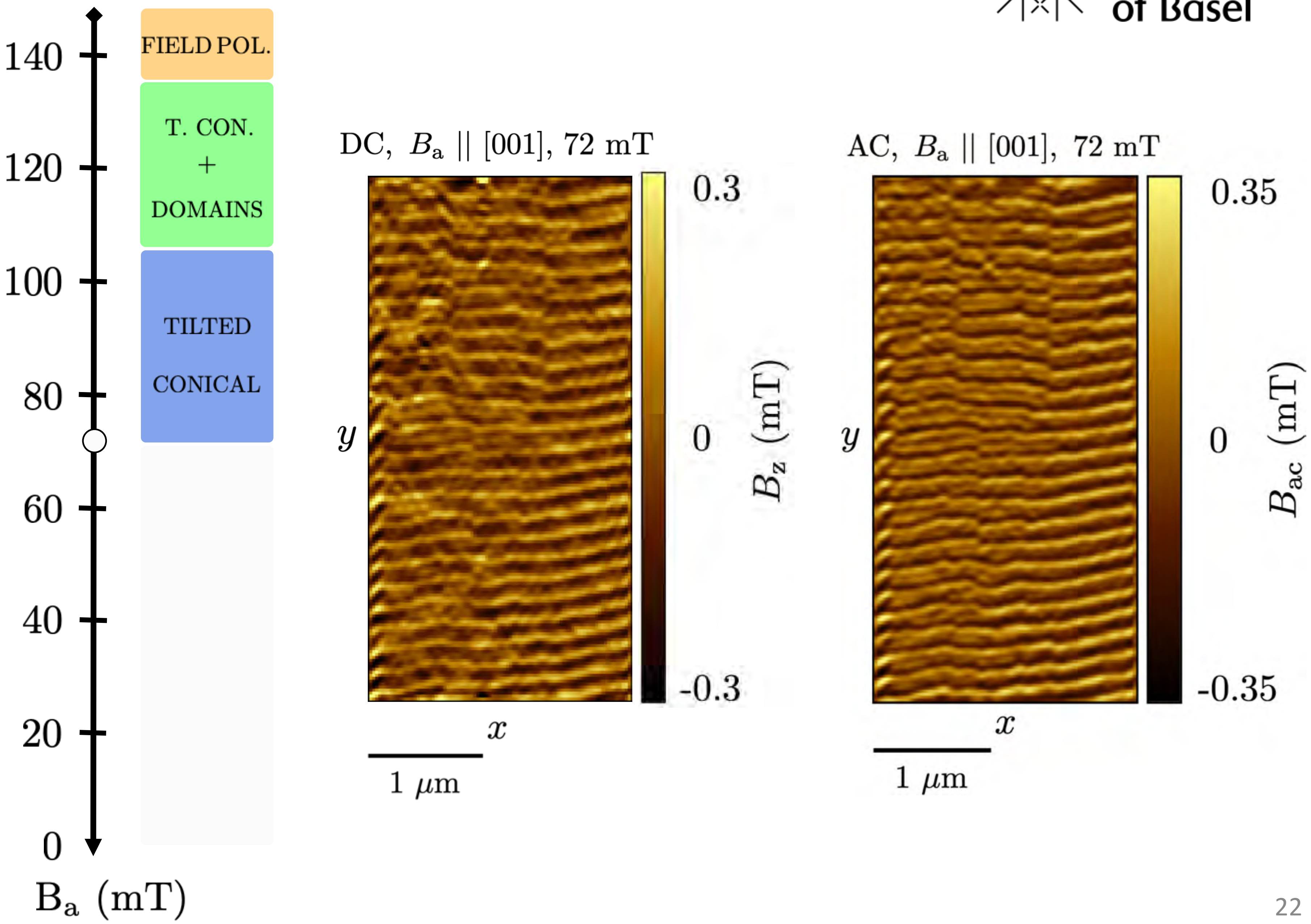

Cu_2OSeO_3 – Field decrease study

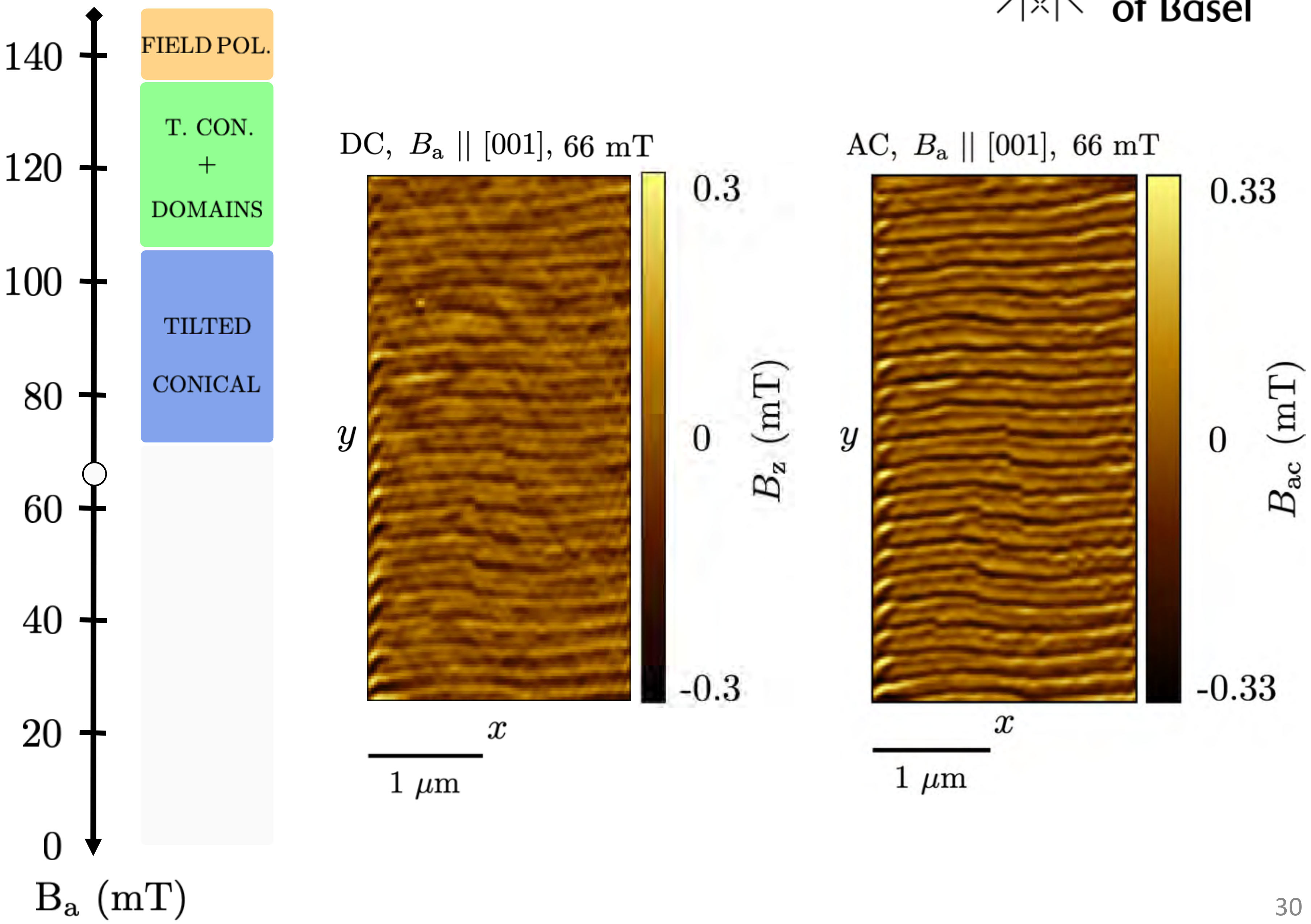

Cu_2OSeO_3 – Field decrease study

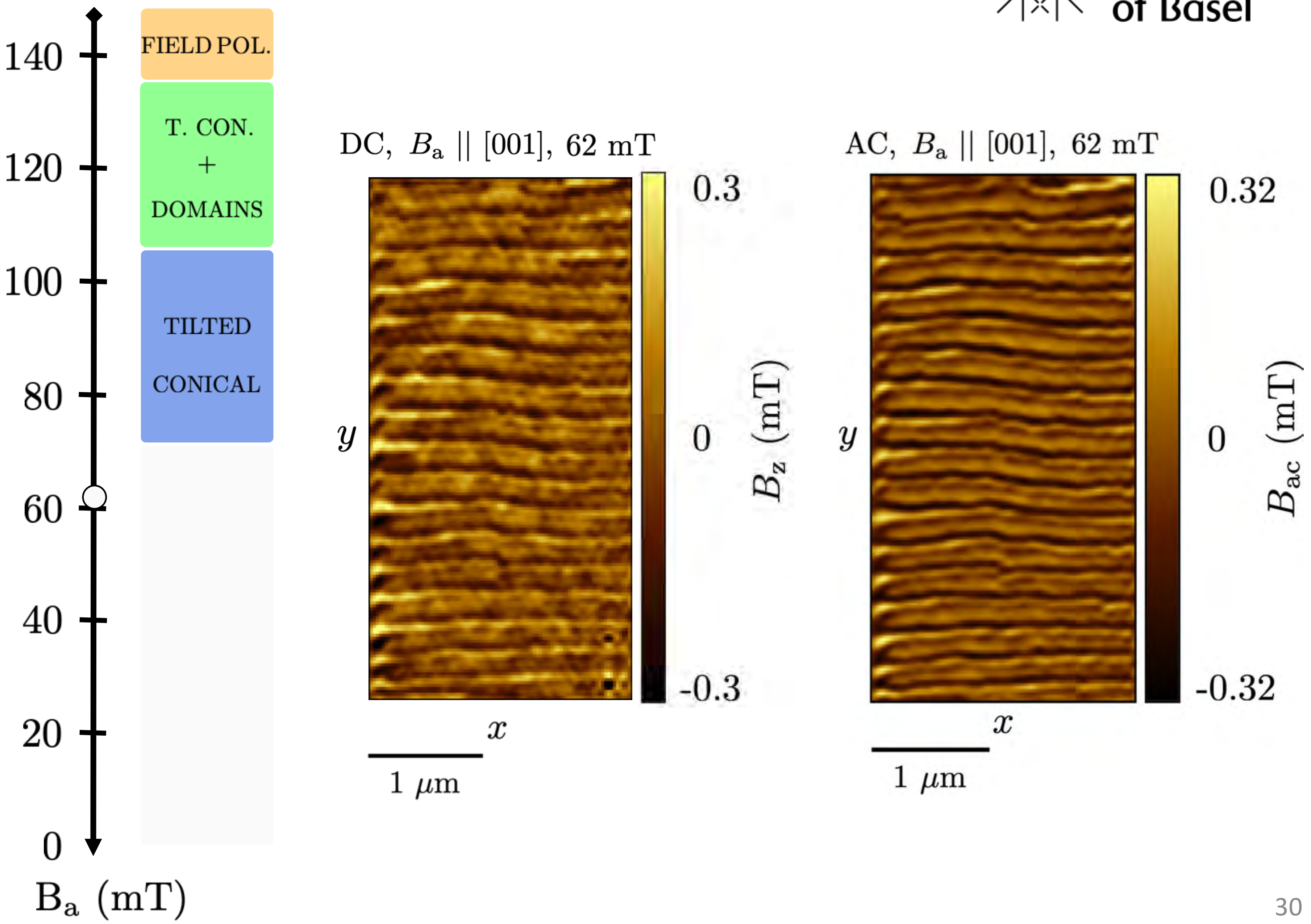

Cu_2OSeO_3 – Field decrease study

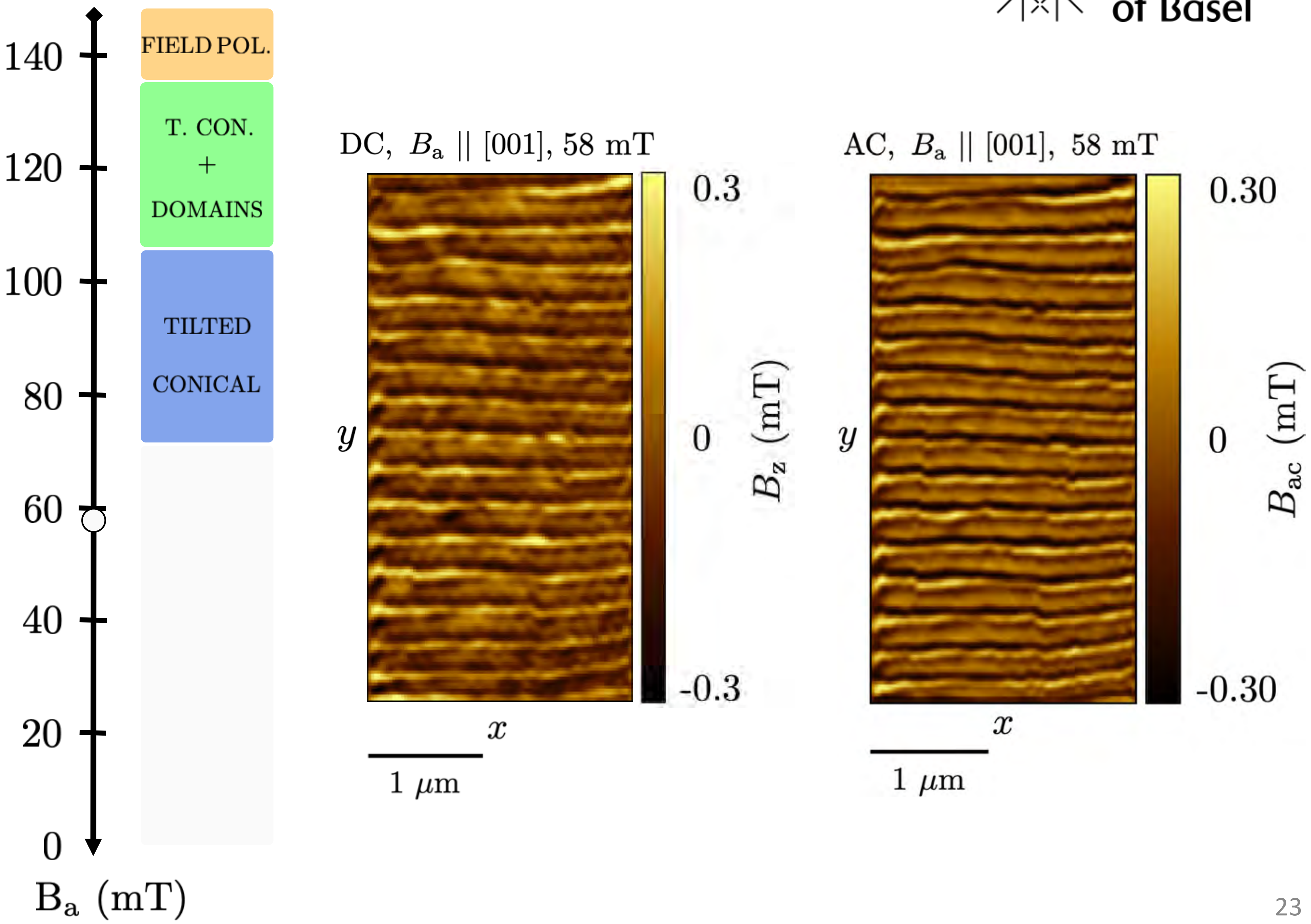

Cu_2OSeO_3 – Field decrease study

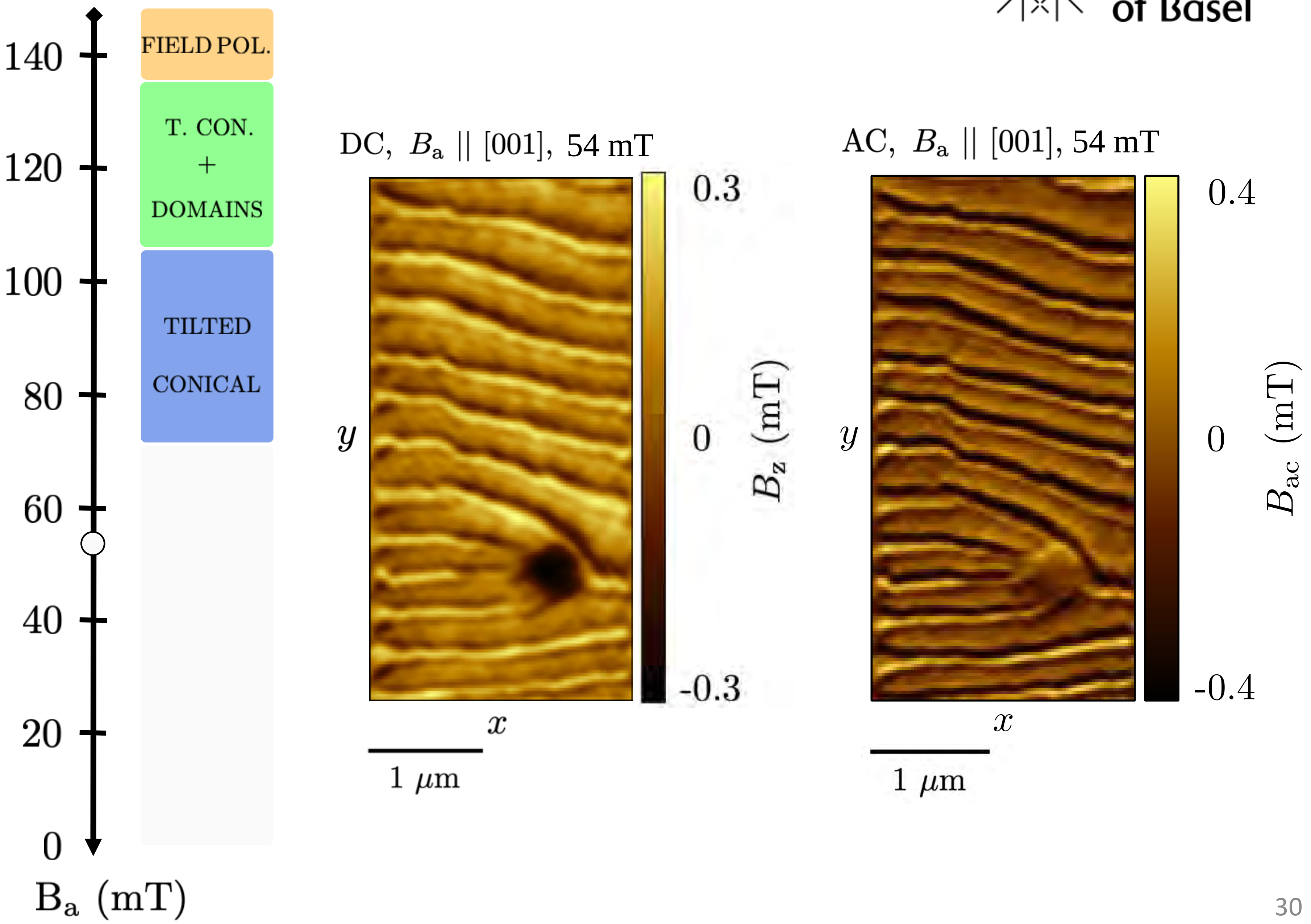

Cu_2OSeO_3 – Field decrease study

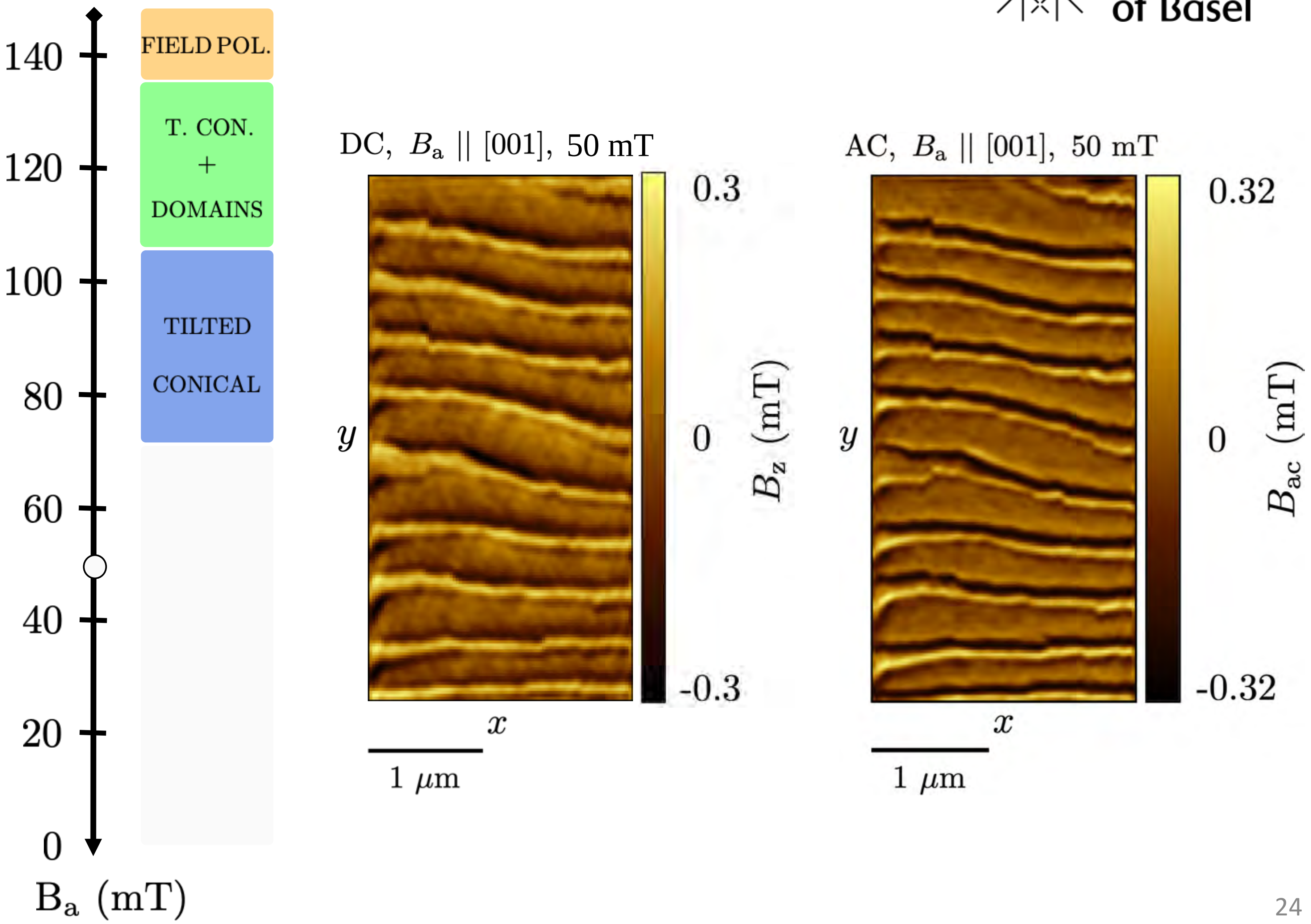

Cu_2OSeO_3 – Field decrease study

University of Basel

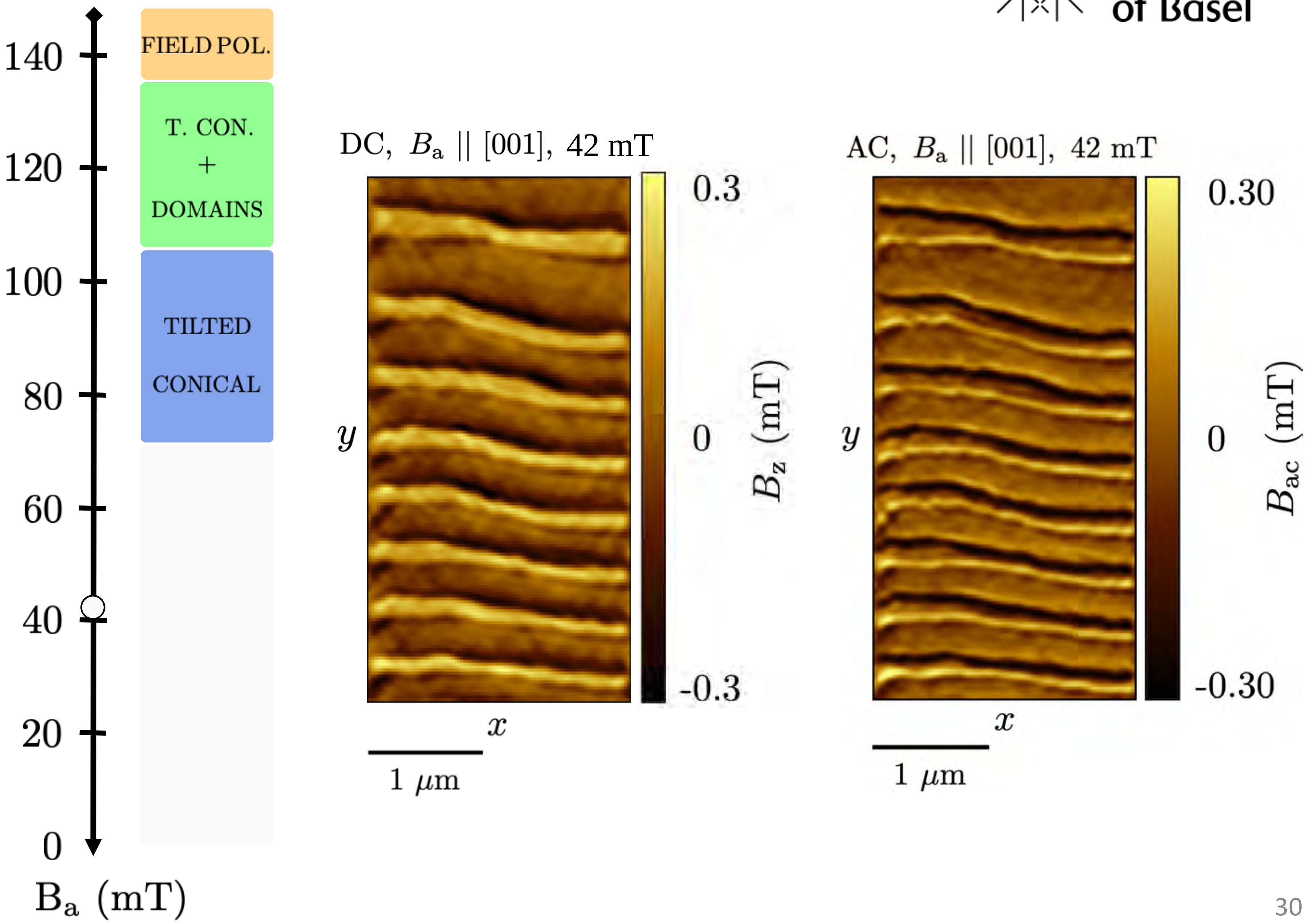

Cu_2OSeO_3 – Field decrease study

University of Basel

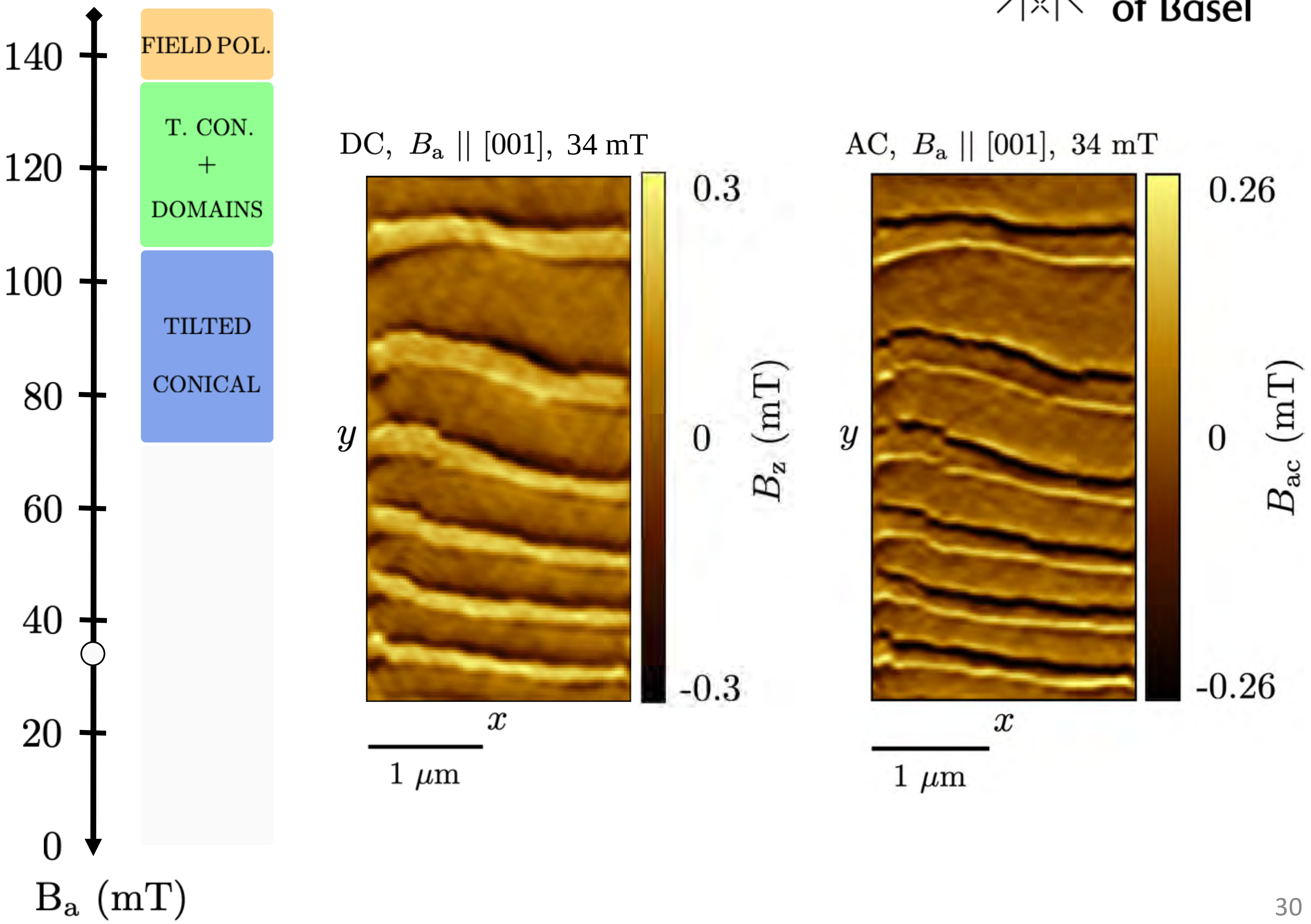

Cu_2OSeO_3 – Field decrease study

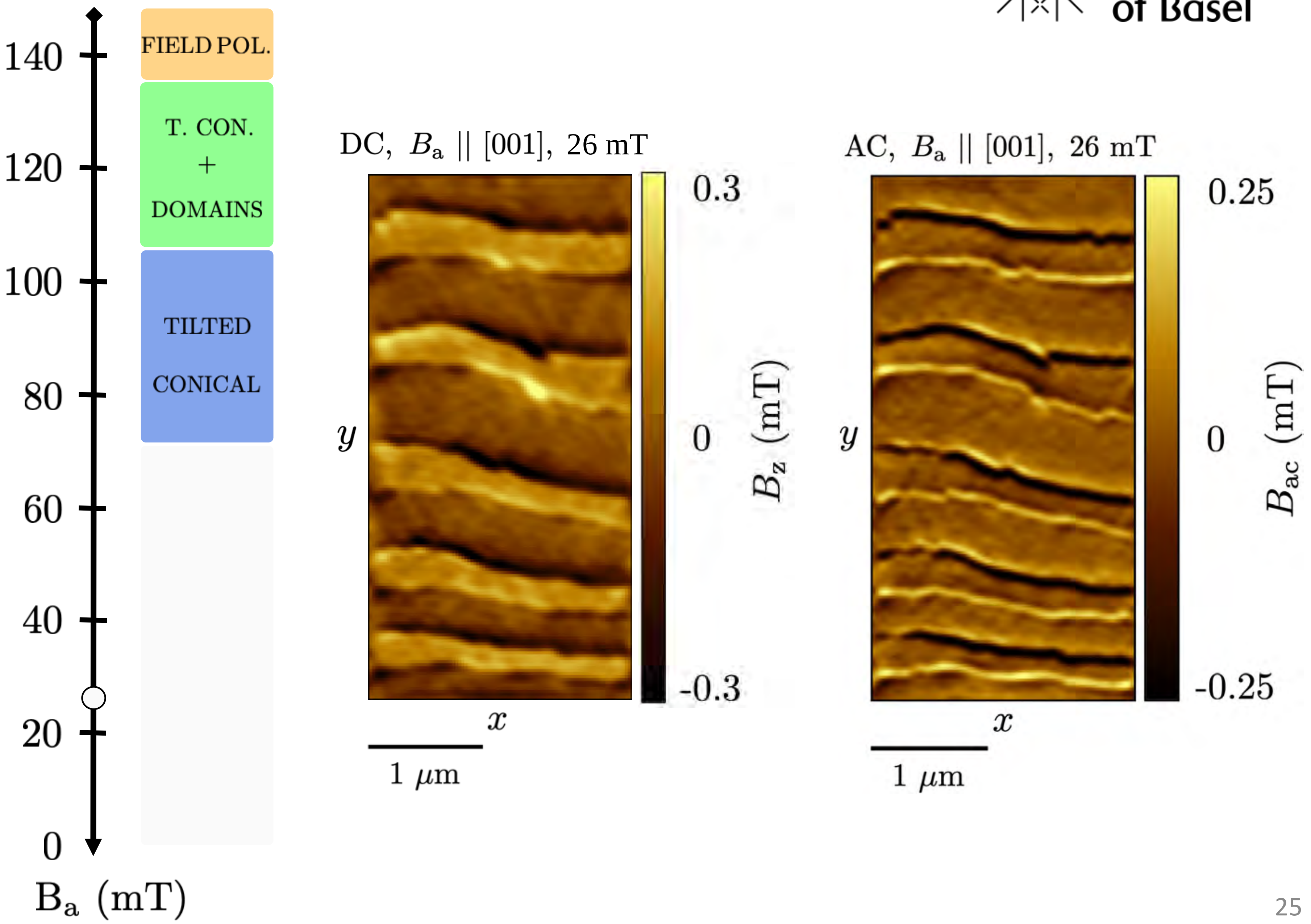

Cu_2OSeO_3 – Field decrease study

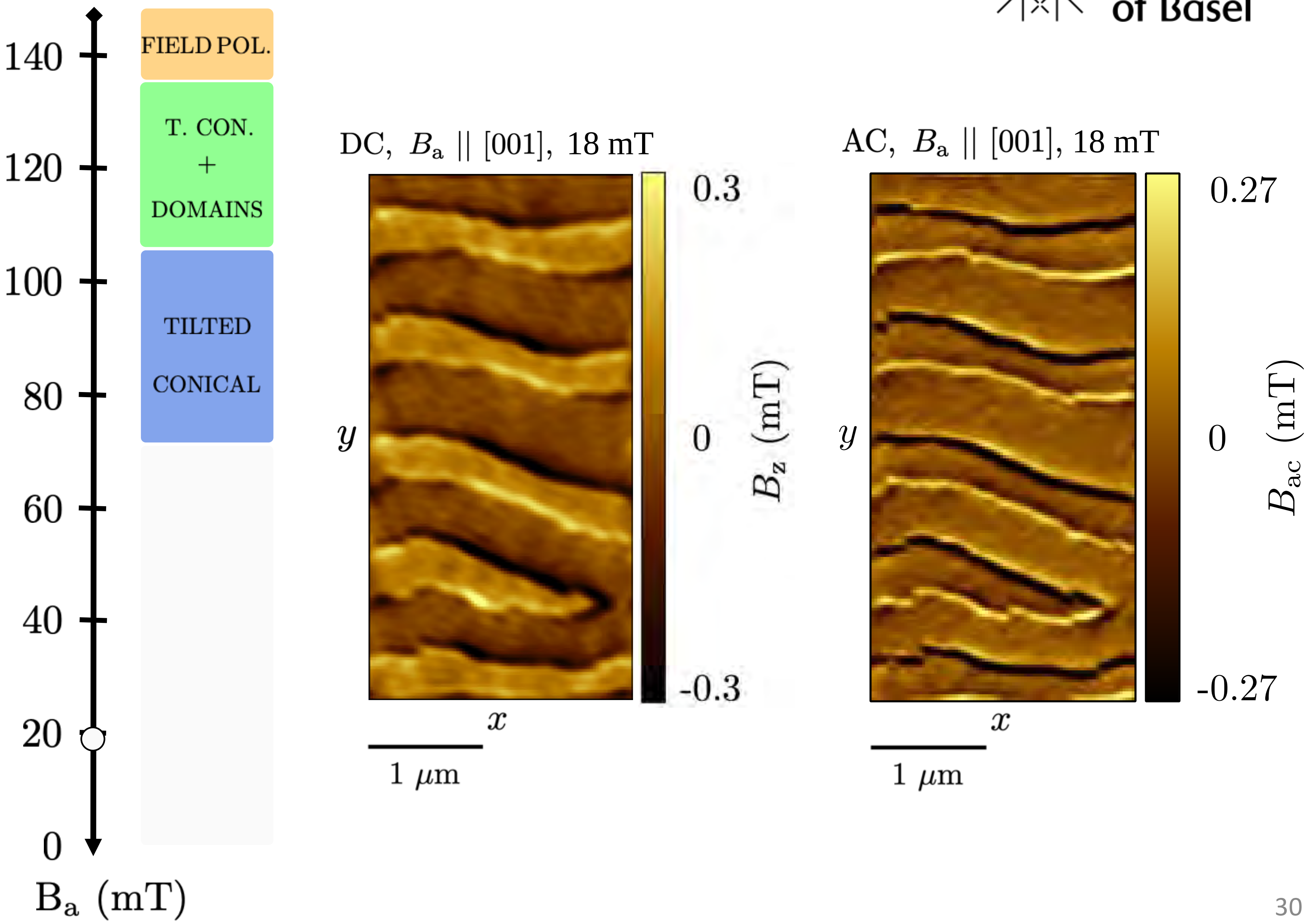

Cu_2OSeO_3 – Field decrease study

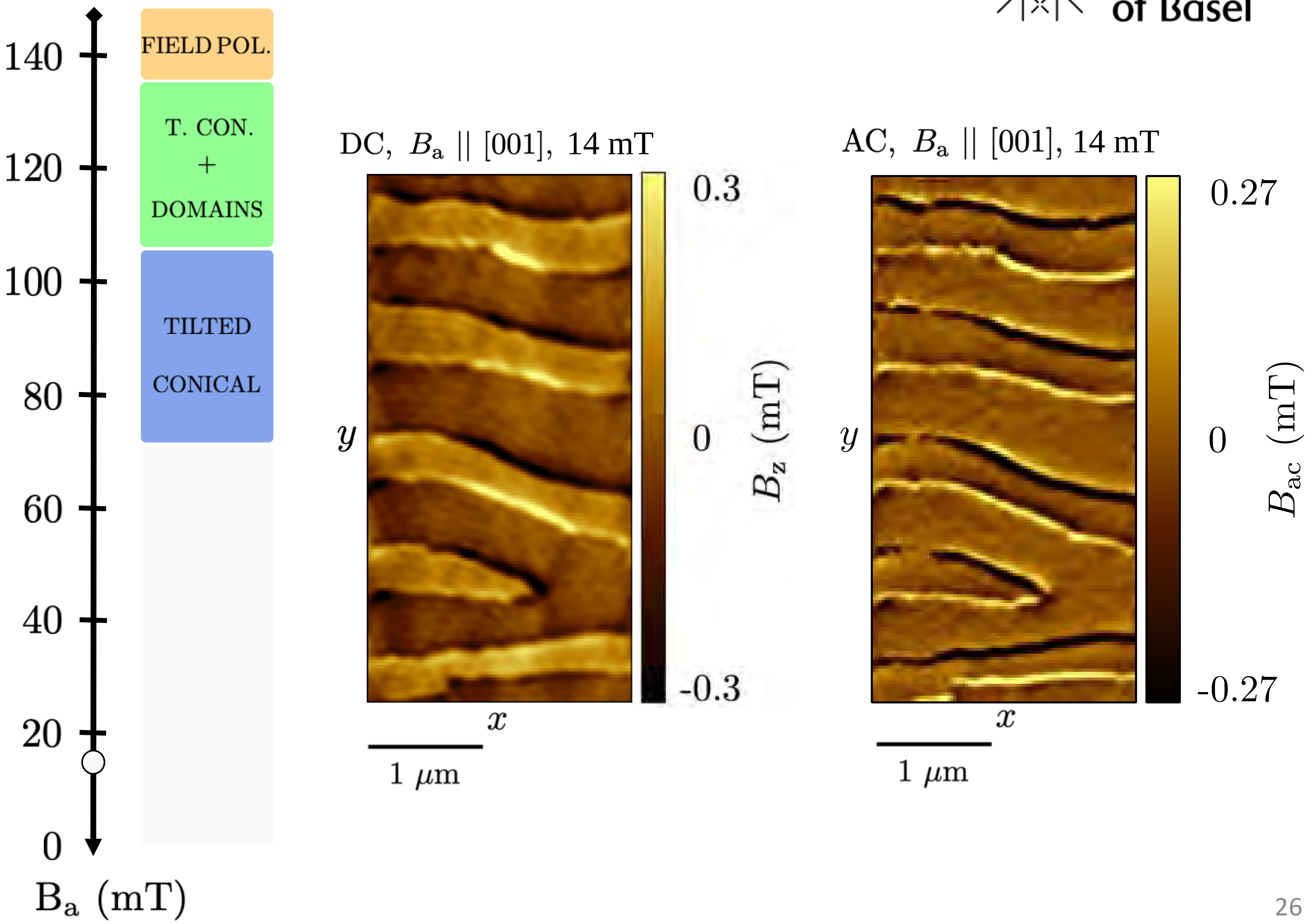

Cu_2OSeO_3 – Field decrease study

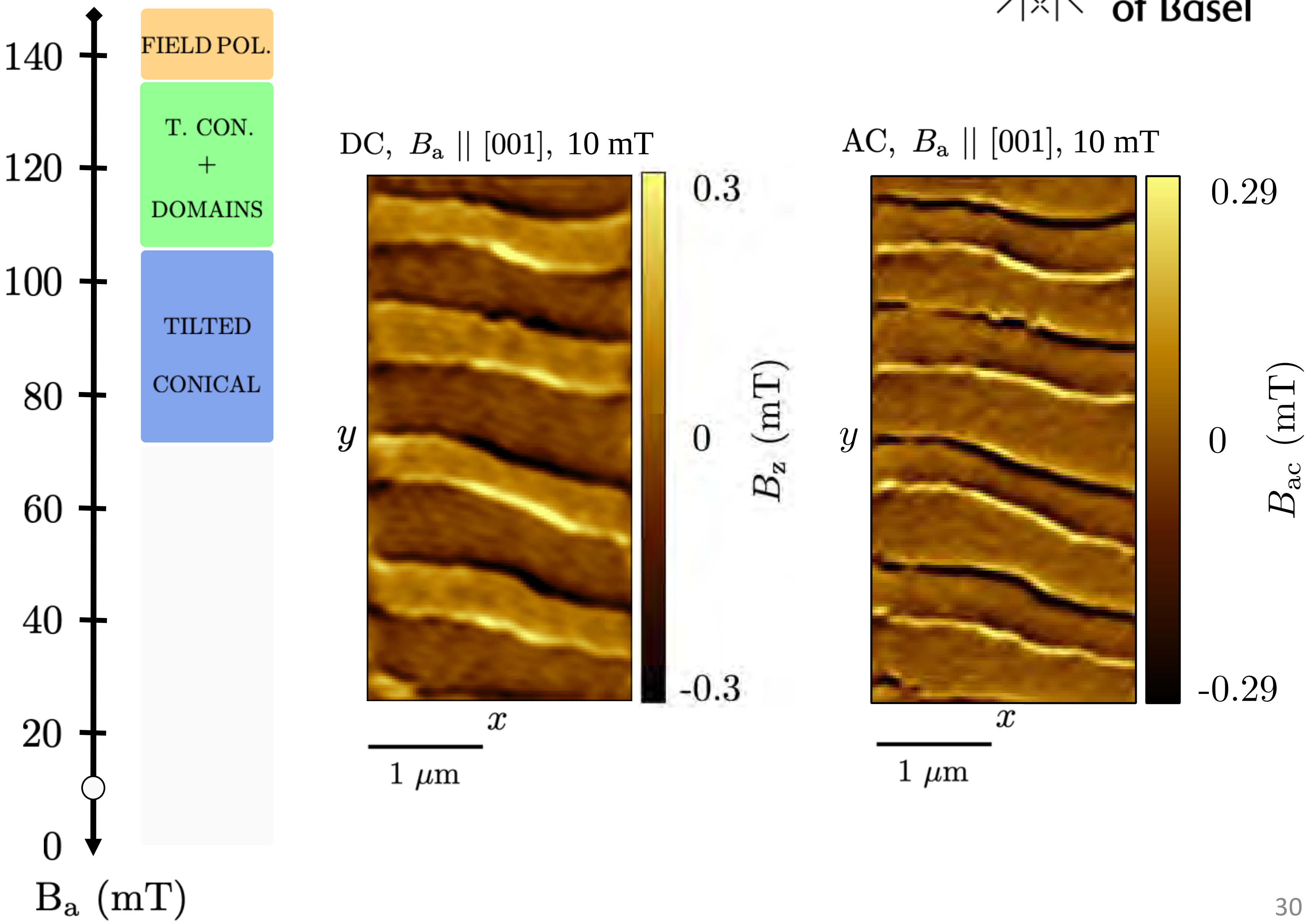

Cu_2OSeO_3 – Field decrease study

University of Basel

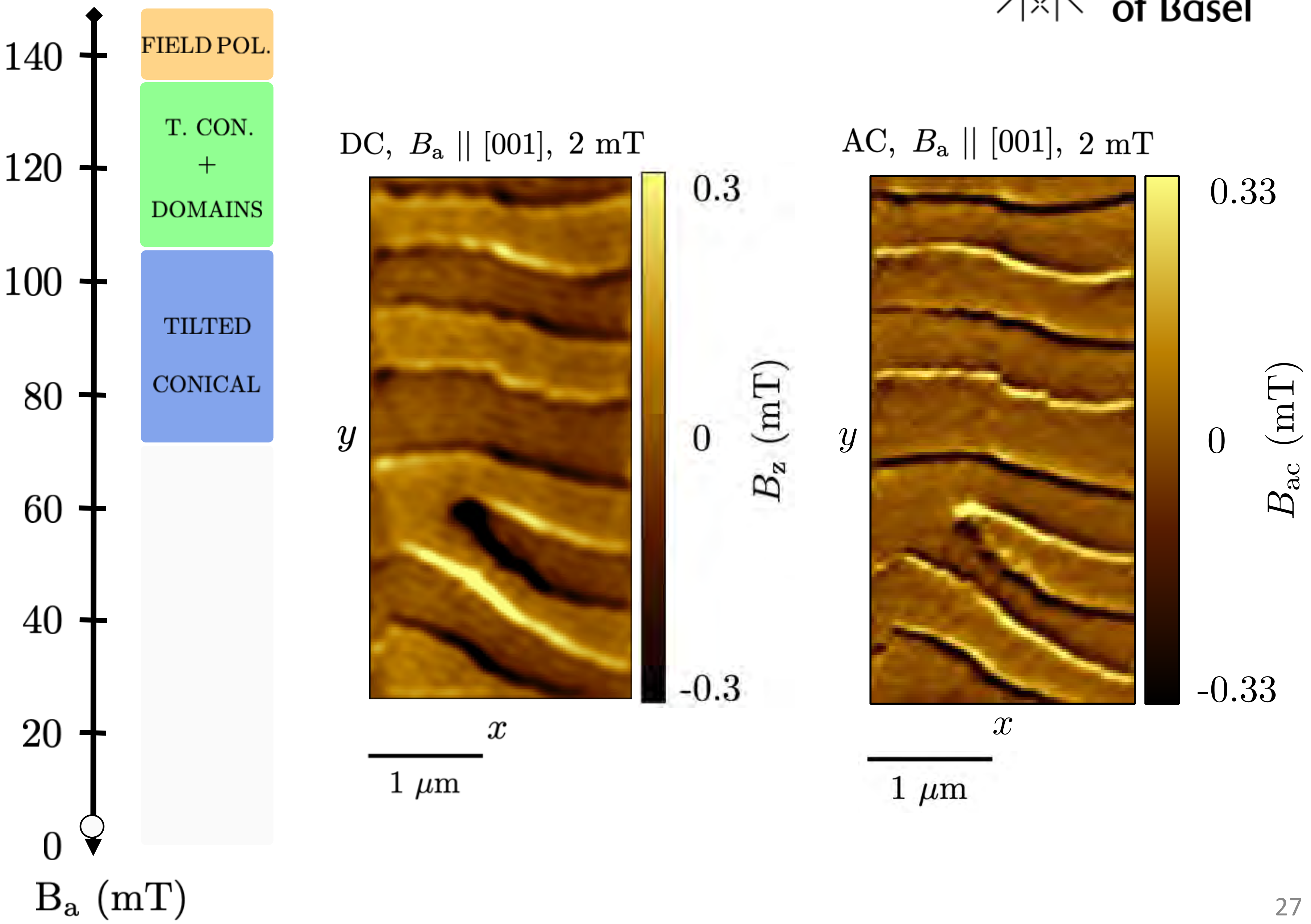

Cu_2OSeO_3 – Field decrease study

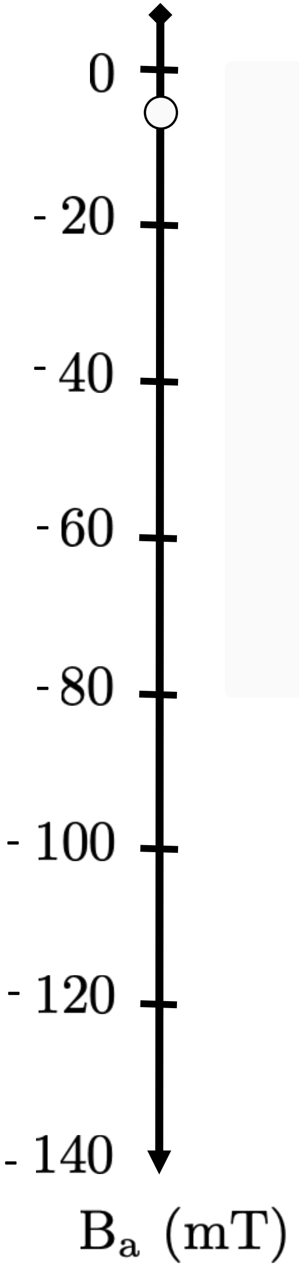

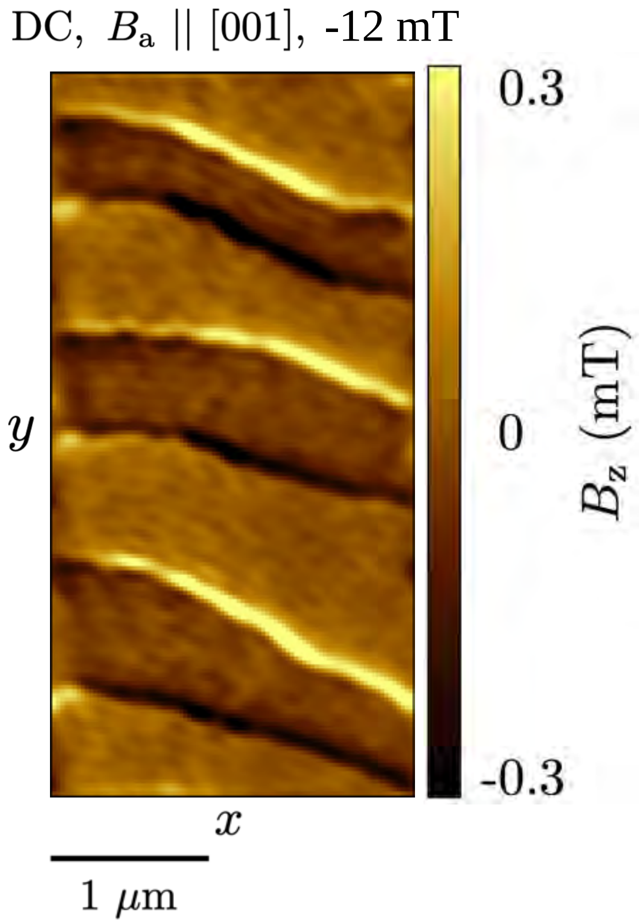

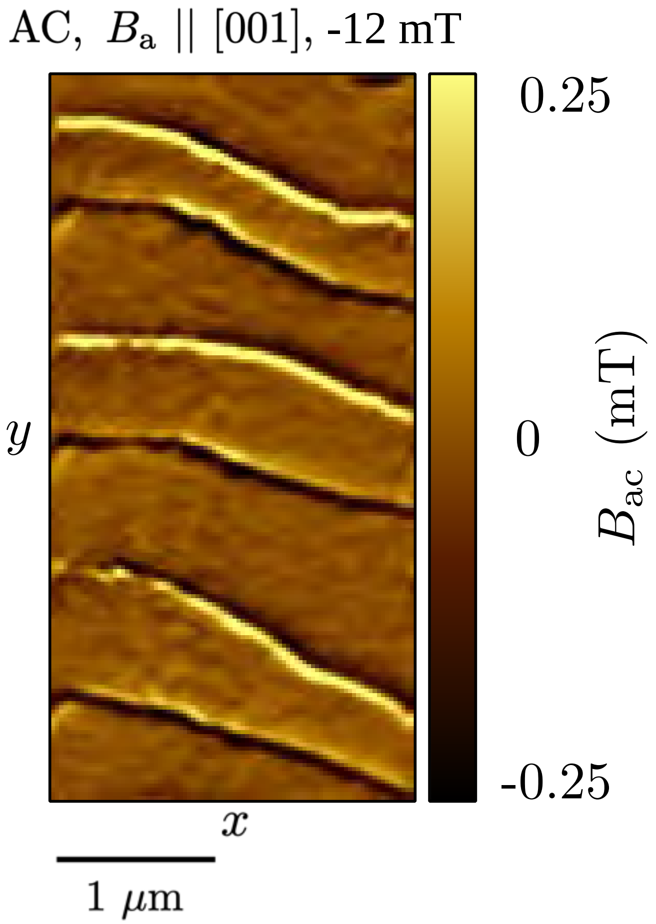

Cu_2OSeO_3 – Field decrease study

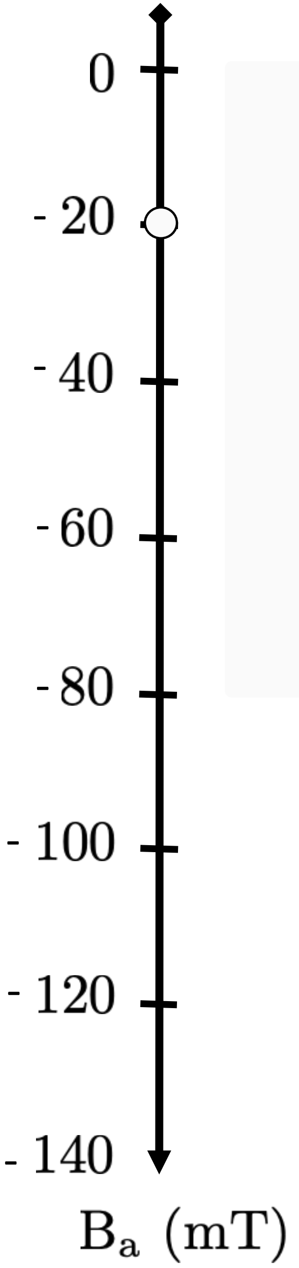

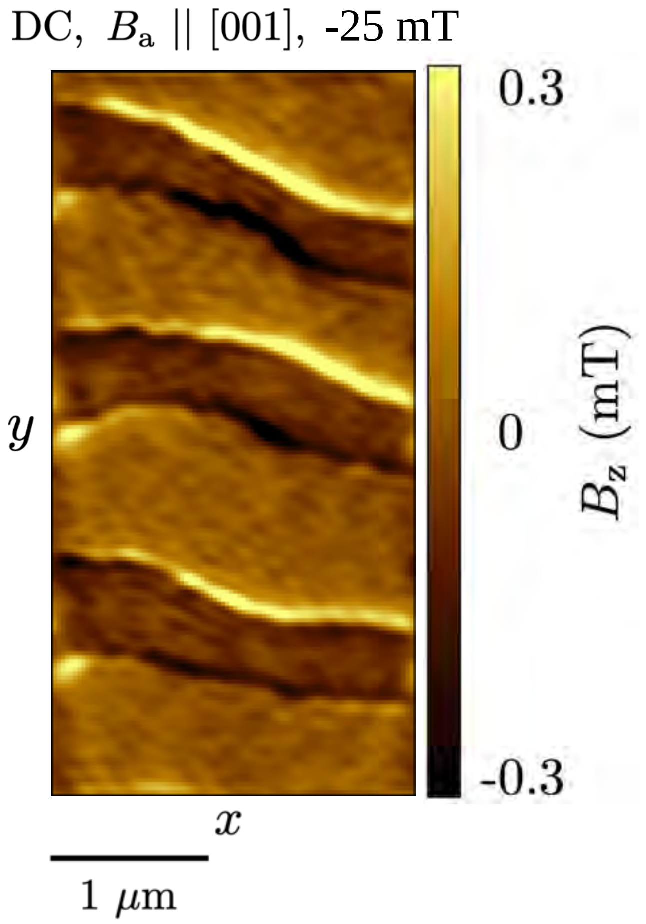

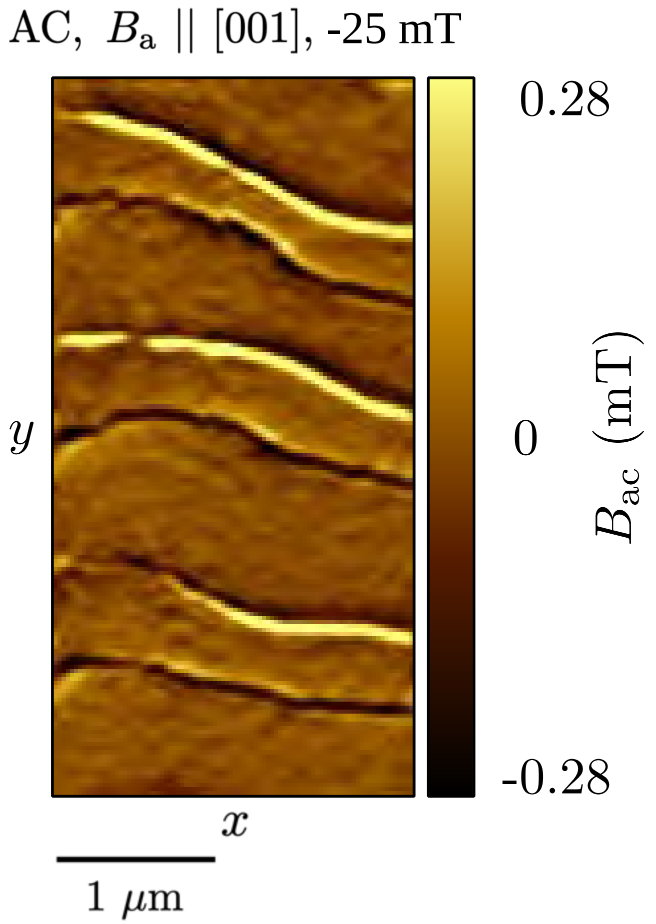

Cu_2OSeO_3 – Field decrease study

University of Basel

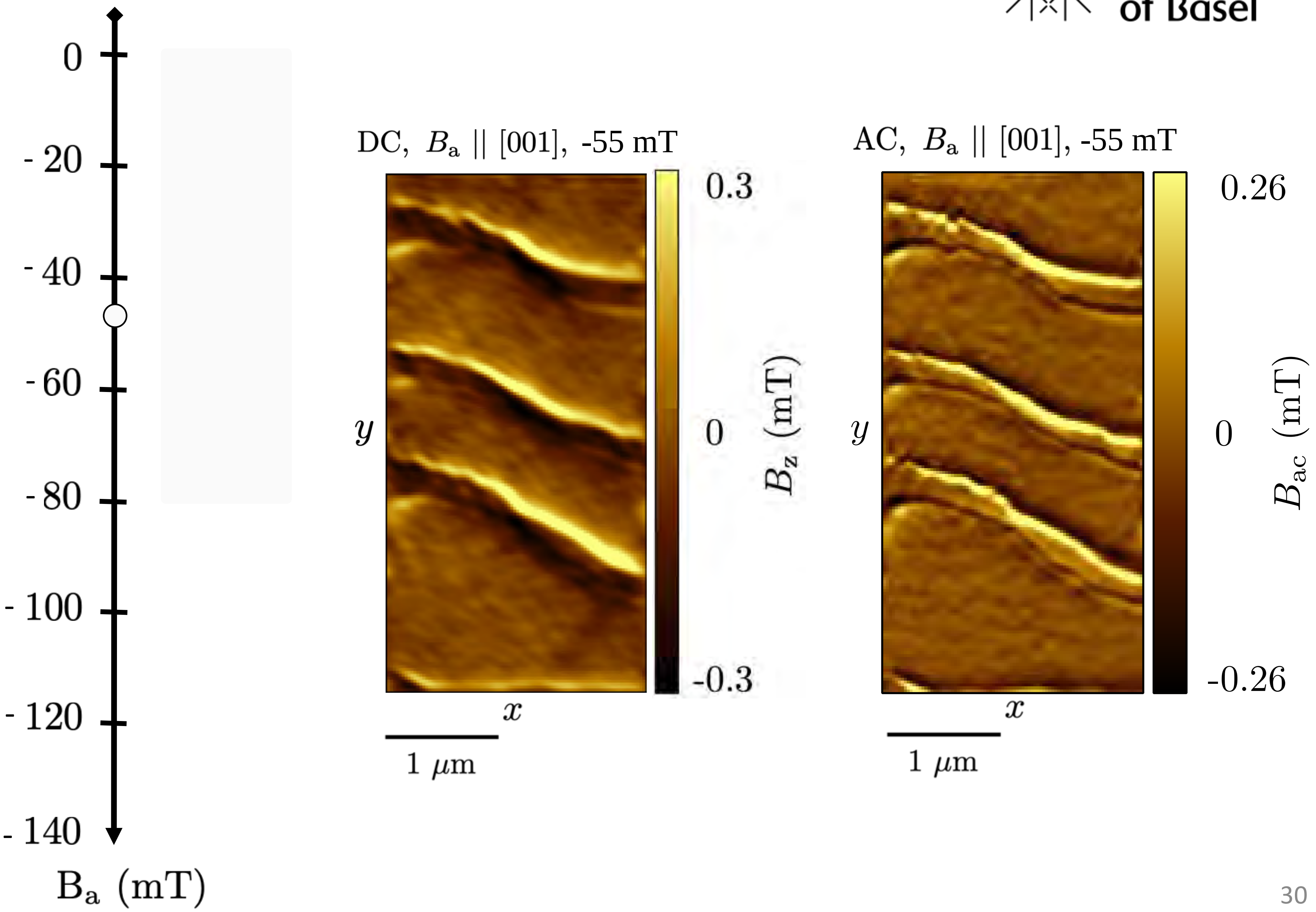

Cu_2OSeO_3 – Field decrease study

University of Basel

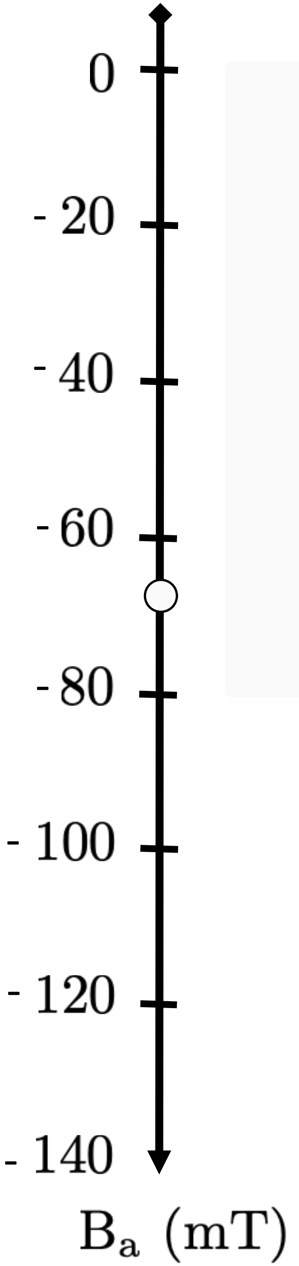

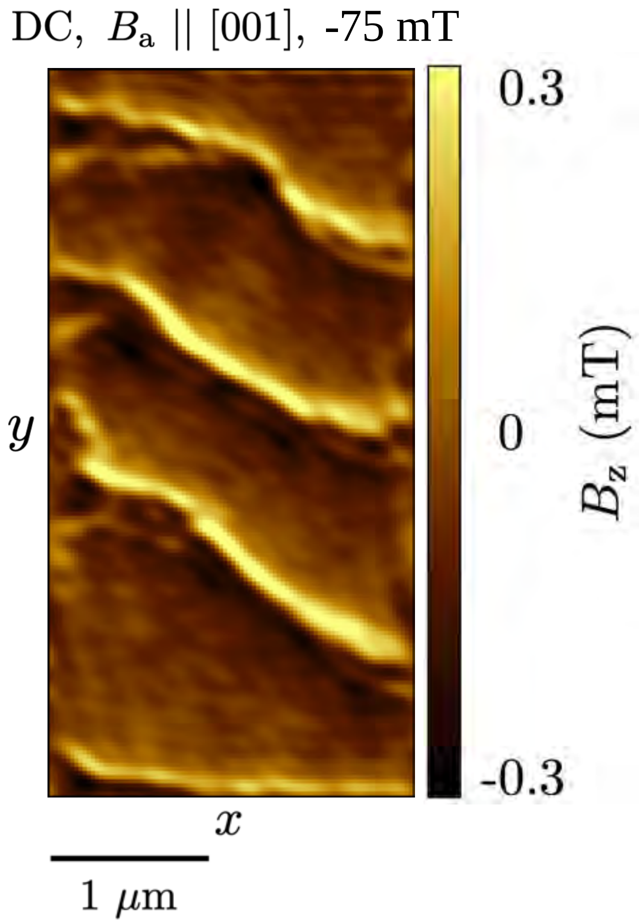

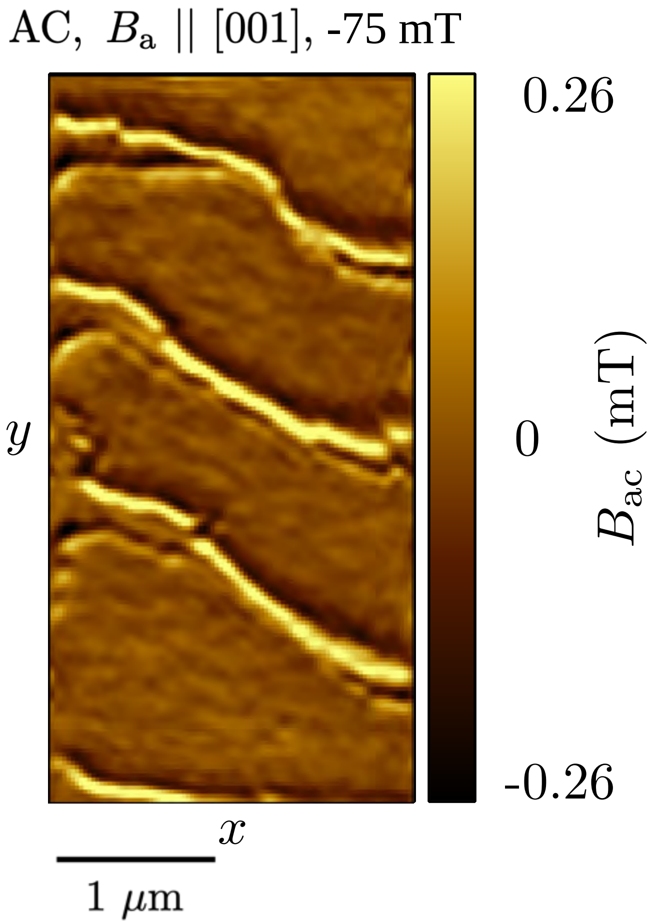

Cu_2OSeO_3 – Field decrease study

University of Basel

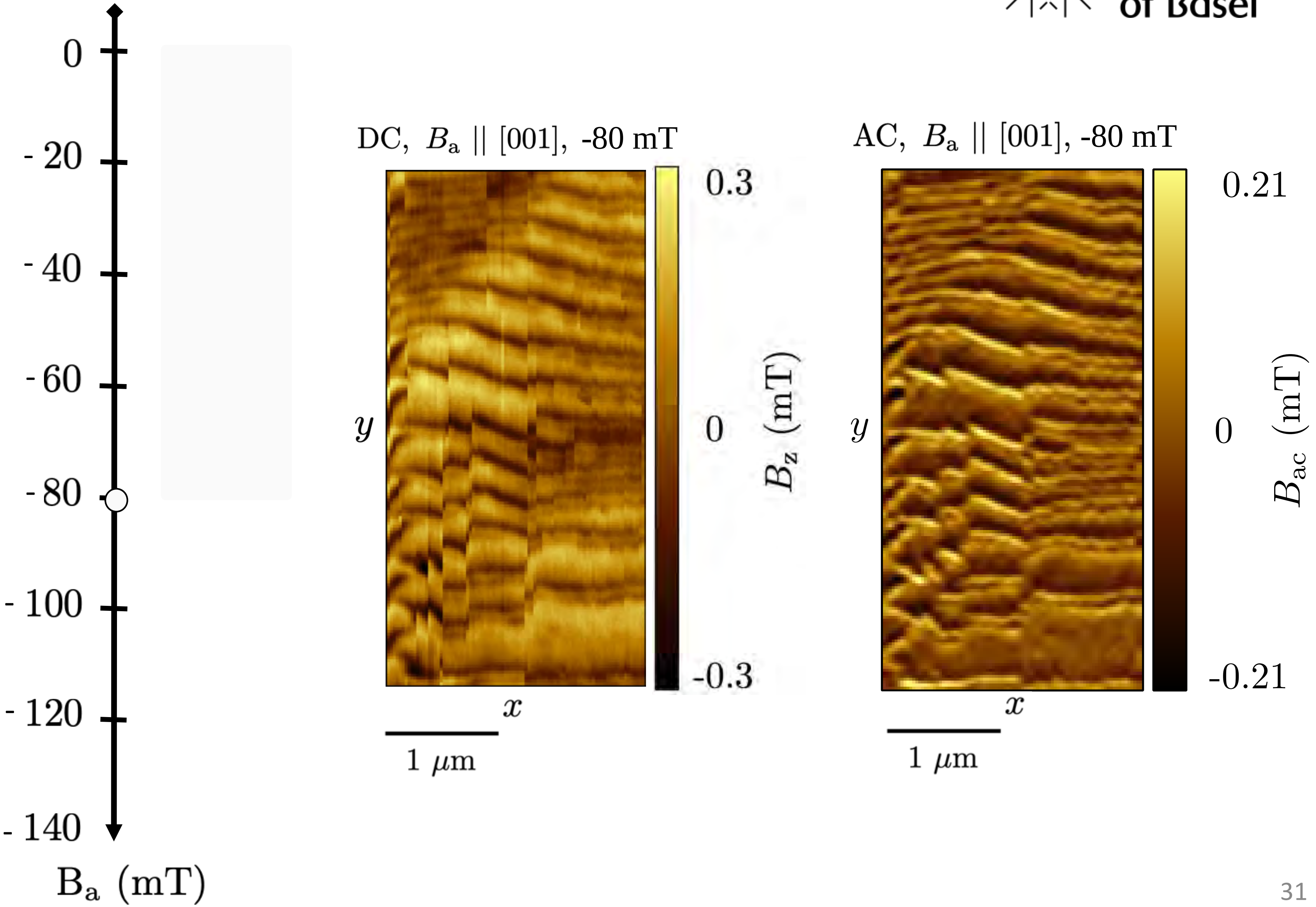

Cu_2OSeO_3 – Field decrease study

University of Basel

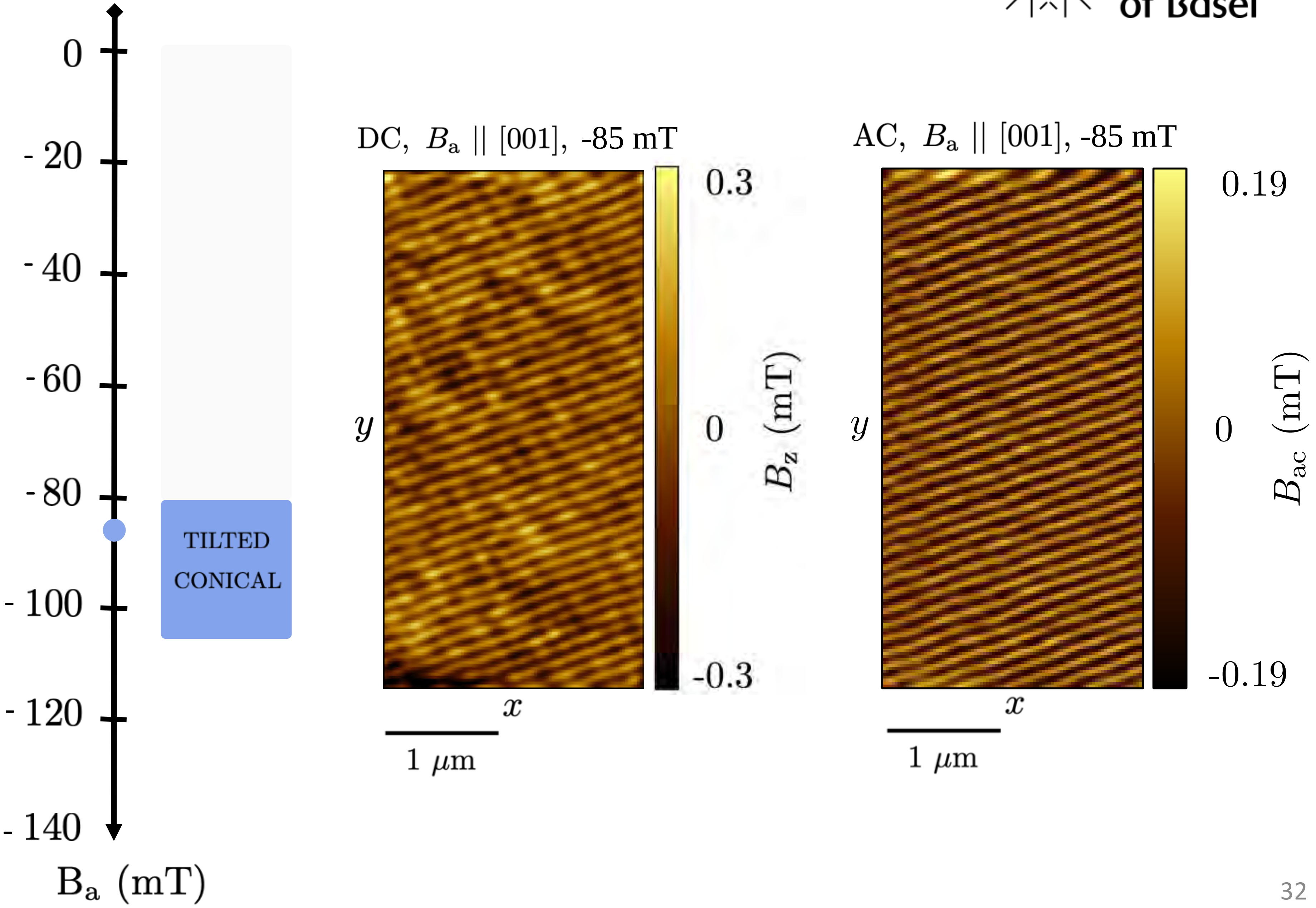

Cu_2OSeO_3 – Field decrease study

University of Basel

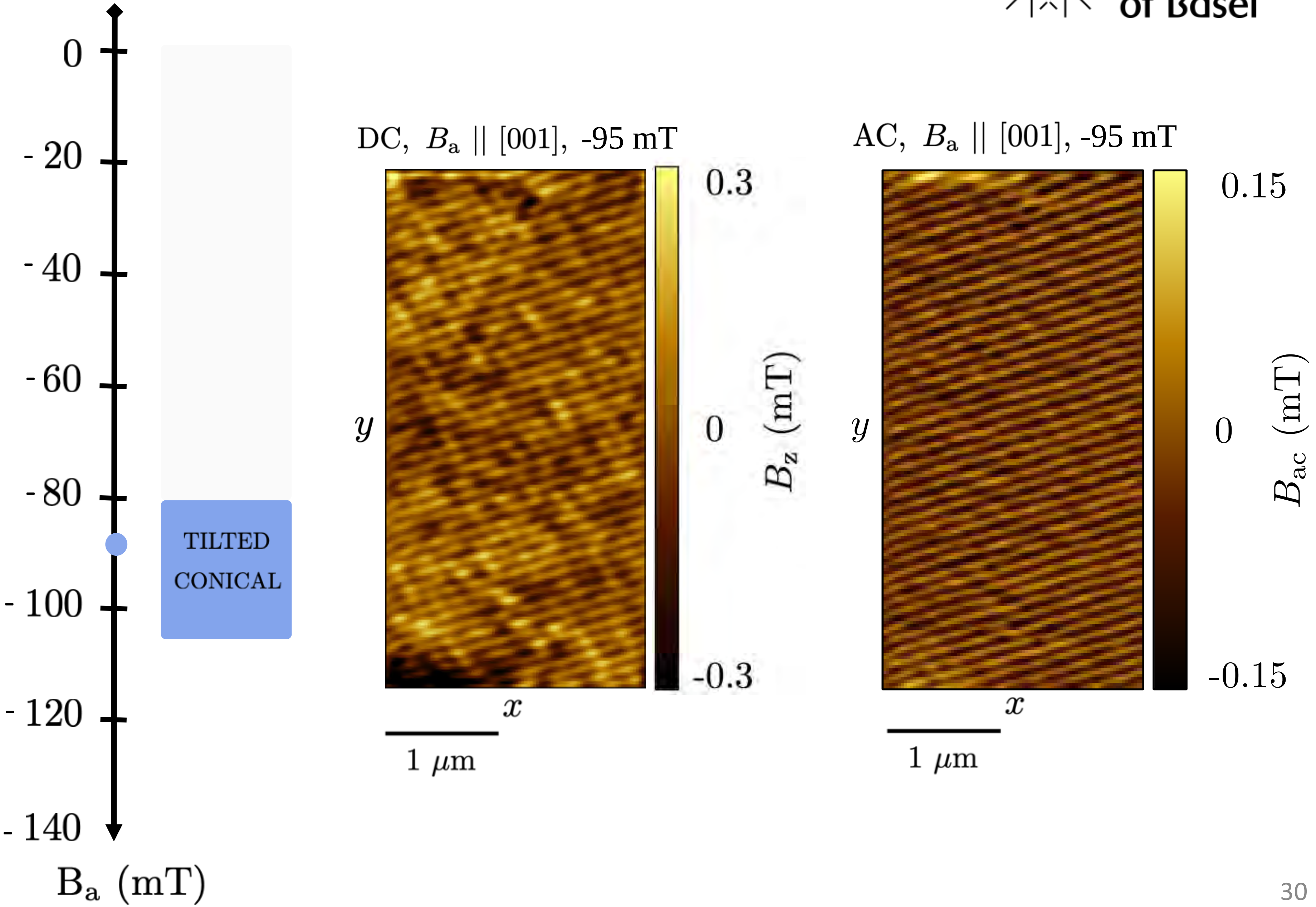

Cu_2OSeO_3 – Field decrease study

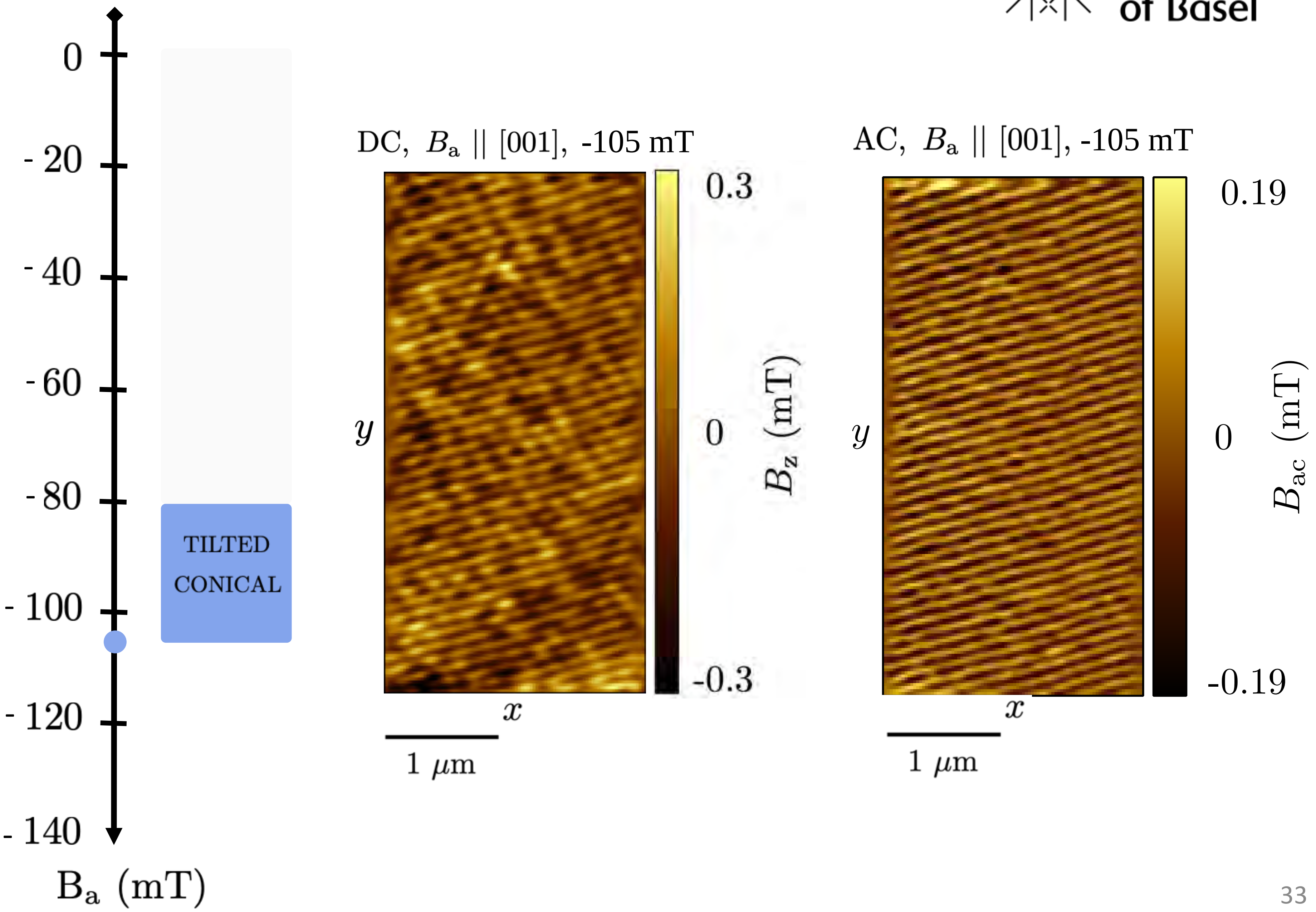

Cu_2OSeO_3 – Field decrease study

University of Basel

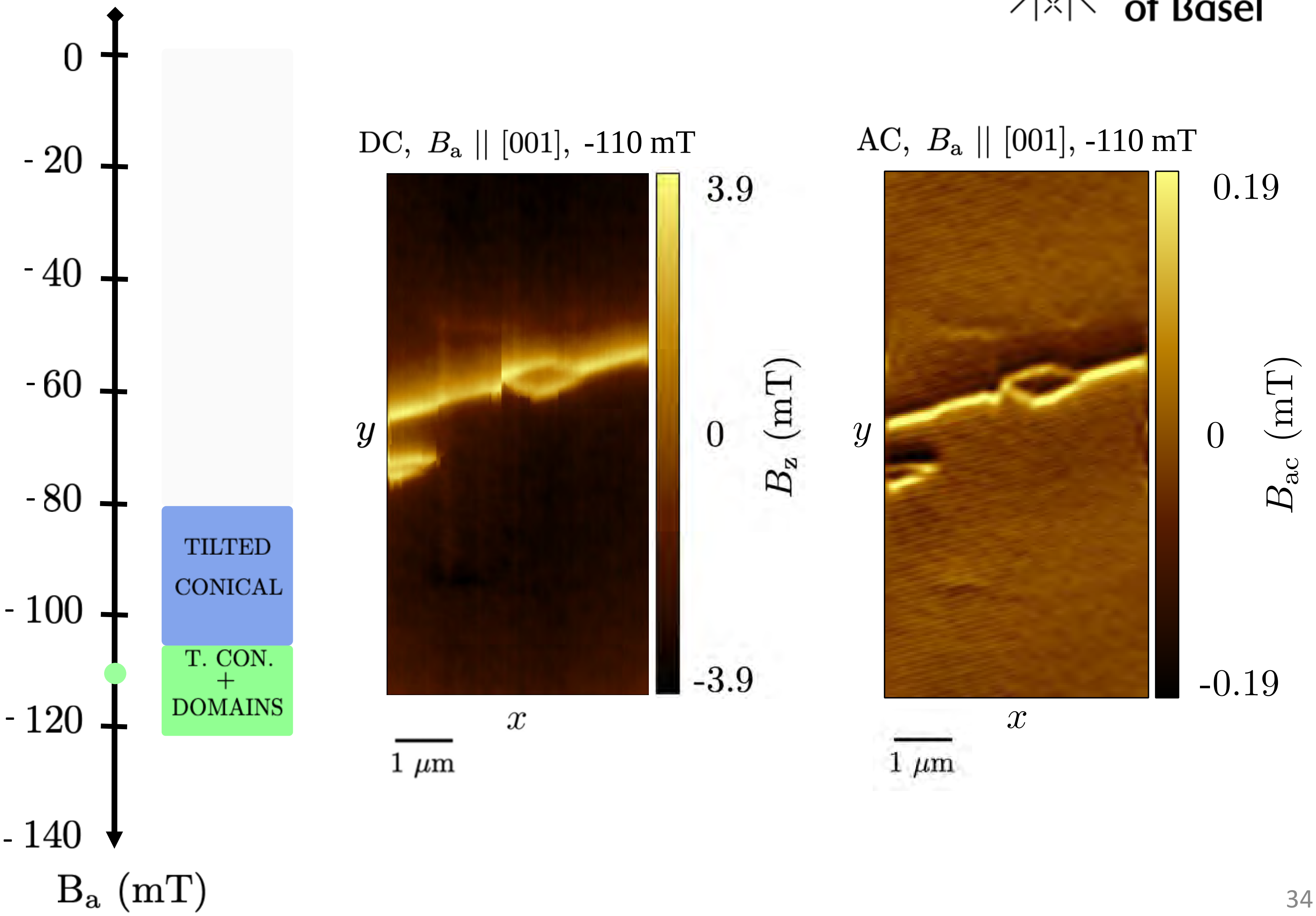

Cu_2OSeO_3 – Field decrease study

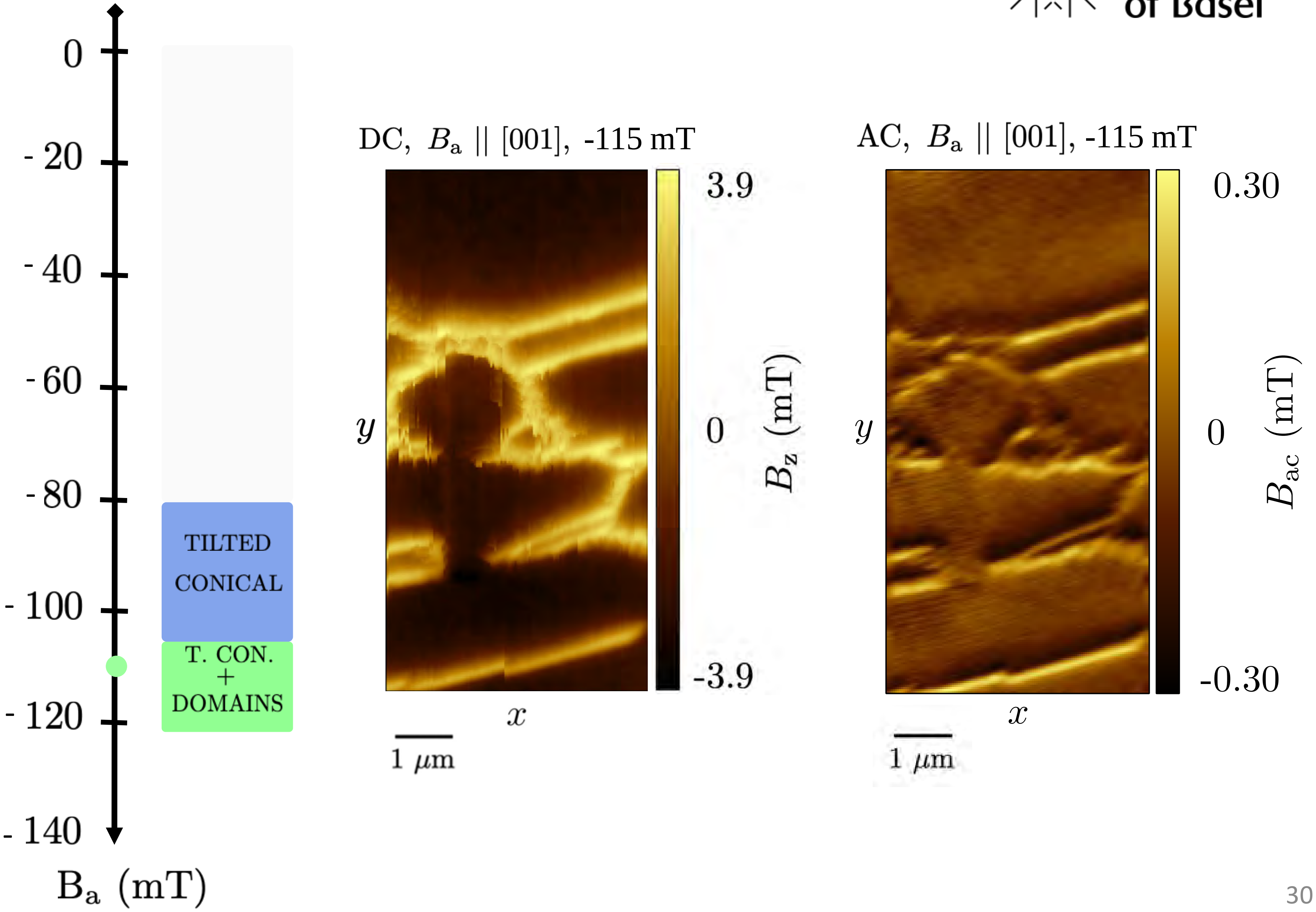

Cu_2OSeO_3 – Field decrease study

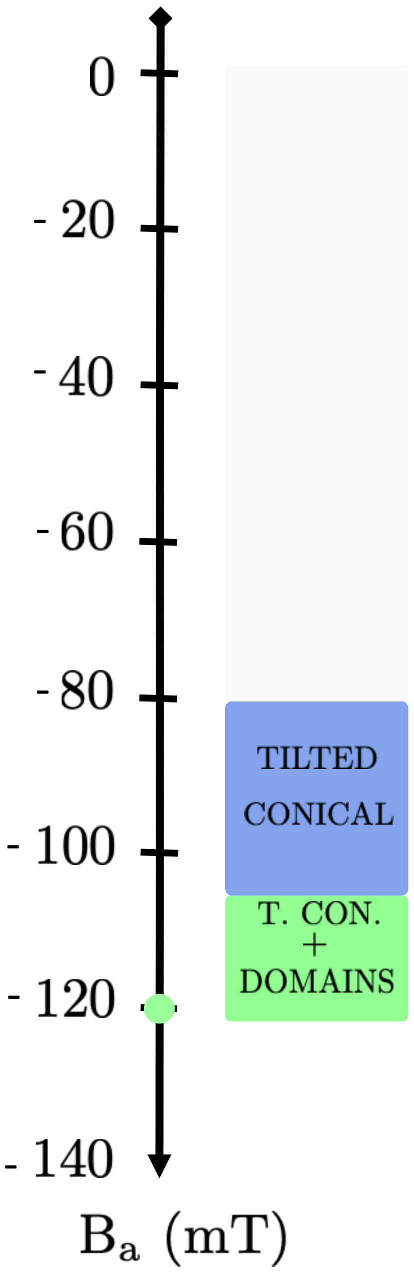

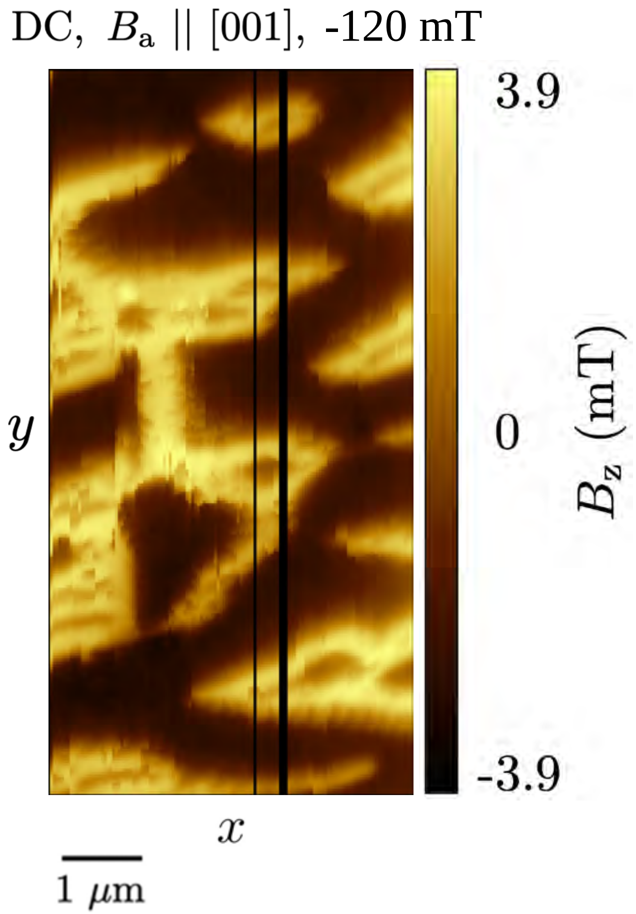

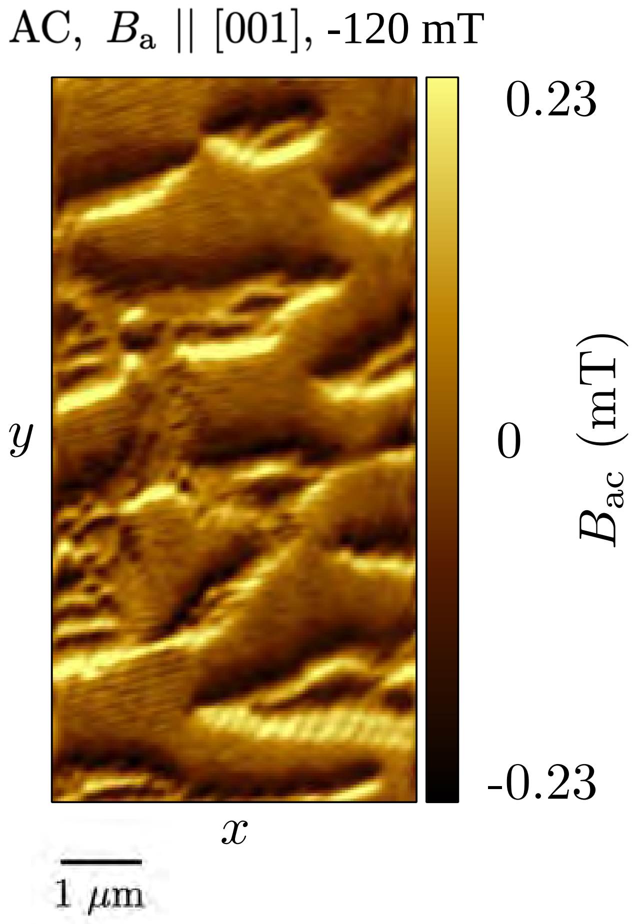

Cu_2OSeO_3 – Field decrease study

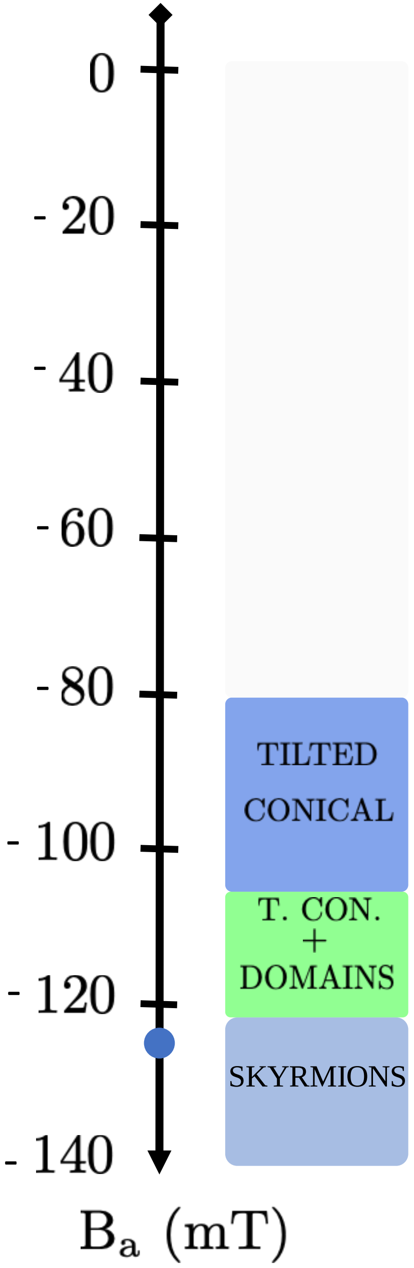

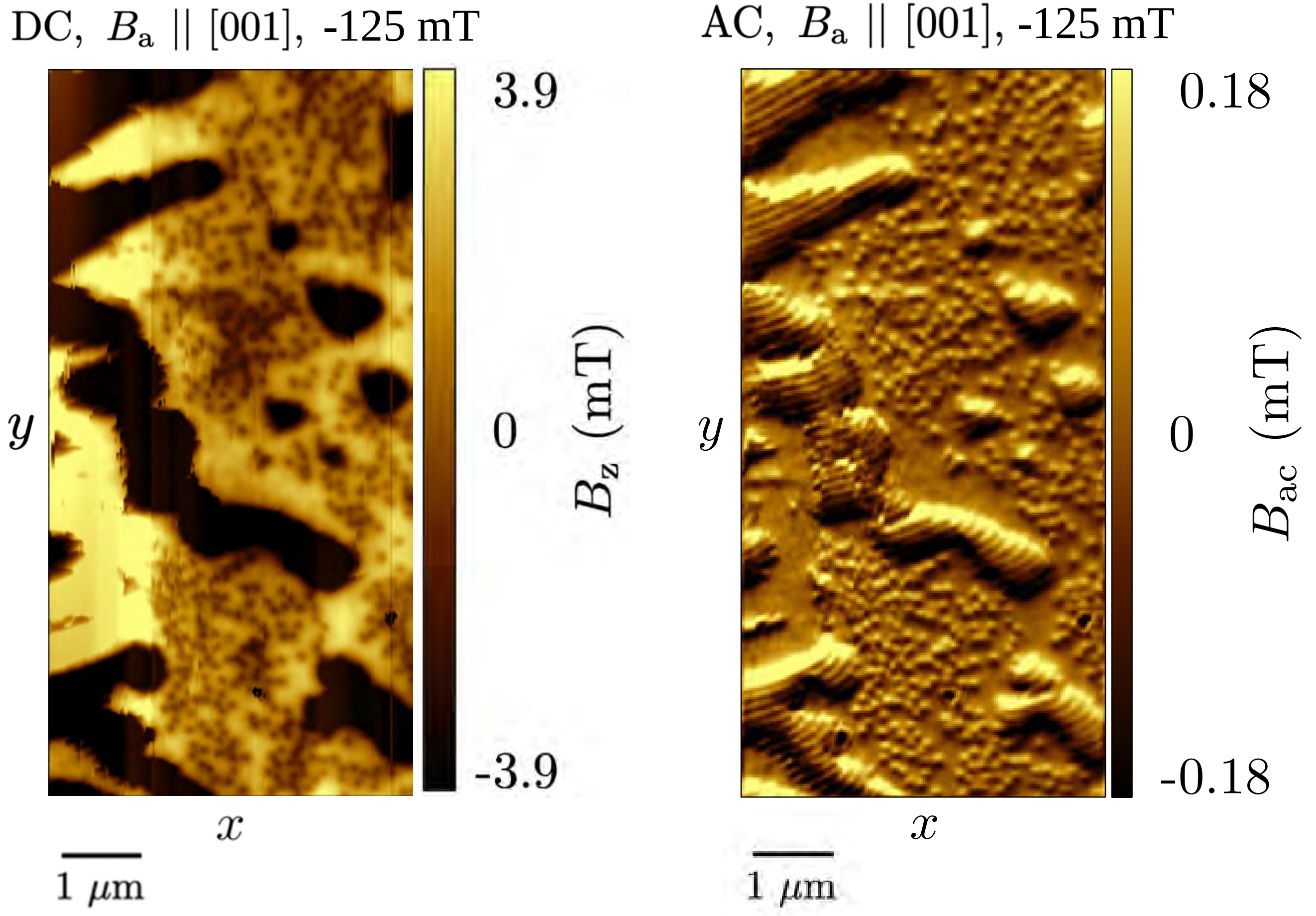

Cu_2OSeO_3 – Field decrease study

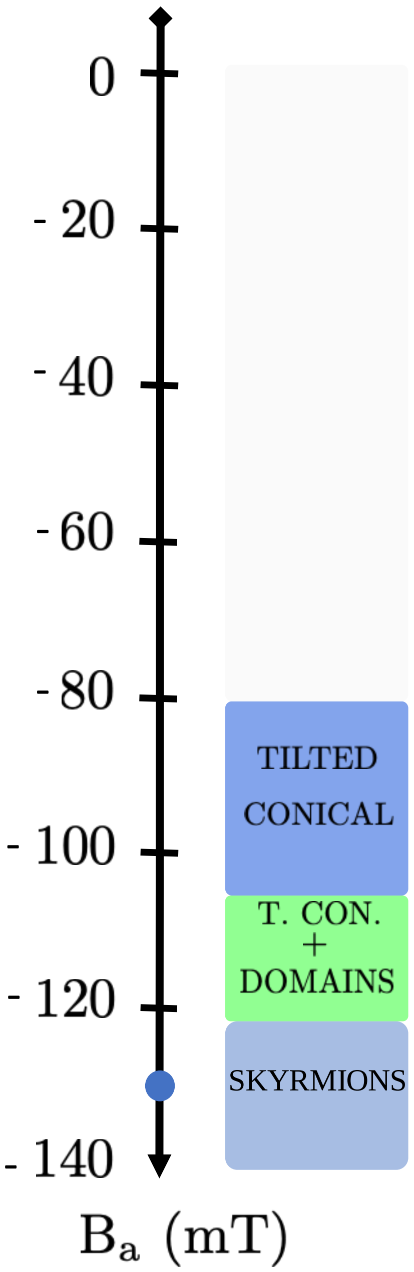

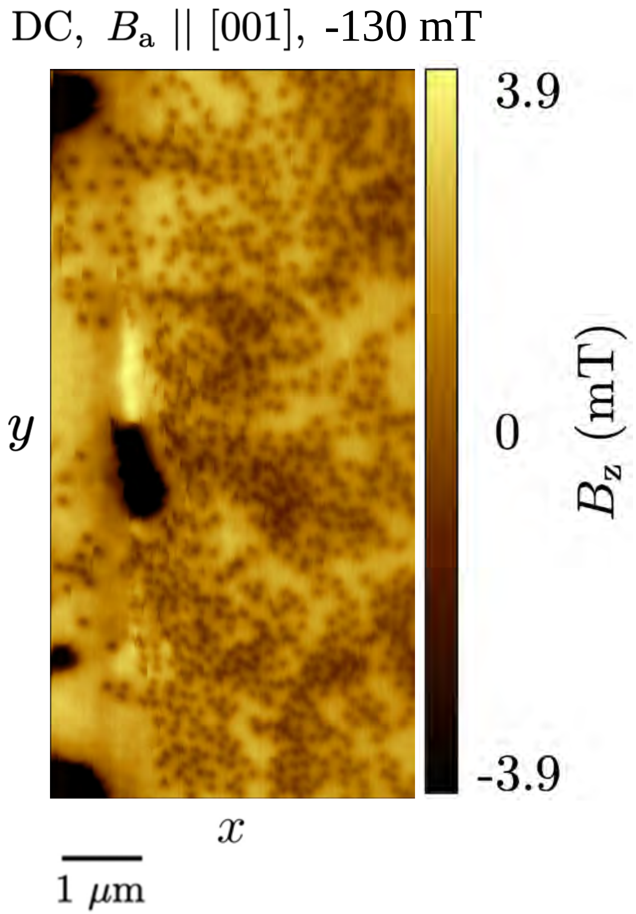

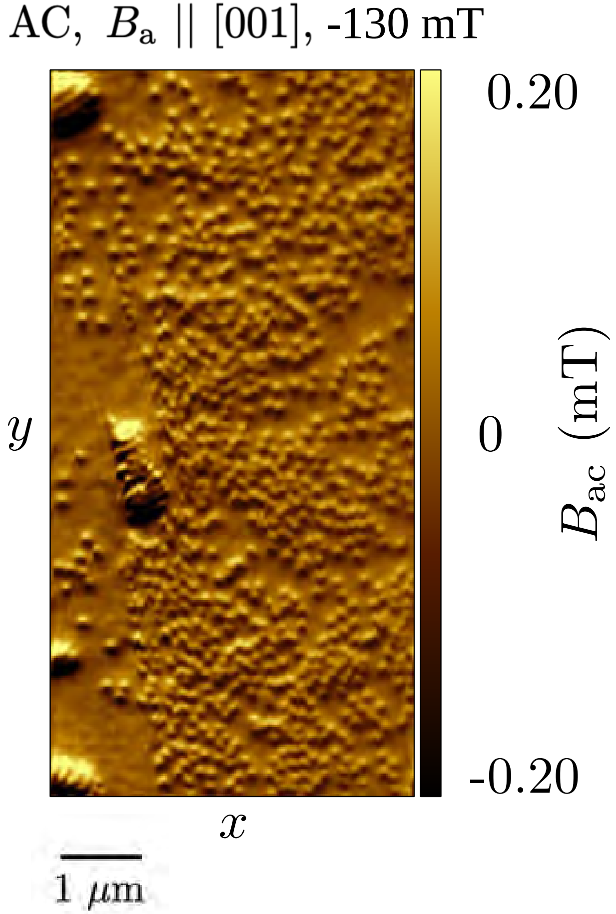

Cu_2OSeO_3 – Field decrease study

University of Basel

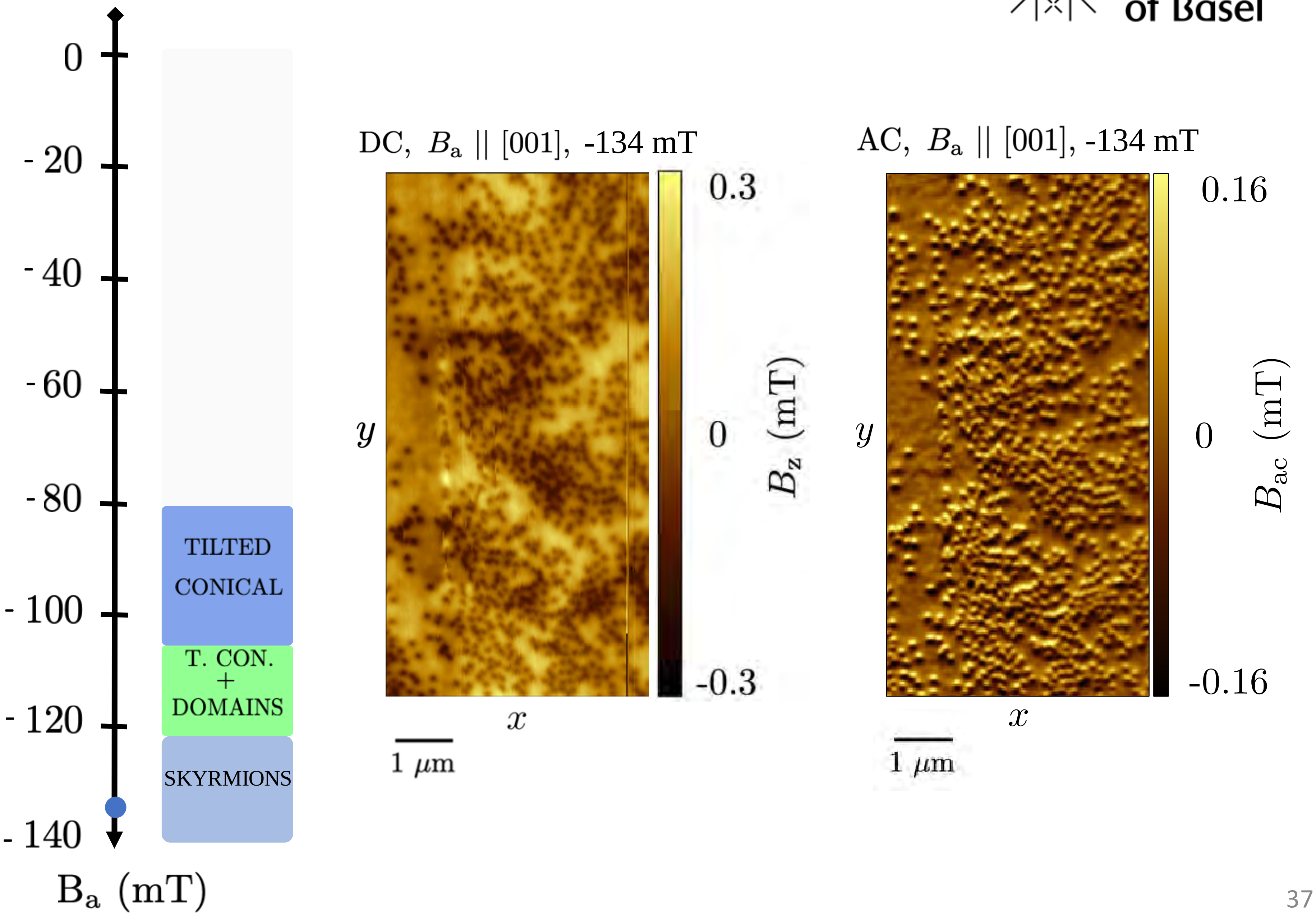

Cu_2OSeO_3 – Field decrease study

University of Basel

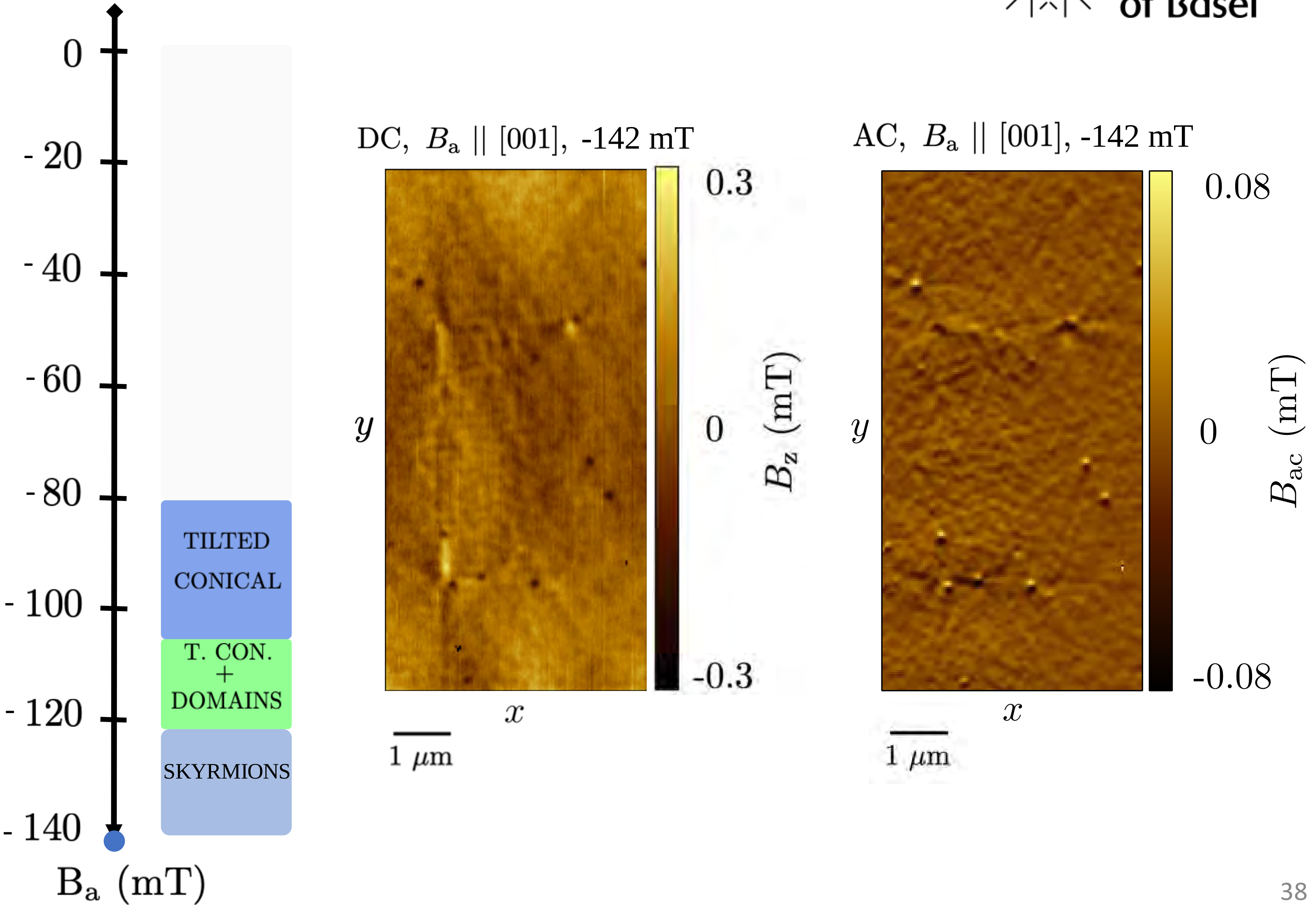

No translational or orientational order

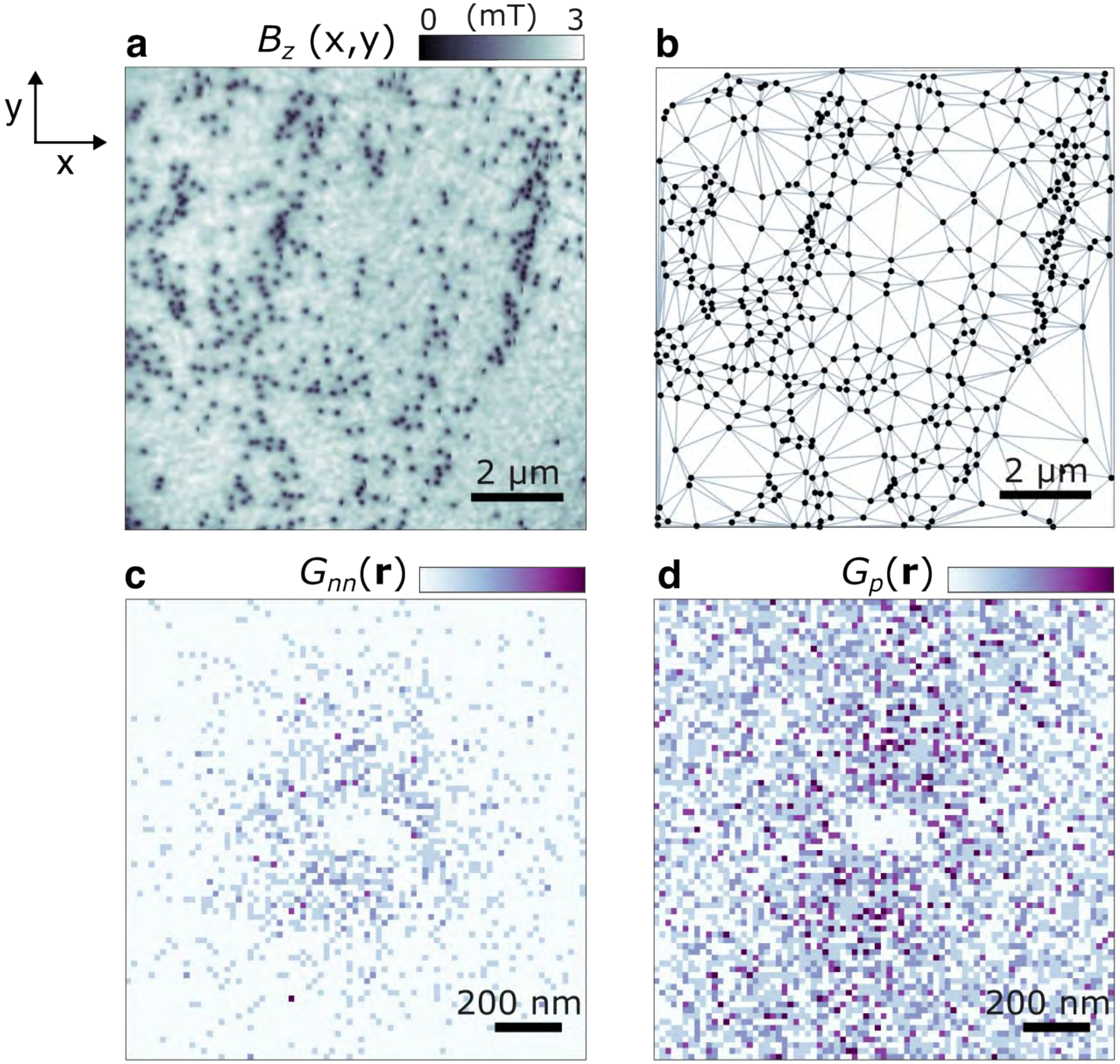

Skyrmion manipulation

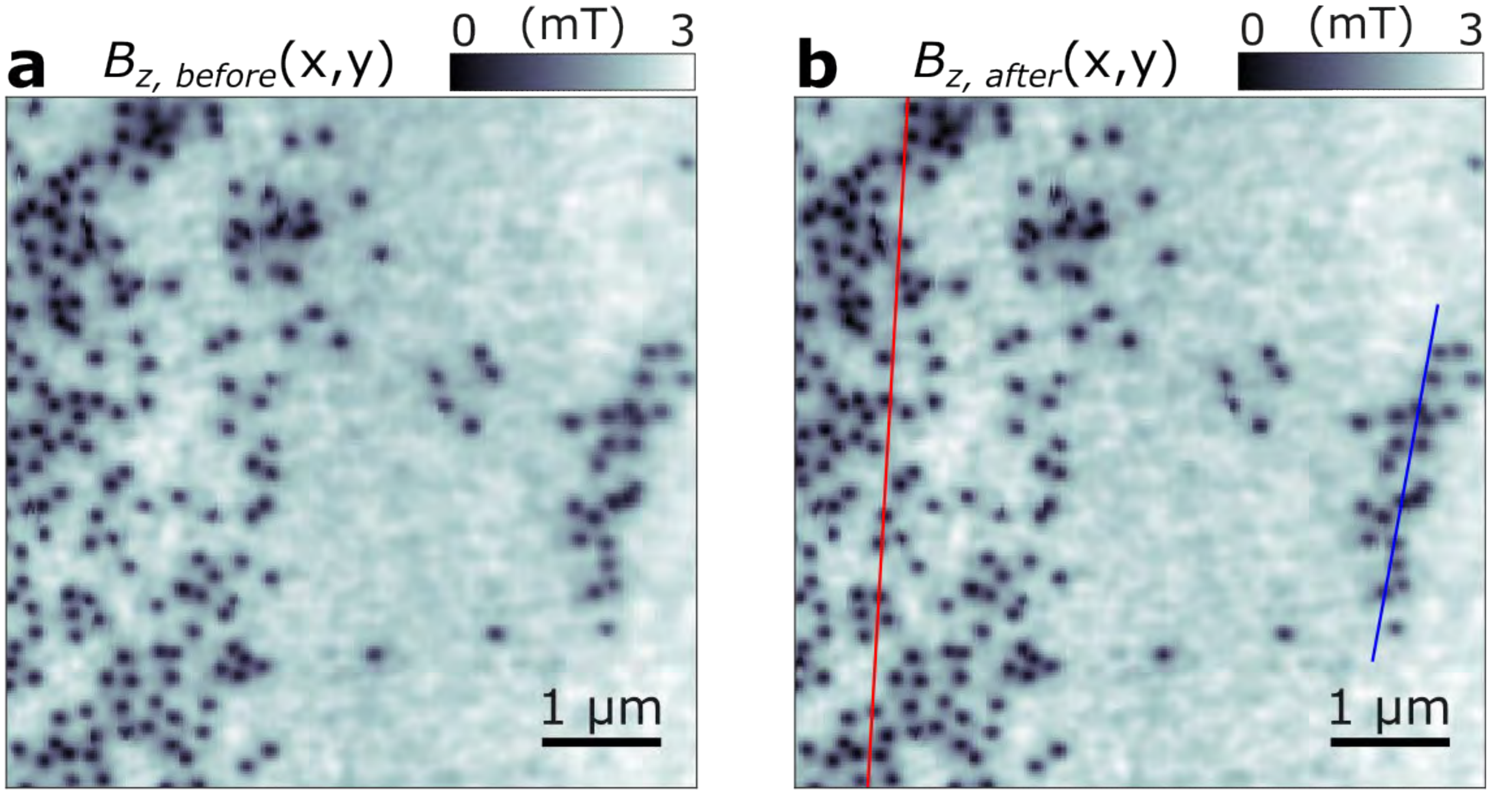

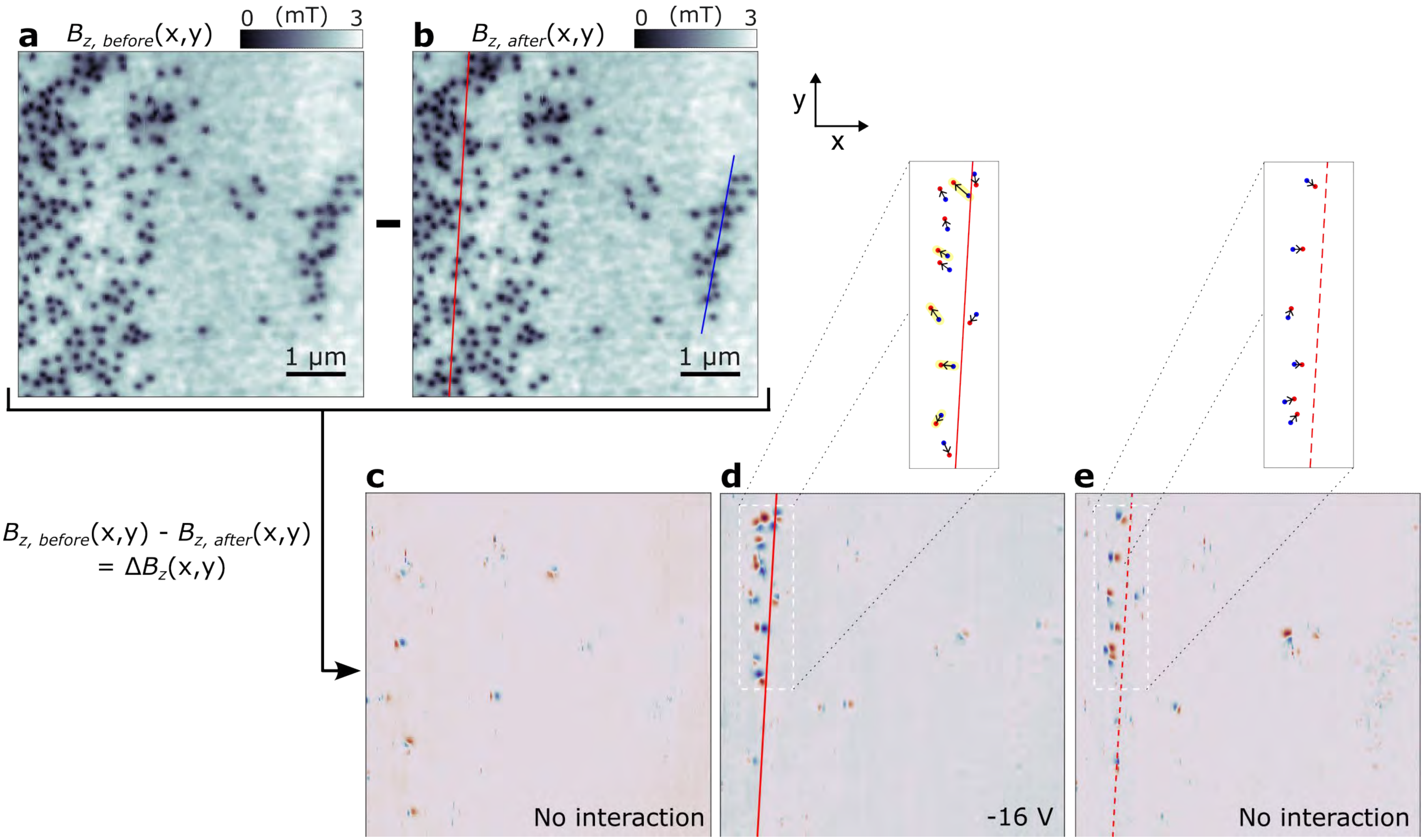

a
$B_{z,\ before}(x,y)$
0 (mT) 3
1 μm
b
$B_{z,\ after}(x,y)$
0 (mT) 3
1 μm
y
x
$B_{z,\ before}(x,y) - B_{z,\ after}(x,y) = \Delta B_z(x,y)$
c
No interaction
d
-16 V
e
No interaction

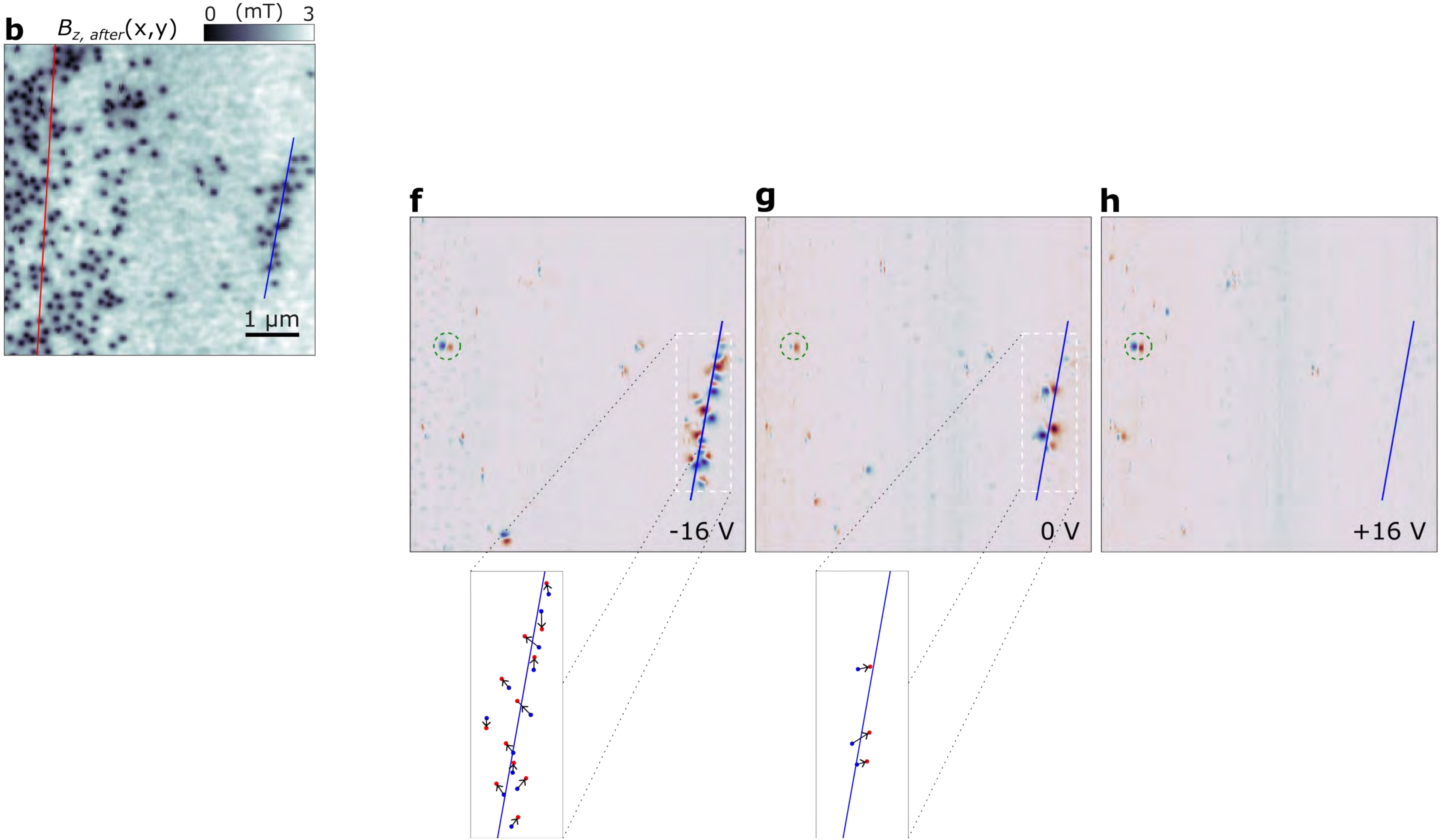

b
$B_{z,\,after}(x,y)$
0 (mT) 3
1 μm
f
g
h
-16 V
0 V
+16 V

Cu_2OSeO_3 Results

- Images of the low-temperature magnetic skyrmion phase at the surface of bulk Cu_2OSeO_3
- Images reveal clusters of skyrmions whose disordered configurations are dominated by pinning effects
- Although some configurations observed at the surface are consistent with what is observed in measurements of the bulk, we find evidence for surface states
- Individual skyrmions can be manipulated by local electric fields in an insulator
- No skyrmions are created or destroyed

Marchiori et al., Romagnoli et al., in preparation

Magnetic imaging by "force microscopy" with 1000 Å resolution

Y. Martin and H. K. Wickramasinghe
IBM T. J. Watson Research Center, P. O. Box 218, Yorktown Heights, New York 10598

(Received 19 December 1986; accepted for publication 19 March 1987)

We describe a new method for imaging magnetic fields with 1000 Å resolution. The technique is based on using a force microscope to measure the magnetic force between a magnetized tip and the scanned surface. The method shows promise for the high-resolution mapping of both static and dynamic magnetic fields.

Appl. Phys. Lett. 50 (20), 18 May 1987

Magnetic force microscopy: General principles and application to longitudinal recording media

D. Rugar, H. J. Mamin, P. Guethner,[a] S. E. Lambert,[b] J. E. Stern,[c] I. McFadyen,[b] and T. Yogi[b]
IBM Research Division, Almaden Research Center, 650 Harry Road, San Jose, California 95120-6099

(Received 15 January 1990; accepted for publication 13 April 1990)

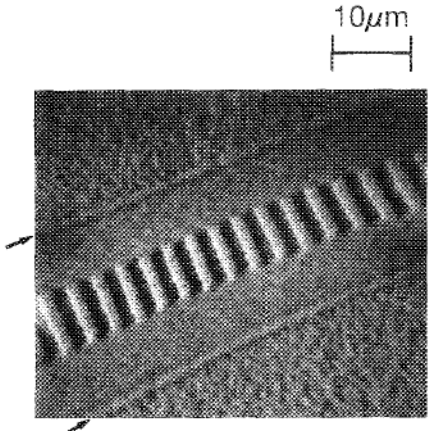

J. Appl. Phys. 68 (3), 1 August 1990

MFM achieves down to 10 nm resolution

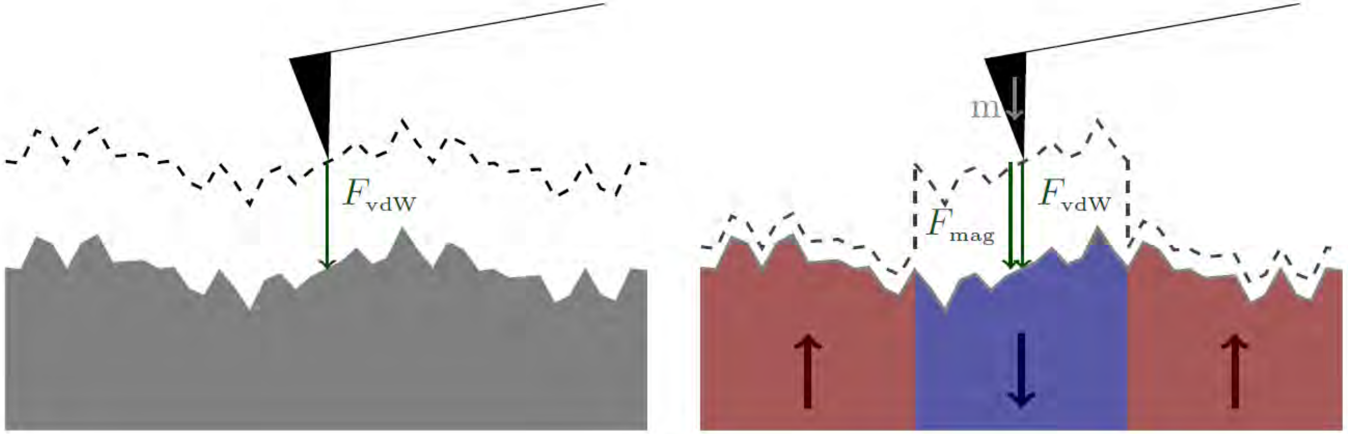

Schwenk, *Ph.D. Thesis in Physics,* University of Basel (2016).

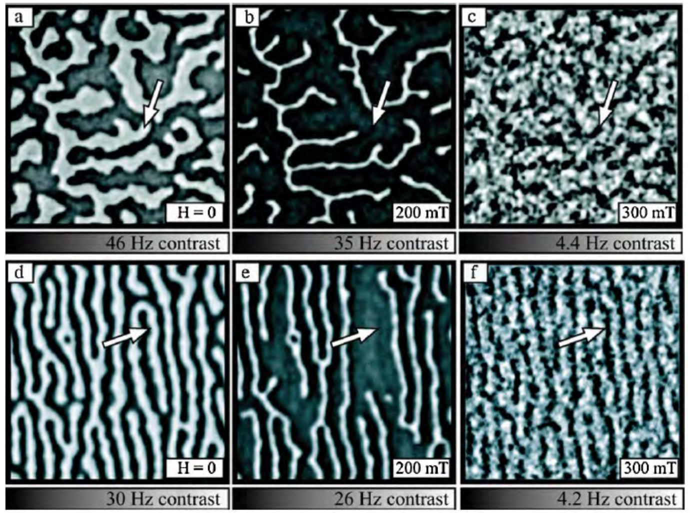

Schmid et al., *Phys. Rev. Lett.* **105**, 197201 (2010).

Nanowires as force sensors and scanning probes

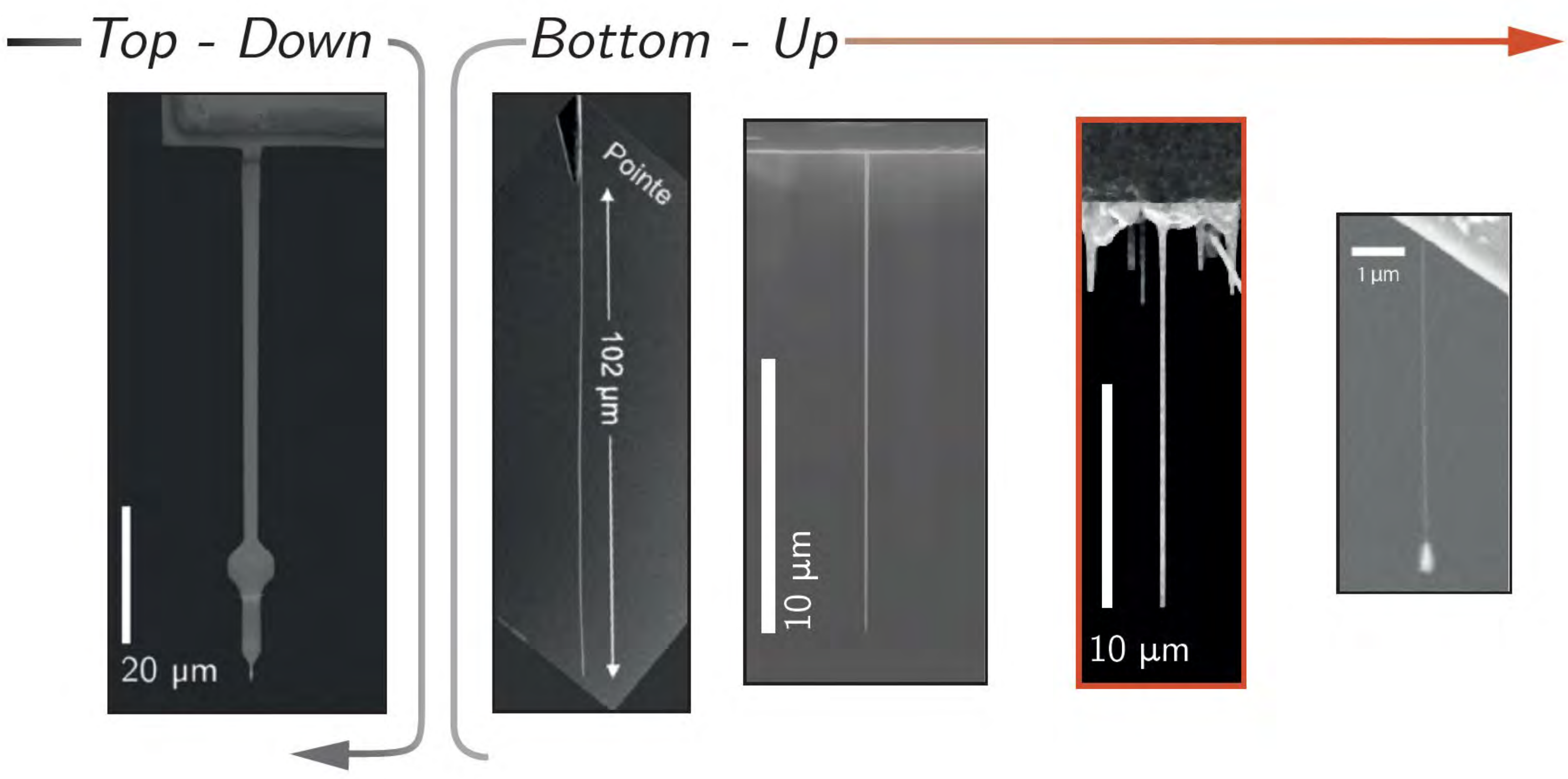

Rossi, *Ph.D. Thesis in Physics,* University of Basel (2019).

NW Cantilevers

Table 1. Experimentally determined parameters of singly-clamped NW cantilevers. Here the diameter d is the average cross-sectional width and $\omega_0/2\pi$ is the average frequency of the fundamental flexural mode doublet. The quality factor Q is the average value of the fundamental flexural mode doublet, taken for a freestanding NW, far from any sample surface and measured at low ambient pressures. RT stands for room temperature.

Material	Cross-section	d (nm)	L (μm)	$\omega_0/2\pi$ (kHz)	k (N m^{-1})	Q	Reference
GaAs/AlGaAs	Hexagonal	350	25	417	1×10^{-2}	50 000 (4 K)	[9, 10]
GaAs	Hexagonal	234	16.8	598	8.3×10^{-3}	46 553 (4 K)	[11]
GaAs	Hexagonal	100	<25	1197	8.3×10^{-3}	4900 (RT)	[12]
GaAs/AlGaAs	Hexagonal	390	20	795	9×10^{-2}	6700 (4K)	[13]
GaAs	Hexagonal	130	14.5	465	—	2000–3000 (RT)	[14]
InAs	Hexagonal	60–80	4–5.5	2023.9	3.6×10^{-3}	1752 (RT)	[15]
SiC	Circular	150	52	113	4×10^{-4}	2890 (RT)	[1]
SiC	Circular	200	50	78	1.5×10^{-4}	1000 (RT)	[16]
SiC	Circular	120	165	6.7	3×10^{-6}	3000 (RT)	[17]
SiC	Circular	284	128	33	—	36 000 (RT)	[18]
SiC	Circular	206	93	43	—	159 000 (RT)	[18]
SiC	Circular	50	7	1519	—	2500 (RT)	[19]
SiC	Circular	300	6	6140	1.5	33 (RT, Air)	[20]
Si	Circular	44	14.4	210.5	2.8×10^{-5}	9250 (RT)	[21]
Si	Circular	46	12.9	273	6.6×10^{-5}	7250 (RT)	[21]
Si	—	35	15	1060	6.5×10^{-4}	25 000 (8 K)	[6]
Si	—	50	15	333	1.5×10^{-4}	18 000 (6 K)	[7]
Si	Circular	50	15	197.5	2.0×10^{-5}	3000–3500 (RT)	[22]
Si	Elongated circular	60, 80	20	342	1×10^{-4}	8150 (4K)	[8]
Si	Hexagonal	100–300	5–10	2000–6000	—	2000 (RT)	[23]
Si	Hexagonal	165	12.7	1772.4	—	3000 (RT)	[24]
Si	Hexagonal	90	9.3	2504.3	—	3000 (RT)	[24]
Si	Hexagonal	100–200	6–8	3500–4000	$2.4 - 5 \times 10^{-2}$	3000–3500 (RT)	[25]
Si	Hexagonal	150 (clamp), 60 (tip)	11.3	2480	—	—	[26]
Si	Hexagonal	39–400	2–20	1000–12 000	—	3000–25 000 (RT)	[27]
Si (metallized)	Hexagonal	142	2.25	200 000	110.3	2000 (25 K)	[28]
Si (metallized)	Hexagonal	118	2.1	188 000	62.9	2500 (25 K)	[28]
Si	Hexagonal	81	1.69	215 000	31.4	5750 (25 K)	[28]
Si	Hexagonal	74	2.77	80 000	6.0	13 100 (25 K)	[28]
CNT	Circular	50	18	270	$\sim 10^{-4}$	250 (RT)	[29]
CNT	Circular	1–3	5	38 178.5	4.5×10^{-8}	2245 (RT)	[30]
CNT	Circular	4	1.2	5955	2.1×10^{-5}	—	[31]
CNT	Circular	—	—	363.5	4.8×10^{-6}	571 (RT)	[31]

Braakman & Poggio, *Nanotechnology* **30**, 332001 (2019).

GaAs NWs

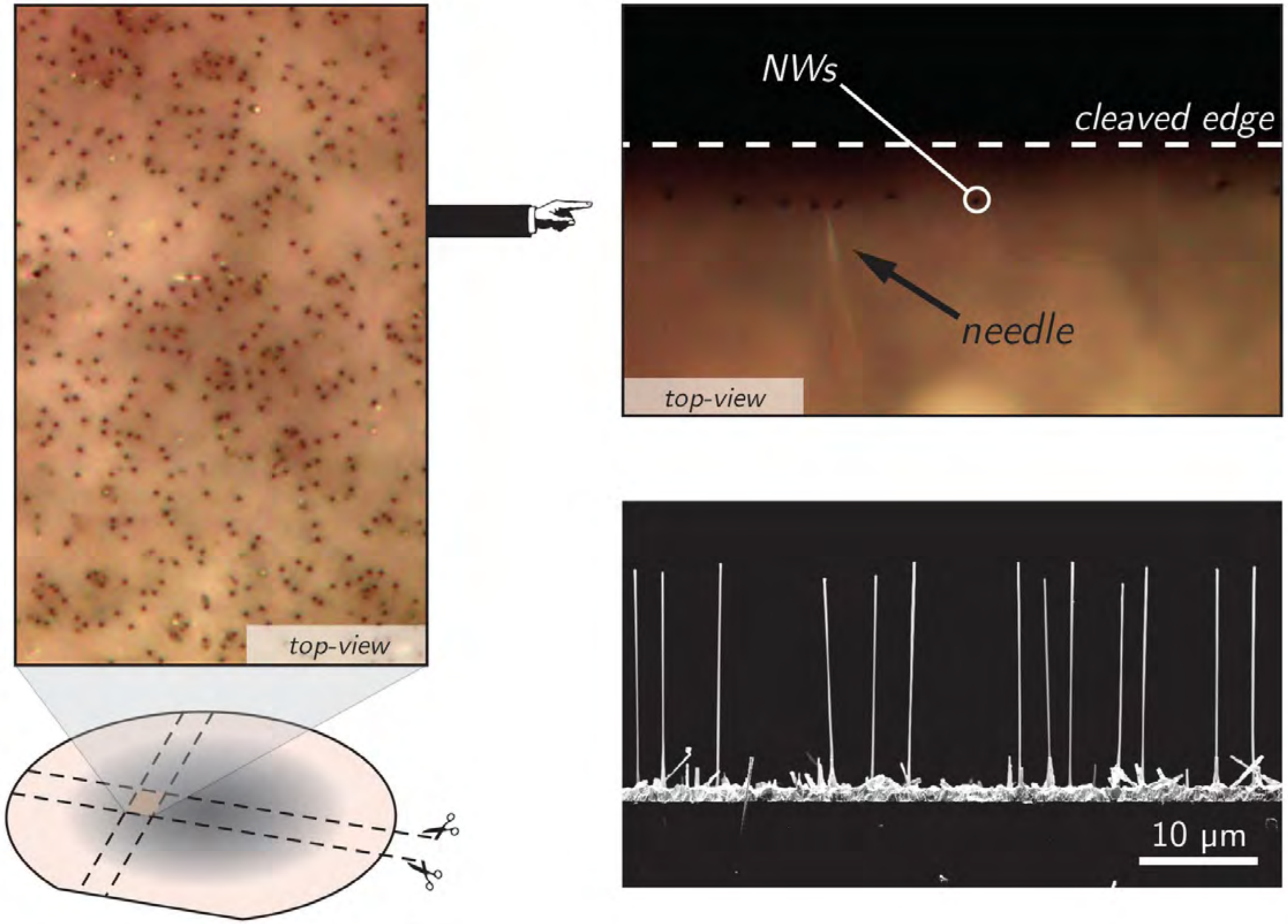

NWs from Fontcuberta group.

NW force microscope

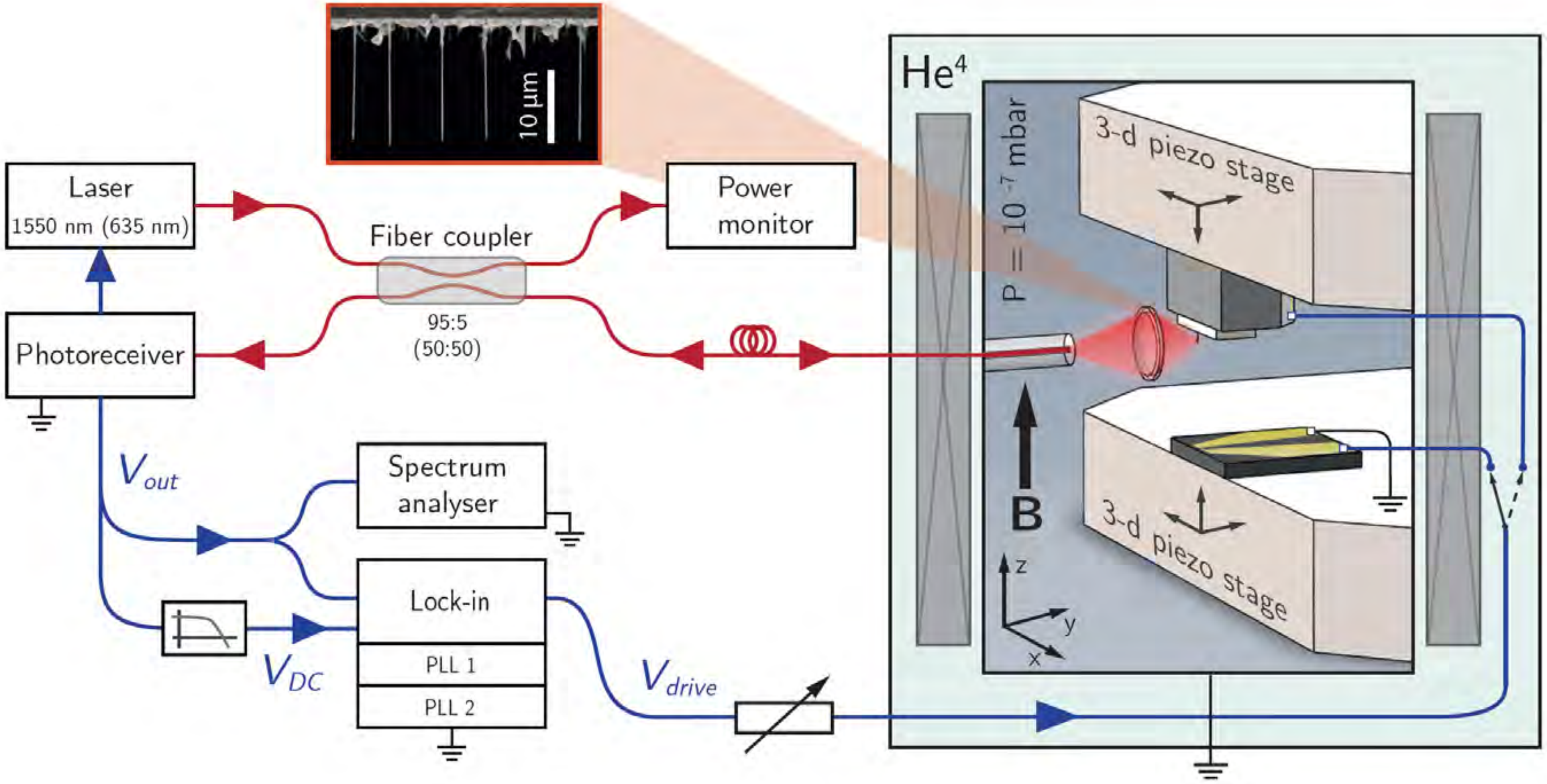

NW force microscope

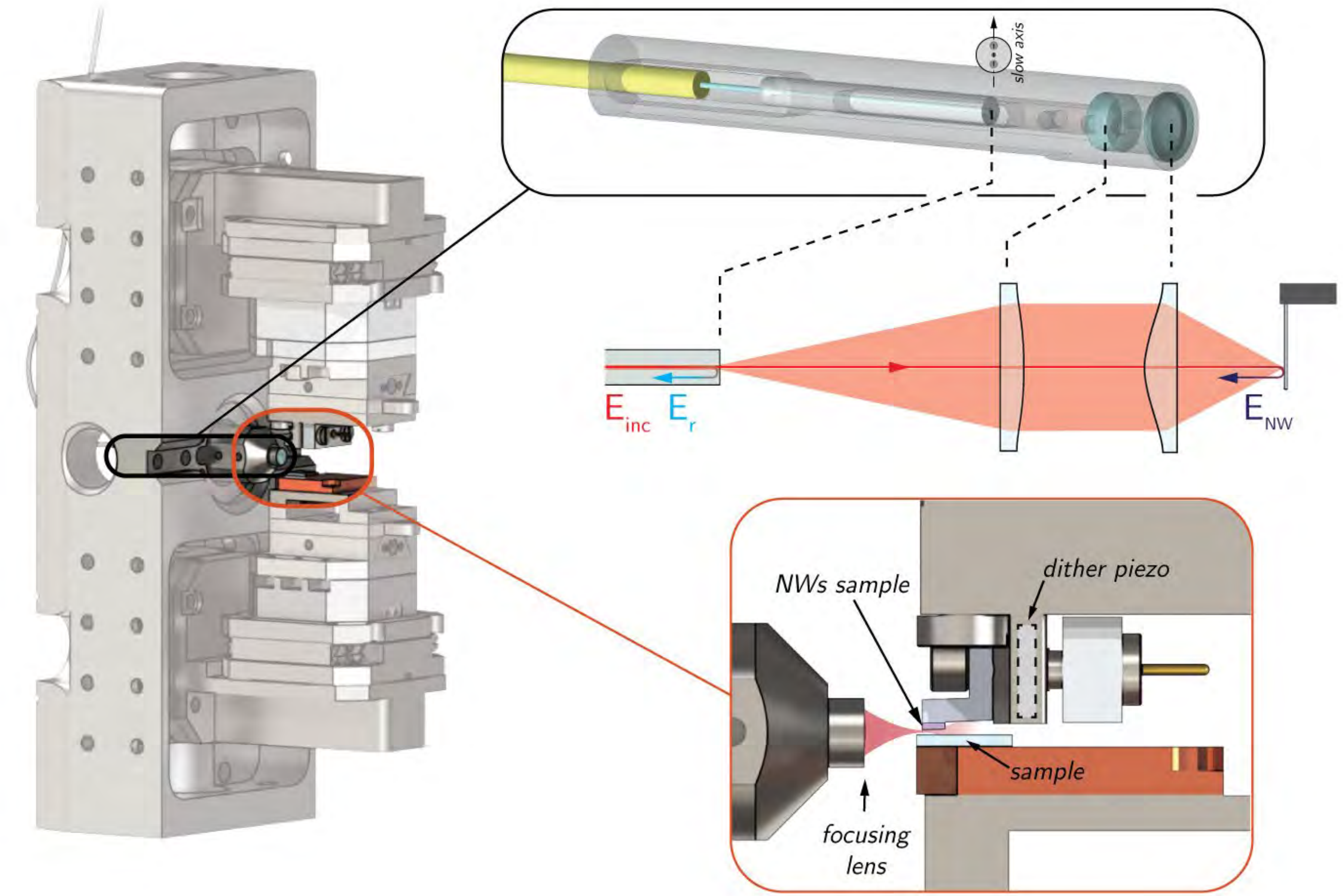

Rossi, *Ph.D. Thesis in Physics,* University of Basel (2019).

Interferometric diplacement detection

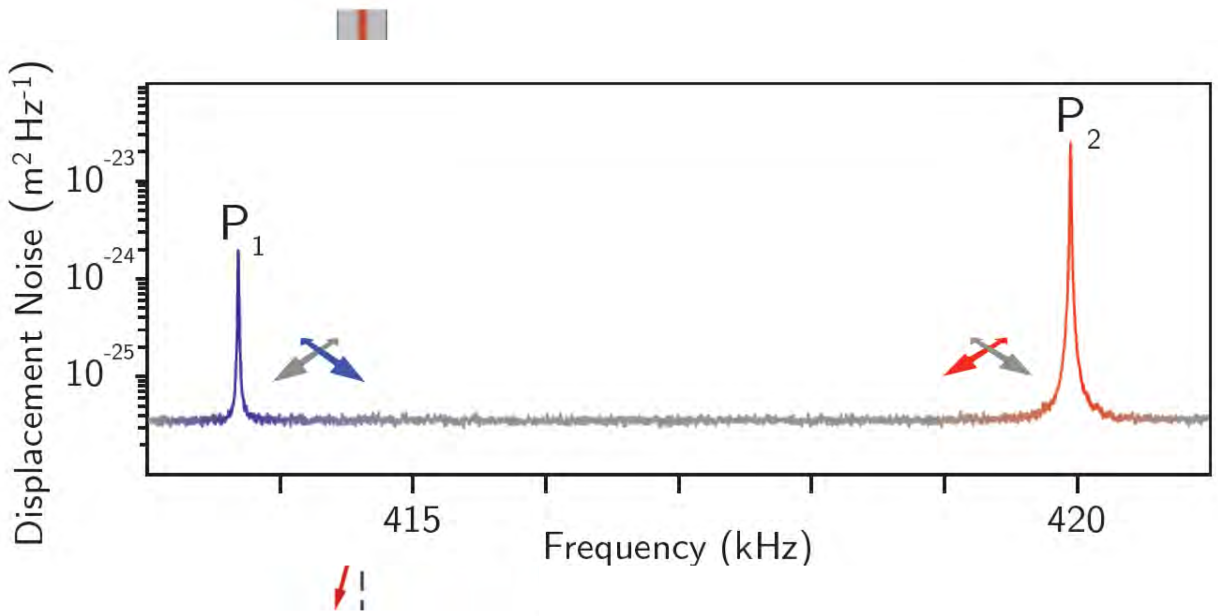

Scanning nanowire microscopy

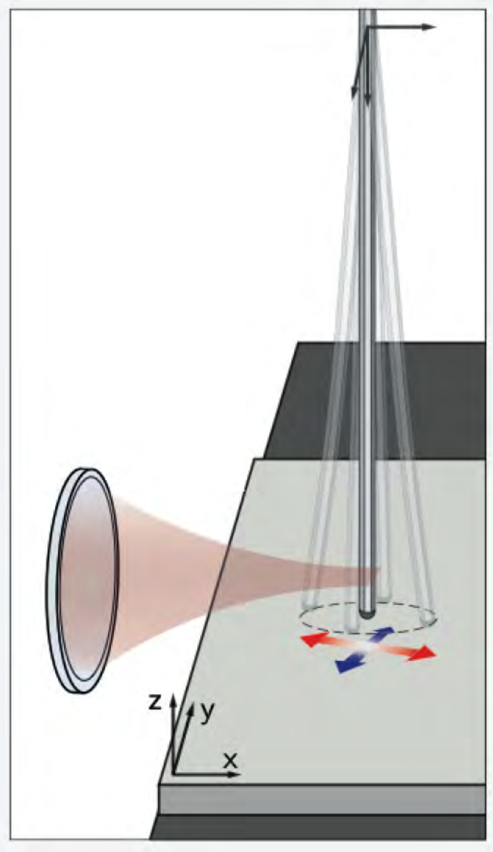

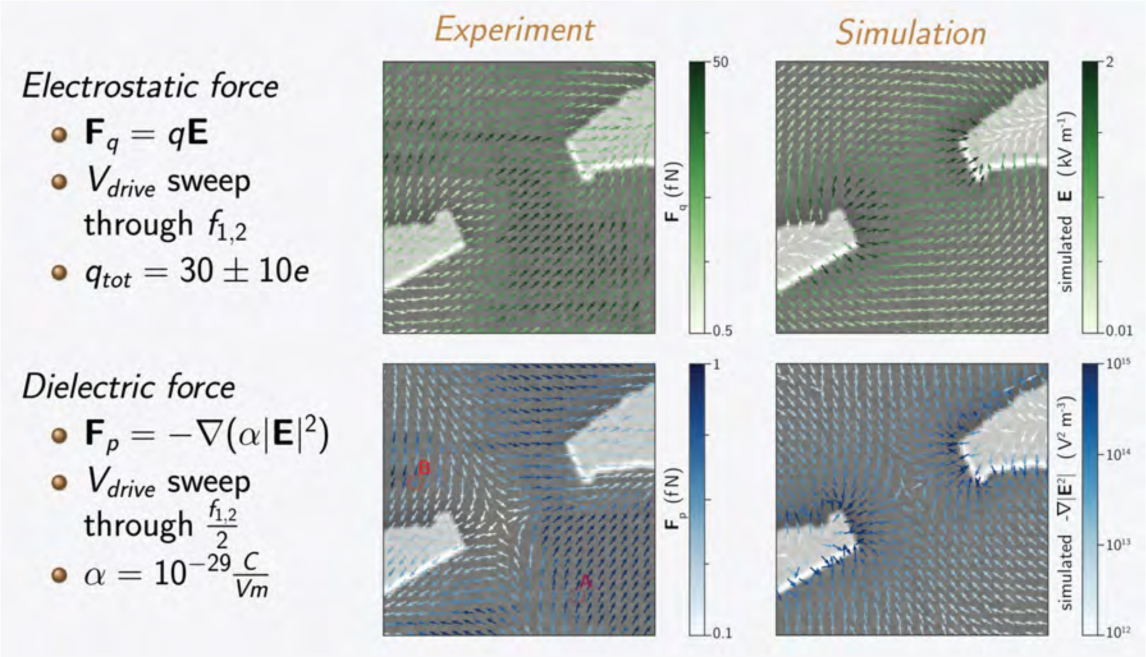

Rossi et al., *Nat. Nanotechnol.* **12**, 150 (2017).

Mercier de Lépinay et al., *Nat. Nanotechnol.* **12**, 156 (2017).

NWs with magnetic tips

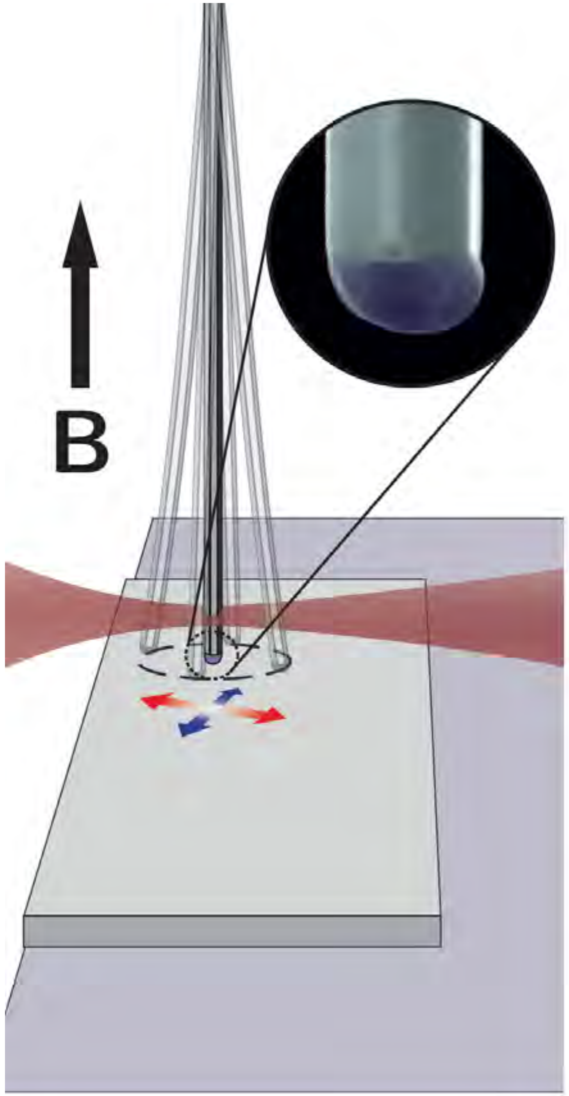

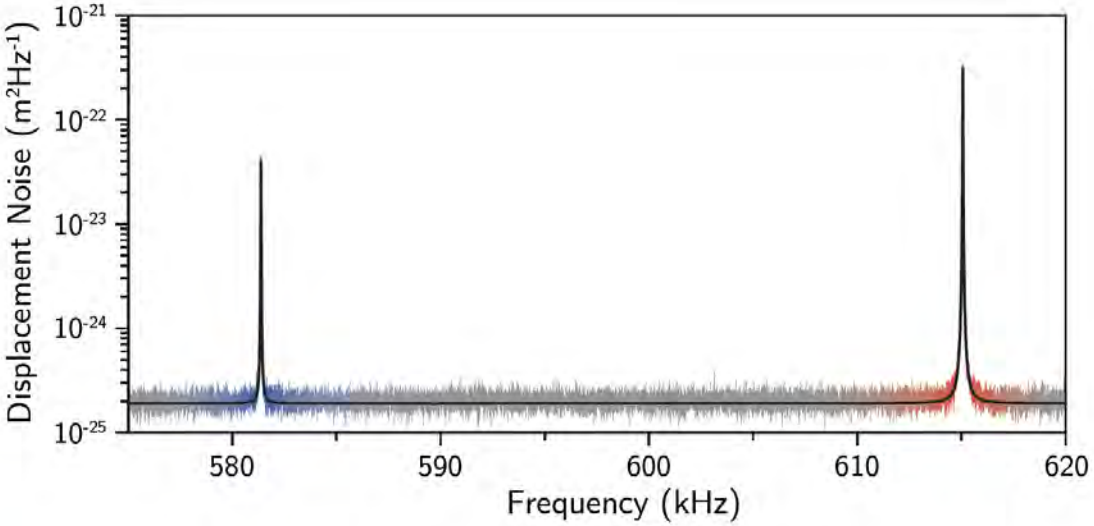

Length $\sim 17 \pm 1\,\mu$m with diameter $\sim 225 \pm 15$ nm

- $f \sim [500 - 700]$ kHz
- $Q \sim [30 - 50] \times 10^3$
- $k \sim [1 - 10]$ mN/m
- $M \sim 700$ fg
- $\Gamma \sim 50 \times 10^{-15}$ kg/s
- $F_{min} \sim 4$ aN/$\sqrt{\text{Hz}}$

Rossi et al., *Nano Lett.* **19**, 930 (2019).

Quantifying sensitivity

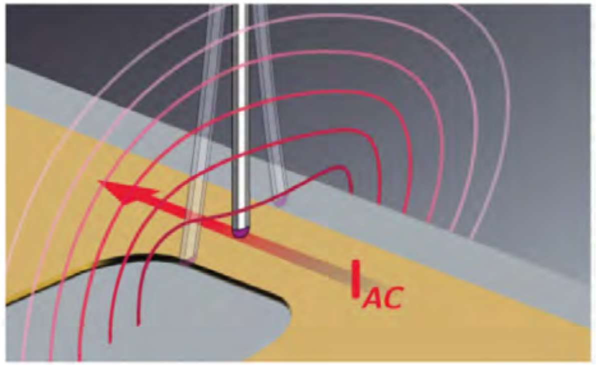

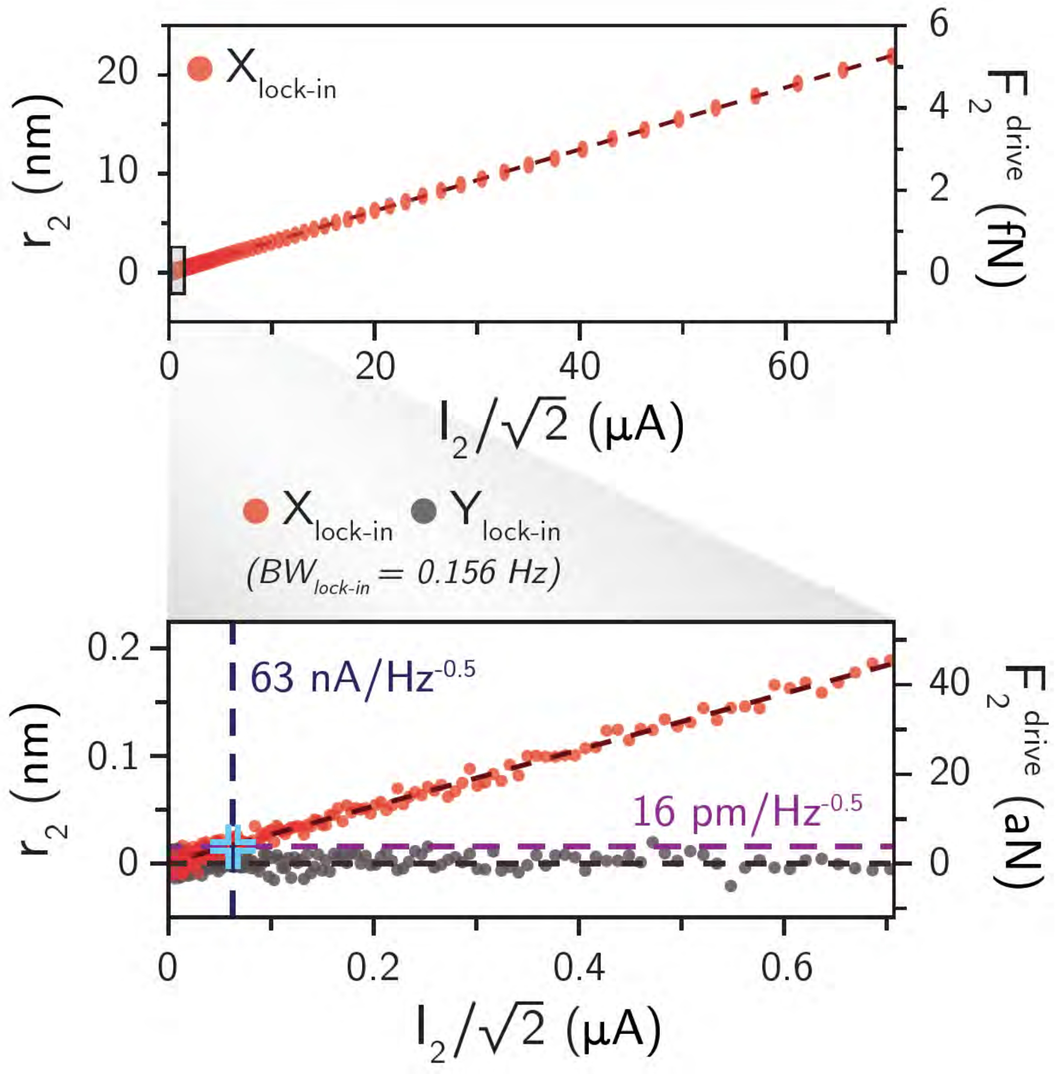

Rossi et al., *Nano Lett.* **19**, 930 (2019).

Quantifying sensitivity

MBE-grown MnAs-tipped NWs

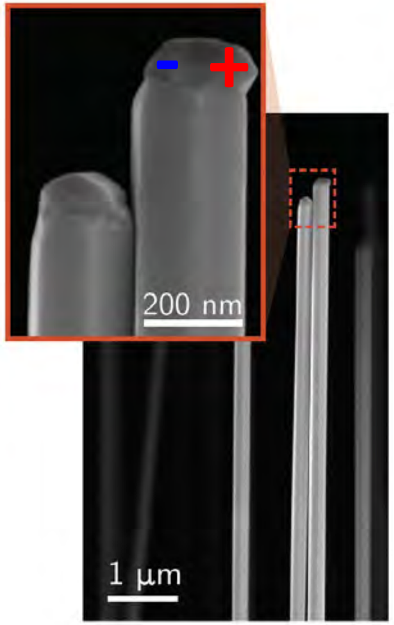

F_{min} = 4 aN/(Hz)$^{1/2}$

At 250 nm spacing:

dB/dx_{min} = 11 mT/m(Hz)$^{1/2}$

Kirtley, *Rep. Prog. Phys.* **73**, 126501 (2010)

Quantifying sensitivity

MBE-grown MnAs-tipped NWs

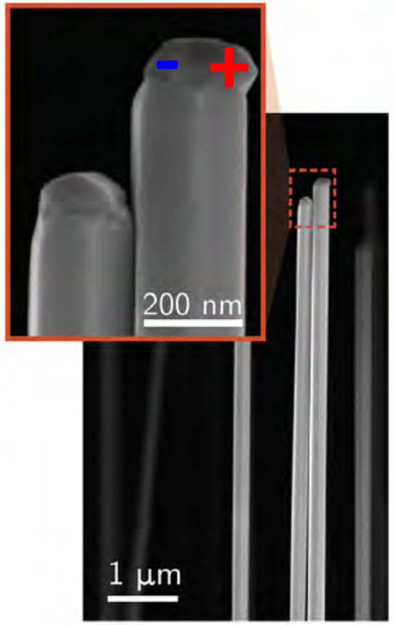

F_{min} = 4 aN/(Hz)$^{1/2}$

<u>At 250 nm spacing:</u>

dB/dx_{min} = 11 mT/m(Hz)$^{1/2}$

M_{min} = 50 μ_B/(Hz)$^{1/2}$

Φ_{min} = 1 $\mu\Phi_0$/(Hz)$^{1/2}$

I_{min} = 10 nA /(Hz)$^{1/2}$

Kirtley, *Rep. Prog. Phys.* **73**, 126501 (2010)

Nanowires as force sensors and scanning probes

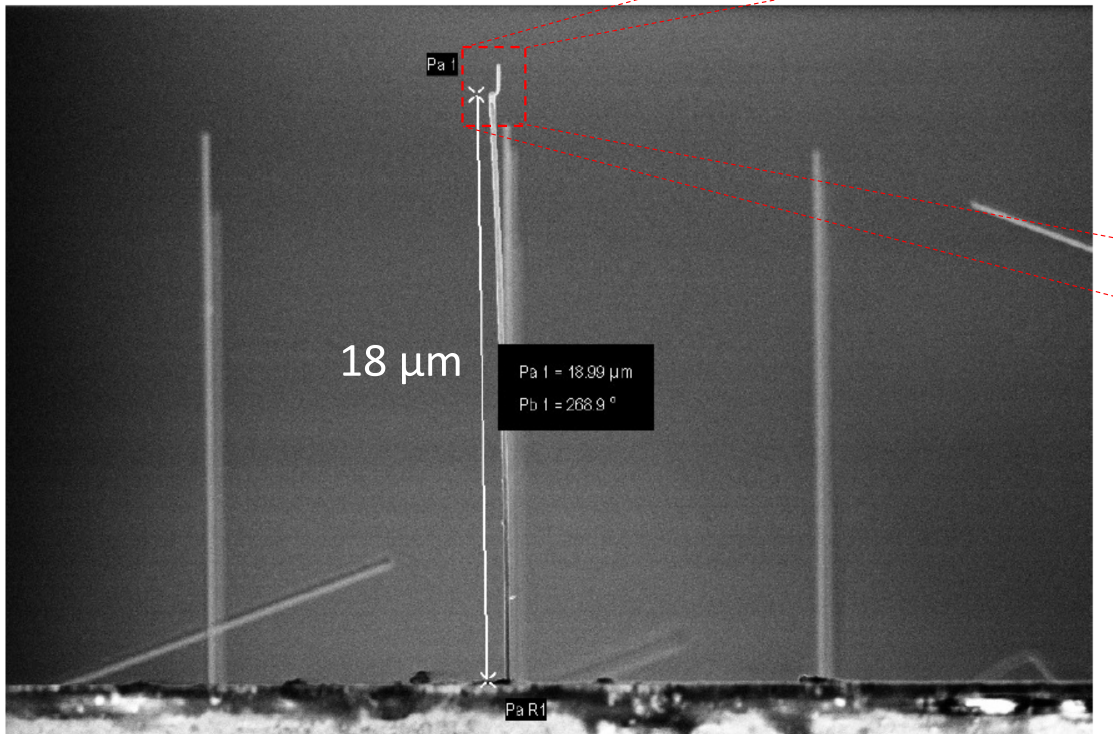

Si NWs (Budakian Group, Waterloo)

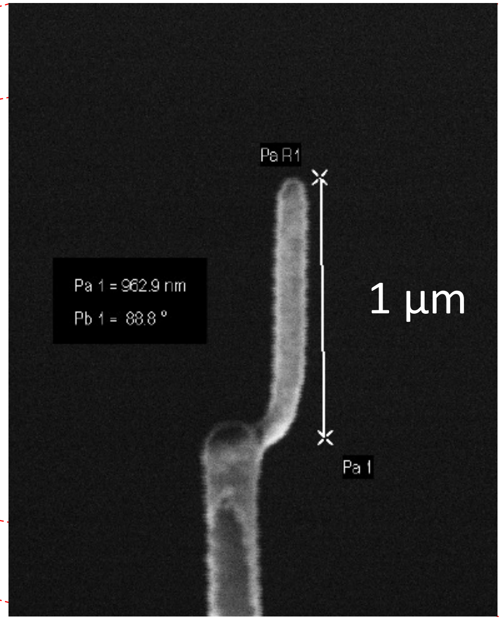

FEBID deposited Co magnetic tip

Magnetic Force Microscopy of bilayer $EuGe_2$

Hinrich Mattiat

Ph.D. Student

Lukas Schneider

Ph.D. Student

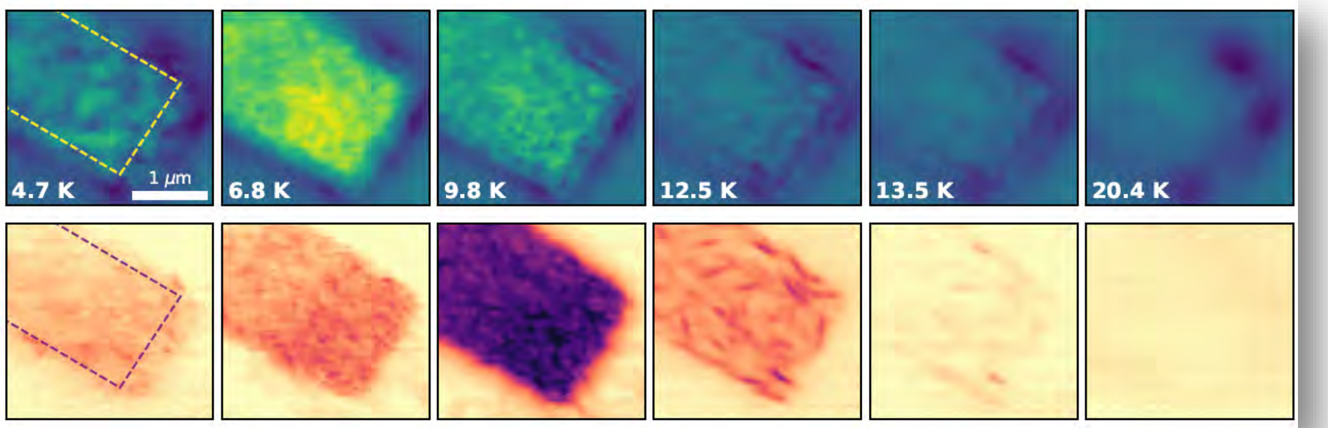

<u>NWs:</u>

Raffi Budiakian

Waterloo, Canada

<u>Samples:</u>

Vyacheslav Storchak

Kurchatov Institute, Russia

Magnetism in 2D $EuGe_2$

- Monolayer exhibits in-plane ferromagnetism (FM)
- Multi-layer (bulk) is stacked antiferromagnetically (AFM)
- layer dependent transition from AFM to FM evolves gradually from bulk to the monolayer, with evidence of a coexistence of both AFM and FM orders (exchange bias)

MBE grown side view top view

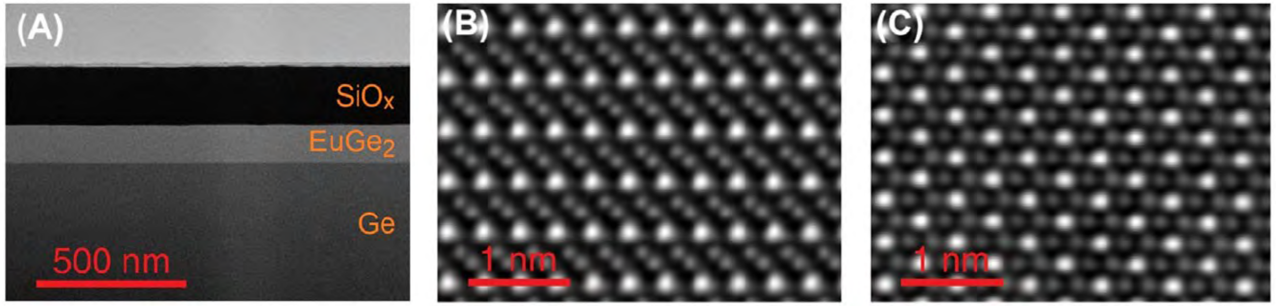

Averyanov et al., *Nano Research* **13**, 3396 (2020); Tokmachev et al., *Materials Horizons* **6**, 1488 (2019).

Bilayer $EuGe_2$: Samples

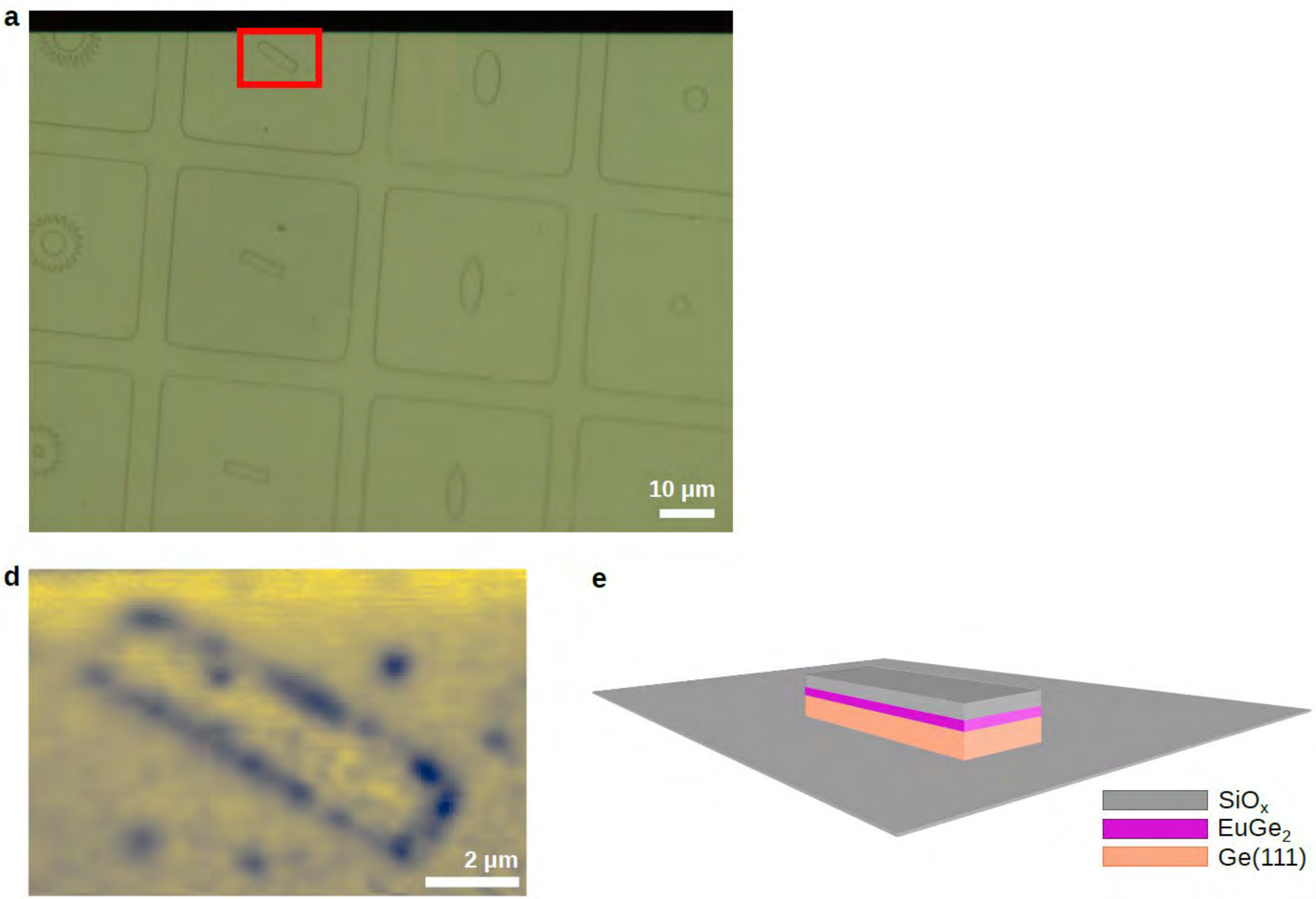

Bilayer $EuGe_2$: Applying out-of-plane field

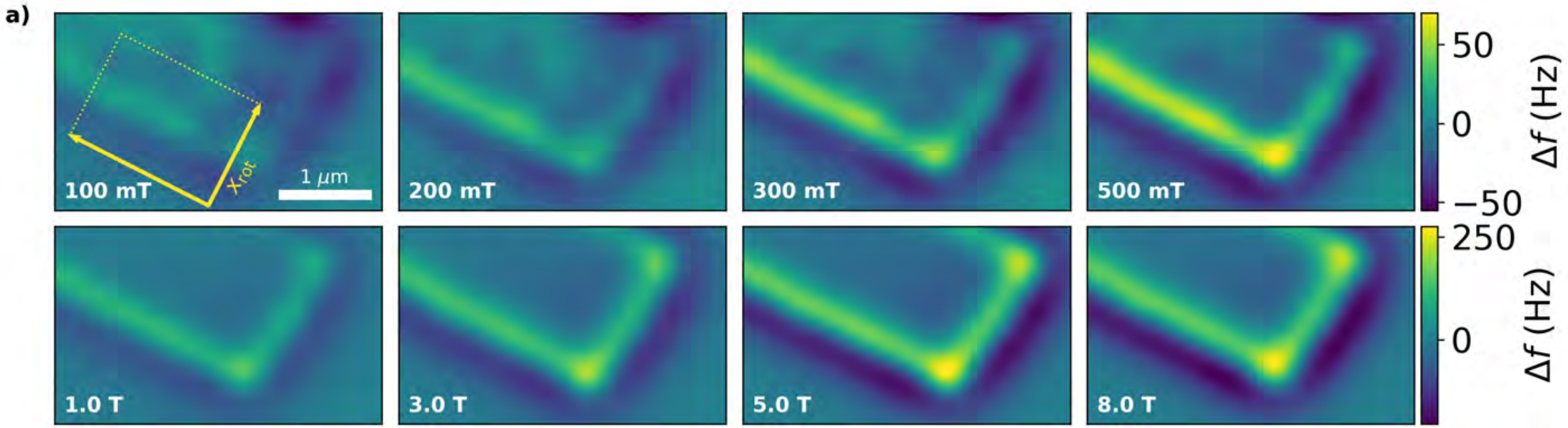

Bilayer $EuGe_2$: Temperature dependence

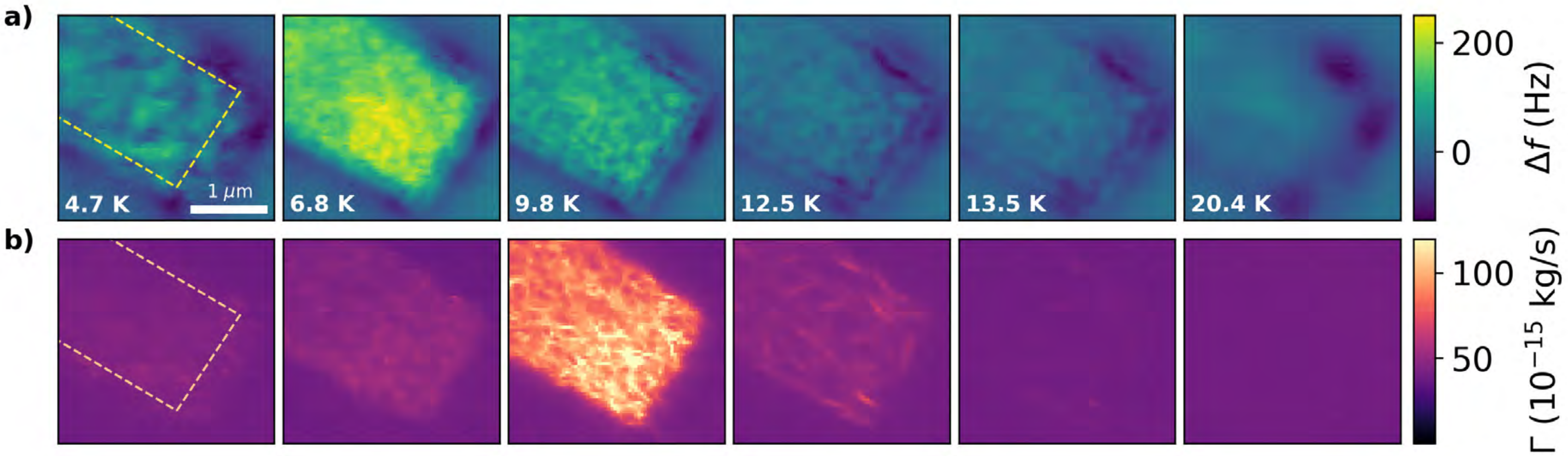

Bilayer $EuGe_2$: Temperature dependence

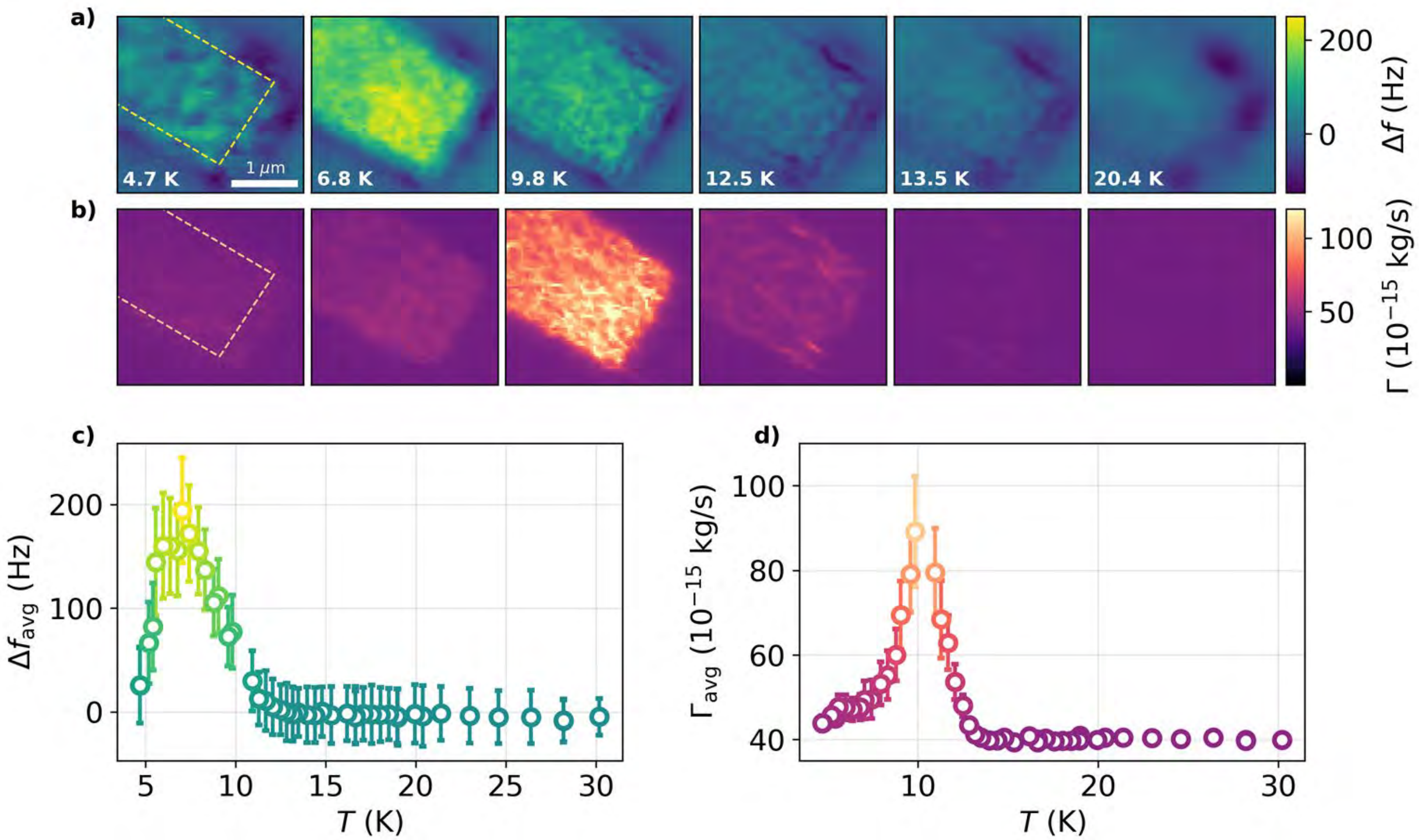

Bilayer $EuGe_2$ Results

- Out-of-plane magnetic saturation above 4 T
- Temperature-dependent measurements in remanence show magnetic phase transition around 10 K
- Images suggest FM/AFM domains with characteristic length of order 100 nm

POGGIO LAB

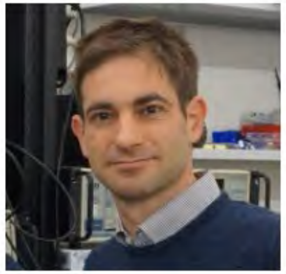
Prof. Martino Poggio
Principal Investigator


Dr. Floris Braakman
Research Scientist


Dr. Boris Groß
Research Scientist


Dr. Estefani Marchiori
Post-doctoral Researcher


Dr. Francesco Fogliano
Post-doctoral Researcher


Dr. Kousik Bagani
Post-doctoral Researcher


Giulio Romagnoli
Post-doctoral Researcher


David Jaeger
Ph.D. Student


Hinrich Mattiat
Ph.D. Student


Lukas Schneider
Ph.D. Student


Andriani Vervelaki
Ph.D. Student


Daniel Jetter
Ph.D. Student


Luca Forrer
Ph.D. Student


Mathias Claus
Ph.D. Student


Liza Žaper
Ph.D. Student


Aurèle Kamber
Ph.D. Student


Aris Lafranca
Master Student

poggiolab.unibas.ch

Recent related references from our group

- **<u>Reviews</u>**
  - Magnetic field imaging for 2D materials: *Nat. Rev. Phys.* **4**, 49 (2022).
  - NW AFM/MFM: *Nanotechnology* **30**, 332001 (2019).

- **<u>Scanning SQUID microscopy</u>**
  - Nb and MoGe SQUID-on-tips: *Appl. Phys. Lett.* **122**, 192603 (2023).
  - Imaging superconducting qubit devices: *Appl. Phys. Lett.* **121**, 052601 (2022).
  - SQUID-on-lever: *Phys. Rev. Appl.* **17**, 034002 (2022)
  - Artificial spin ice: *ACS Nano* **13**, 13910 (2019)
  - Vortices in MoSi: *Phys. Rev. B* **100**, 104504 (2019)
  - Ferromagnetic nanotubes: *Nano Lett.* **18**, 964 (2018)

- **<u>NW MFM</u>**
  - MFM with FEBID NWs: *Phys. Rev. Appl.* **13**, 044043 (2020).
  - NW MFM: *Nano Lett.* **19**, 930 (2019).
  - NW AFM: *Nat. Nanotechnol.* **12**, 150 (2017).